COMPLIANT ROBOTIC STRUCTURES – PART II

Second Report to DARPA

June 1, 1985 – May 31, 1986

James F. Wilson

Department of Civil and Environmental Engineering

Duke University

Durham, North Carolina 27706

July, 1986

86 10 21 066

COMPLIANT ROBOTIC STRUCTURES - PART II

Second Report to DARPA

June 1, 1985 - May 31, 1986

James F. Wilson

Department of Civil and Environmental Engineering

Duke University

Durham, North Carolina 27706

July, 1986

QUALITY INSPECTED 1

Accession For		
NTIS GRA&I	☒	
DTIC TAB	☐	
Unannounced	☐	
Justification	*per ltr*	
By		
Distribution/		
Availability Codes		
Dist	Avail and/or Special	
A-1		

REPORT DOCUMENTATION PAGE

Form Approved
OMB No 0704-0188
Exp Date: Jun 30, 1986

1a. REPORT SECURITY CLASSIFICATION	1b RESTRICTIVE MARKINGS
Unclassified	

2a. SECURITY CLASSIFICATION AUTHORITY	3. DISTRIBUTION/AVAILABILITY OF REPORT
2b. DECLASSIFICATION/DOWNGRADING SCHEDULE	APPROVED FOR PUBLIC RELEASE DISTRIBUTION UNLIMITED

4 PERFORMING ORGANIZATION REPORT NUMBER(S)	5. MONITORING ORGANIZATION REPORT NUMBER(S)
DUKE-CE-001-86-2	

6a. NAME OF PERFORMING ORGANIZATION	6b OFFICE SYMBOL (If applicable)	7a. NAME OF MONITORING ORGANIZATION
Duke University	CE	ONRRR

6c. ADDRESS (City, State, and ZIP Code)	7b. ADDRESS (City, State, and ZIP Code)
Durham, NC 27706	Georgia Institute of Technology 2060 O'Keefe Building Atlanta, GA 30332

8a. NAME OF FUNDING/SPONSORING ORGANIZATION	8b. OFFICE SYMBOL (If applicable)	9. PROCUREMENT INSTRUMENT IDENTIFICATION NUMBER
DARPA (DOD)		MDA903-84-C-0243

8c. ADDRESS (City, State, and ZIP Code)	10. SOURCE OF FUNDING NUMBERS			
	PROGRAM ELEMENT NO.	PROJECT NO.	TASK NO.	WORK UNIT ACCESSION NO.
DARPA/ISTO 1400 Wilson Boulevard Arlington, VA 22209				

11. TITLE (Include Security Classification)

Compliant Robotic Structures - Part II

12. PERSONAL AUTHOR(S)
Wilson, James F.

13a. TYPE OF REPORT	13b. TIME COVERED	14. DATE OF REPORT (Year, Month, Day)	15. PAGE COUNT
second year rept.	FROM 6/1/85 TO 5/31/86	1985, July	

16. SUPPLEMENTARY NOTATION

17.	COSATI CODES		18. SUBJECT TERMS (Continue on reverse if necessary and identify by block number)
FIELD	GROUP	SUB-GROUP	Bellows, cylindrical shells, manipulators nonlinear deformations, orthotropic shells, robotics

19. ABSTRACT (Continue on reverse if necessary and identify by block number)

This is a continuation of studies on complaint robotic structures, which are tube-like, continuously flexible arms or fingers that are designed to extend, bend or twist when pressurized. Conceptual designs are tempered by a knowledge of muscle structure in selected animals.

The results of the second year studies are reported in three chapters. Chapter I presents an overview of muscle structure and function in a variety of soft animal parts. Chapter II focuses on large deformations of compliant torsion elements for robotic wrist action. Chapter III deals with the analysis and conceptual design of compliant robotic arms undergoing large deformations.

Keywords: computer programs, cylindrical shells, manipulators.

20 DISTRIBUTION/AVAILABILITY OF ABSTRACT	21. ABSTRACT SECURITY CLASSIFICATION
☒ UNCLASSIFIED/UNLIMITED ☐ SAME AS RPT. ☐ DTIC USERS	unclassified

22a. NAME OF RESPONSIBLE INDIVIDUAL	22b. TELEPHONE (Include Area Code)	22c OFFICE SYMBOL
Robert L. Rosenfeld	202-694-3624	ISTO

DD FORM 1473, 84 MAR 83 APR edition may be used until exhausted. All other editions are obsolete.
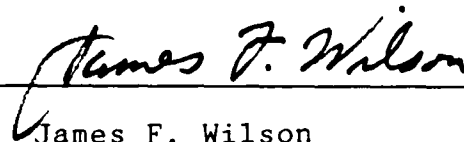
TABLE OF CONTENTS

SUMMARY

This is the second year report which is a part of a three-year study on compliant robotic structures. Such structures are constructed of continuously flexible elastomeric tubes that extend, bend or twist when pressurized. The motion of each tube element under pressure depends on its directional stiffness, achieved through the orientation of wall corrugations and reinforcement. Tube elements placed in series or parallel are being designed as robotic fingers and arms that are fast-acting and have potential payload to self weight ratios as high as 10/1 for laboratory-scale models and up to 3/1 for full-scale prototype arms.

The first two years of this study have involved the formulation and solution of mathematical models for the mechanical behavior of single and multiple elastomeric structures. The formulation of these models has been tempered by the knowledge of the muscle morphology and function in animal hydrostats. In this regard, Chapter I describes fourteen soft animal parts (worm bodies, cephalopod appendages, and vertebrate tongues) and the mechanical principles operating in these structures as they move during muscle contractions. Chapter II presents a general, nonlinear mathematical model of orthotrophic cylindrical shells that undergo large rotations when pressurized. The numerical solutions may be directly employed in the design of rugged, lightweight actuators to achieve wrist action.

Chapter III deals with three topics: the detailed elastic analysis of the load-deformation behavior of bellows; the use of this general analysis in the design of strings of bending elements suitable for use as robotic arms; and a general analysis of the elastica, or the finite deformation patterns achieved in cantilevered element strings (or arms) under internal pressure and end forces due to its payload. This report ends with a brief description of a novel compliant, robotic arm based on satellite bellows elements, analogous to the longitudinal muscles in the appendages of animal hydrostats.

ACKNOWLEDGMENTS

James F. Wilson

James F. Wilson

Professor and
Principal Investigator

Chapter I

MUSCLE MORPHOLOGY AND FUNCTION IN

ANIMAL HYDROSTATS

Lisa J. Croner

INTRODUCTION

This chapter is about muscle. In particular, it presents an overview
of a zoologist's understanding of how muscles work in a variety of
animals' soft parts, in the hope that animal structure can serve as a
source of ideas for the design of flexible robotic manipulators. I have
been asked by the engineers involved in the design of flexible manipulators
to consider soft animal parts as muscular beams which undergo various
contortions when selected muscles contract. To this end, I devote the
first two parts of the chapter to a description of representative
cross-sections of fourteen soft, roughly cylindrical animal parts, and to a
discussion of the simple mechanical principles operating in these
structures when the muscles in them shorten.

In the third part of the chapter I present a brief discussion of
remaining questions which are likely to be relevant to animal-inspired
flexible robot design. I present these questions here to suggest subjects
ripe for analysis in future incarnations of this project.

MECHANICS OF MUSCULAR HYDROSTATS

General Principles

Muscle is familiar to us as the tissue whose activity results in animal motion. In simple terms, a muscle cell is an elongated body which contains a constant volume of cytoplasm and which has the ability to become shorter and fatter forcefully when stimulated electrically. This shape change of the individual muscle cell is converted into a shape change of a body part when many muscle cells pull and push on the tissues surrounding them. The stiffness, elasticity, and other material properties of these tissues are thus extremely important in determining the body changes resulting from a muscle contraction.

"Muscular hydrostats" are animal structures in which cell cytoplasm and/or the constant volume of soft tissue act(s) as a hydrostatic skeleton to transmit the work of contracting muscle (Kier, 1983). Worm bodies, cephalopod appendages, and vertebrate tongues are examples of muscular hydrostats. The tissues comprising them are deformable and make up a constant volume of material. The contraction of muscles surrounding and embedded in such tissue causes changes in the dimensions of the animal structure; because the volume is constant, this results in changes in other dimensions of the structure. This idea is now the basis for the standard analysis of movement in soft-tissue, constant volume structures (Chapman, 1958; Chapman, 1975; Clark, 1964; Kier, 1983; Kier and Smith, 1985; Wainwright,1982).

Two generalizations can be made about the muscular hydrostats I will describe. These generalizations facilitate the development of a model which can be used to explain the movements of these structures. First, they are all either roughly cylindrical in shape or consist of two cylinders separated by a membrane. Second, the muscles in these structures are found oriented in any of three directions (Figure 1). Muscles may be oriented parallel to the long axis of the cylindrical structure; these are "longitudinal" muscles. Muscles may be oriented perpendicular to the long axis of the structure in "circular", "transverse" or "radial" arrays. Muscles may wrap around the periphery of the structure at an oblique angle to the long axis; these are "oblique" muscles (Kier and Smith, 1985).

Muscular hydrostats are capable of making any of four basic movements. They may extend, shorten, bend, and/or twist. The arrangement of muscles within the structures determines the mechanical principles utilized in producing these movements. These principles have
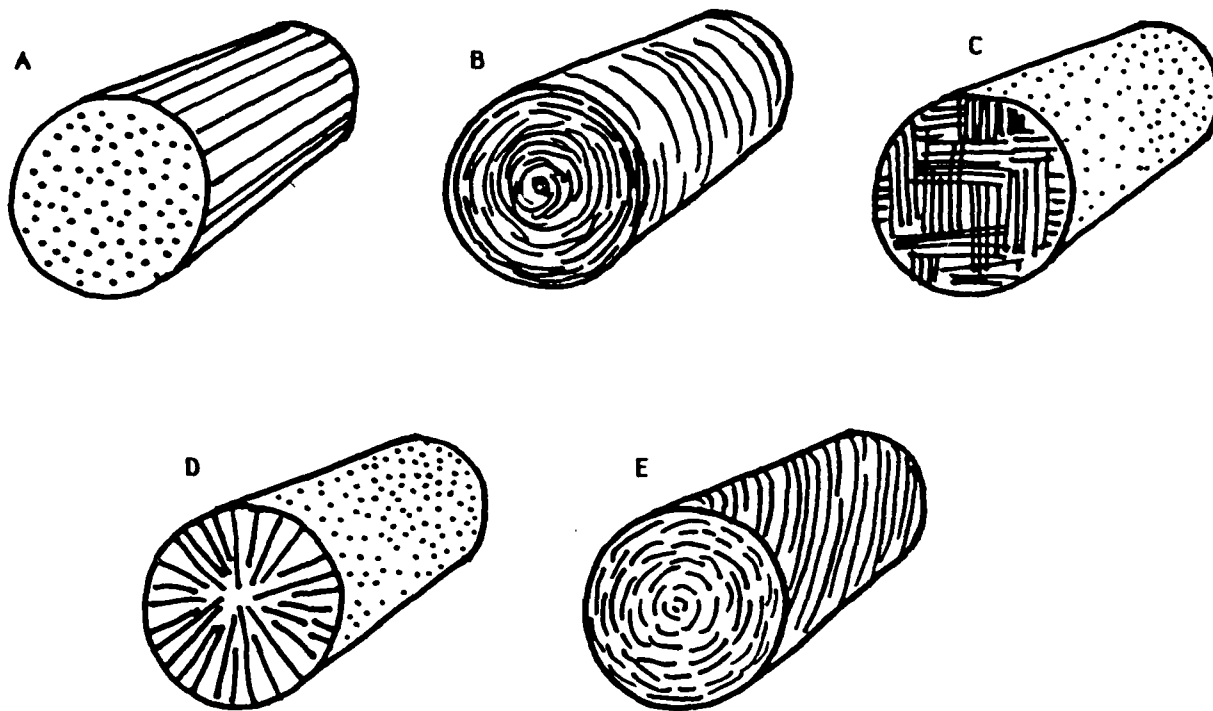
Figure 1. Orientation of muscles found in cylindrical muscular hydrostats. a) Longitudinal
muscles. b) Circular muscles. c) Transverse muscles. d) Radial muscles. e) Oblique
muscles.

been described by various researchers. Most recently, Kier and Smith (1985) have outlined the mechanics of muscular hydrostats, and the following discussion reflects in large part their views.

Elongation

Elongation of a soft, constant volume cylinder occurs when its cross-sectional area decreases. A decrease in cross-sectional area is produced by the contraction of muscles perpendicular to the long axis of the cylinder. Hence, one would expect to find circular, radial, or transverse muscles in soft, cylindrical animal parts which are known to elongate.

The contraction of oblique muscles oriented at an angle ø greater than $54^{0}44'$ to the long axis of the cylinder will also cause elongation. Figure 2 demonstrates why this is so. A constant volume cylinder wrapped for one turn by a single oblique fiber is slit longitudinally to display the surface as a flat sheet, as shown in Figure 2B. The length, radius, and volume of a right circular cylinder in relation to ø are respectively

$$L = D \cos ø$$
$$r = D \sin ø / 2\pi$$
$$V = \pi r^{2} L$$

where D is the length of the oblique fiber. Substituting for r and L, the volume is

$$V = D^{3} \sin^{2} ø \cos ø / 4\pi.$$

The oblique fiber length is then

$$D = (4\pi V / \sin^{2} ø \cos ø)^{1/3},$$

and

$$D/V^{1/3} = (4\pi / \sin^{2} ø \cos ø)^{1/3}.$$

For a constant volume, $D/V^{1/3}$ varies directly with D and thus serves as a "fiber length parameter".

The fiber length parameter can now be plotted against fiber angle ø; such a plot is shown in Figure 2C. The fiber is shortest when the fiber angle is $54^{0}44'$, and increases in length as the angle approaches 0^{0} or 90^{0}.
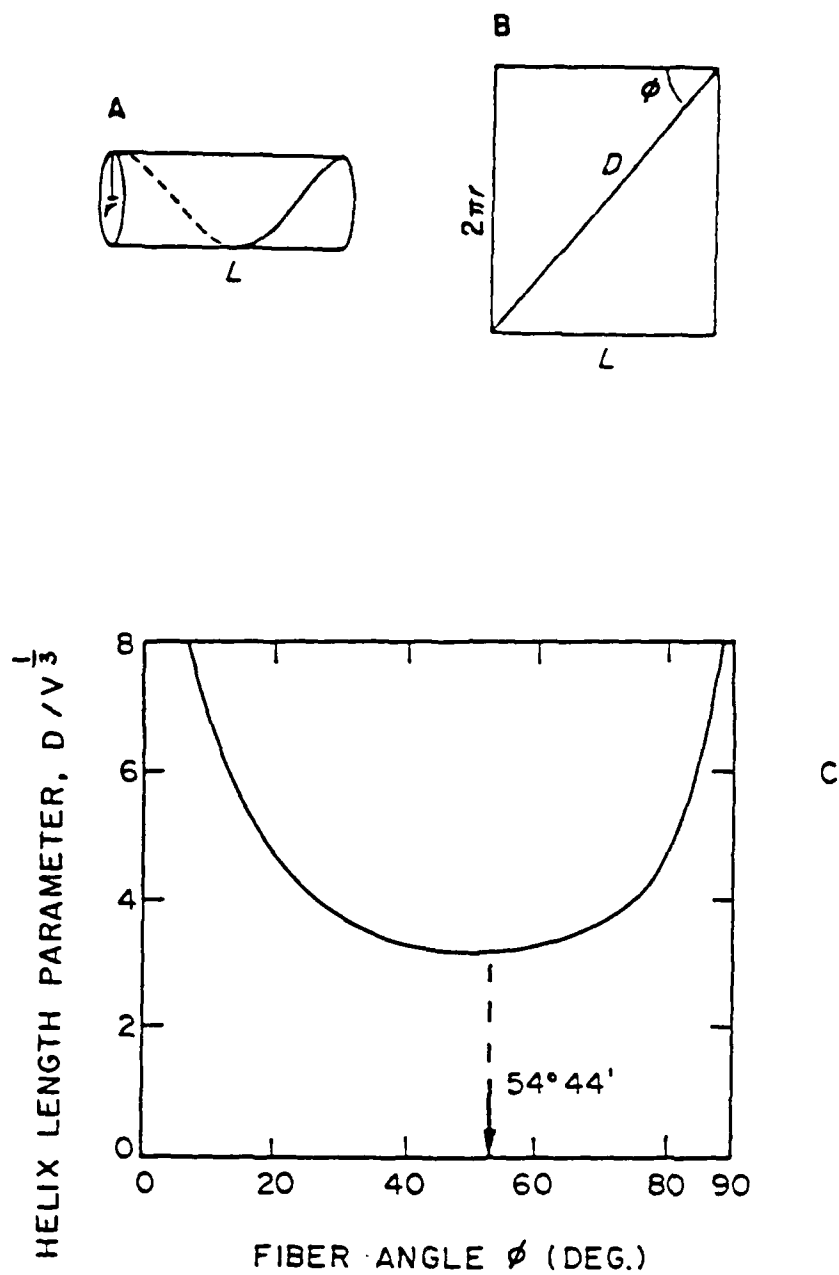
Figure 2. Diagram illustrating the effect of fiber angle on the length of a helical fiber wrapping a constant volume cylinder. See explanation in text. Adapted from Kier and Smith, 1985.

The shortening of a fiber oriented at less than $54°44'$ will increase the fiber angle, and will thus result in a decrease in the length of the cylinder. The shortening of a fiber oriented at greater than $54°44'$ will decrease the fiber angle, thus resulting in an increase in the length of the cylinder. Therefore, oblique musculature can contribute to elongation and shortening of cylindrical muscular hydrostats.

The amount and speed of elongation produced by a given decrease in diameter are affected by the ratio of the length to the width of the cylinder. This is demonstrated as follows. Consider a right circular cylinder of constant volume,

$$V = \pi d^2 L/4 = \pi d_0^2 L_0/4$$

where d and L are the diameter and length respectively, and the subscript zero denotes initial dimensions. The diameter-length relationship is therefore

$$d/d_0 = (L_0/L)^{1/2}.$$

This relationship is plotted in Figure 3. Suppose that the initial state, where $d/d_0 = L/L_0 = 1$, is designated as position A on the plot, and that initially the diameter is one-half the length, or $d_0 = L_0/2$, as shown by cylinder A. Then, if the diameter is increased by a factor of two ($d = 2d_0$), the length must decrease by a factor of four ($L = L_0/4$), as shown by cylinder B. However, if the diameter is decreased by a factor of two, the length increases fourfold, as shown by cylinder C.

It is clear from Figure 3 that a given decrease in diameter produced by action of radial, circular, or transverse muscles causes a greater change in length in a cylinder with a relatively high length/diameter ratio than in one with a lower ratio. The speed of elongation is similarly greater in cylinders with high length/diameter ratios. Therefore, it takes a smaller amount of radial, transverse, or circular muscle contraction to elongate a relatively long and thin cylindrical muscular hydrostat than it does to elongate a shorter and fatter one. One would expect, then, soft, cylindrical animal parts which elongate a great deal to be long and thin.
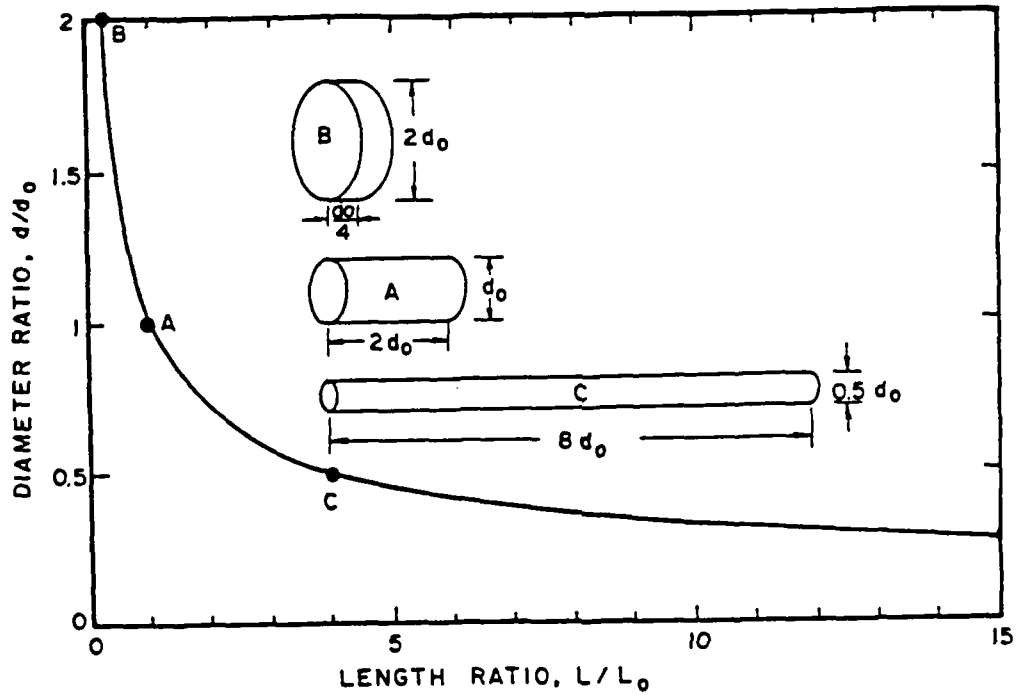
Figure 3. Length-diameter relation for a constant volume right circular cylinder. Adapted from Kier and Smith, 1985.

Shortening

Shortening is produced by the contraction of longitudinal muscles or of oblique muscles oriented at less than $54°44'$ to the long axis (Fig. 2). The amount of extension determines the amount of longitudinal muscle contraction necessary to shorten a muscular hydrostat. The longitudinal muscles of an extensible structure may have to operate over a range of 300% extension and contraction. Obliquely striated muscle cells are thought to be capable of operating over this range (Lanzavecchia and Arcidiacono, 1981).

The muscle cells of some long, thin, extensible structures, however, are not obliquely striated, and cannot function beyond elongations of roughly 40% (Rice, 1973). The contribution of these muscles to shortening an extensible structure can be increased if the longitudinal muscles are longer than the structure itself--in other words, if the longitudinal muscles running through an appendage insert more deeply in the body of the animal than does the appendage itself. For example, a longitudinal muscle 1.4 times the length of the structure it shortens will undergo a 40% elongation during an 80% elongation of the structure.

Bending

Bending of a cylindrical muscular hydrostat is produced by the simultaneous contraction of the longitudinal muscles on one side of the cylinder and the circular, radial, or transverse muscles perpendicular to the long axis. The material properties of tissues composing the muscular hydrostats I will discuss are such that contraction of the longitudinal muscles alone would result in a shortening and widening of the cylinder. Contraction of circular, radial, or transverse muscles prevents the diameter of the cylinder from increasing, and thus prevents shortening from occurring. In this case, contraction of longitudinal muscles can only shorten one side of the cylinder, and thus the cylinder bends. If longitudinal muscles are placed along the periphery of the cylinder, the bending moment exerted by a given contraction of these muscles is greater than it would be if they were placed closer to the center of the cylinder. Animals that have soft cylindrical parts with both longitudinal muscles and circular, radial, or transverse muscles and with the longitudinal muscles located just beneath the skin of the structure would probably,

therefore, include forceful bending as part of the animals' repertoire of motions.

Longitudinal muscles located close to the axis or center of the cylindrical structure can also contribute to bending. For a given amount of contraction, they will do so with a smaller mechanical advantage than longitudinal muscles located more peripherally. They will also, however, do so more quickly, and thus with a greater "speed advantage". One would expect that longitudinal muscles in a structure that bends very quickly and without need of great force would be found near the central axis of the structure.

Twisting

Twisting is produced by the contraction of obliquely oriented muscle fibers. The direction of twisting depends on the handedness of the oblique muscles. If right- and left-handed oblique muscles contract independently, both clockwise and counter-clockwise twisting is possible. If they contract simultaneously, the structure will resist twisting in both directions.

As described above, oblique muscle contraction may also cause elongation and shortening of a structure, depending on the longitudinal angle of these muscles. At $54^\circ 44'$, these muscles are at their minimum length; contraction of muscles at this angle will not cause shortening or elongation of the cylinder, but only twisting.

If oblique muscles are placed along the periphery of the cylinder, the moment through which the torque is applied for a given contraction is greater than if the oblique muscles are placed more centrally. Therefore, one would expect oblique muscles used for twisting to be located close to the skin of the structure.

WORM BODIES, CEPHALOPOD APPENDAGES, AND VERTEBRATE TONGUES

The discussion so far has focussed in a general way on the mechanical principles operating in cylindrical muscular hydrostats. In this section I will consider how these principles operate in fourteen flexible animal parts. These structures include some of the appendages of cephalopods (the squid arm, the squid tentacle, the chambered *Nautilus* cirrus, and the *Octopus* arm), some vertebrate tongues (those of pangolins, lizards, and cats), and the bodies of some worms (horsehair worms, leeches, the nematode *Ascaris*, earthworms, two genera of polychaetes, and the onychophoran *Peripatus*).

The muscle organization in each of these structures takes one of three forms. The structures contain 1)longitudinal muscles only, 2) longitudinal muscles and transverse, radial, or circular muscles, or 3) longitudinal muscles; transverse, radial, or circular muscles; and oblique muscles. This represents, in a sense, a progression of muscle organization, in which versatility of motion increases with the addition of each kind of muscle. This does not represent an evolutionary progression, but simply a useful organizing principle. The structures will be discussed with reference to this progression.

Structures with Longitudinal Muscles Only

In the generalized muscular hydrostat discussed above, the contraction of longitudinal muscles can cause shortening or can contribute to bending. However, the absence of muscles whose contraction could exert transverse tension complicates matters in structures with only longitudinal muscles.

Shortening requires subsequent elongation to return contracted longitudinal muscles to their resting lengths. Elongation results from a decrease in diameter caused by the contraction of radial, circular, or transverse muscles. Elongation can also result from elasticity of tissue deformed by shortening. If these muscles are absent and tissue elasticity is not significant, elongation cannot occur. Shortening would therefore be a devastating motion for such animals to make, and one would expect them to devise mechanisms, either neural or mechanical, to prevent this.

Bending requires that some mechanism prevent an increase in diameter while longitudinal muscles on one side of the hydrostat contract. The prevention of an increase in diameter need not be an active muscular process, but can result from mechanical properties of tissue surrounding

the hydrostat. By preventing an increase in diameter, tissue with appropriate properties would also prevent shortening.

Thus one would expect that cylindrical muscular hydrostats with longitudinal muscles only might be incapable of shortening, capable of bending, and surrounded by material which would prevent increases in diameter.

Gordius (Figure 4) and *Ascaris* (Figure 5) represent two phyla of worms, Nematomorpha and Nematoda respectively, whose members function with muscles oriented only longitudinally. *Ascaris* moves by thrashing its way through viscous media (Sherman and Sherman, 1976). *Gordius* swims or crawls by means of whiplike motions (Barnes, 1980). A thick cuticle surrounds the bodies of these worms, and it is thought that this cuticle causes the muscles on the dorsal and ventral sides of the worms to act as antagonists (Sherman and Sherman, 1976). In *Ascaris*, the contraction of longitudinal muscles on one side of the worm does not cause shortening because the thick cuticle resists the increase in width associated with shortening. The cuticle is composed of several layers of inextensible fibers, presumably collagen, which wrap in right- and left-handed helices around the worm. These fibers are wrapped at an average angle of $75^{0}30'$ to the longitudinal axis (Harris and Crofton, 1957). As described above (Figure 2), hydrostatic pressure pushing against fibers wrapped around a cylinder at this angle will produce an "elongation force". This force is equivalent to that produced by the contraction of oblique muscles wrapped at this angle. There will be no increase in diameter of the cylinder, and the worm will bend, stretching the longitudinal muscles on the opposite side to that of the contracting longitudinal muscles.

Eakin and Brandenburger (1974) investigated the fine structure of gordian worms and found that the cuticle surrounding the body consists of as many as 36 layers of helically wrapped fibers. Although the angles of these fibers have not been measured, they are probably greater than $54^{0}44'$, since this is required to resist an increase in diameter when hydrostatic pressure increases as a result of longitudinal muscle contraction. The sequence of events producing the whiplike motion of *Gordius* are likely the same as those producing *Ascaris* thrashing.

Structures with Longitudinal and Transverse, Radial, or Circular Muscles

Structures with longitudinal muscles and their antagonists, the circular, radial, or transverse muscles, are capable of elongating,

Figure 4. The Nematomorph worm *Gordius.* a) External view of whole
animal. Adapted from Barnes, 1980. b) Cross-section. Adapted
from Eakin and Brandenburger, 1974.

A

5 mm

0.5 mm

B

CUTICLE

LONGITUDINAL MUSCLE

PHARYNX

LATERAL NERVE CORD

BODY CAVITY
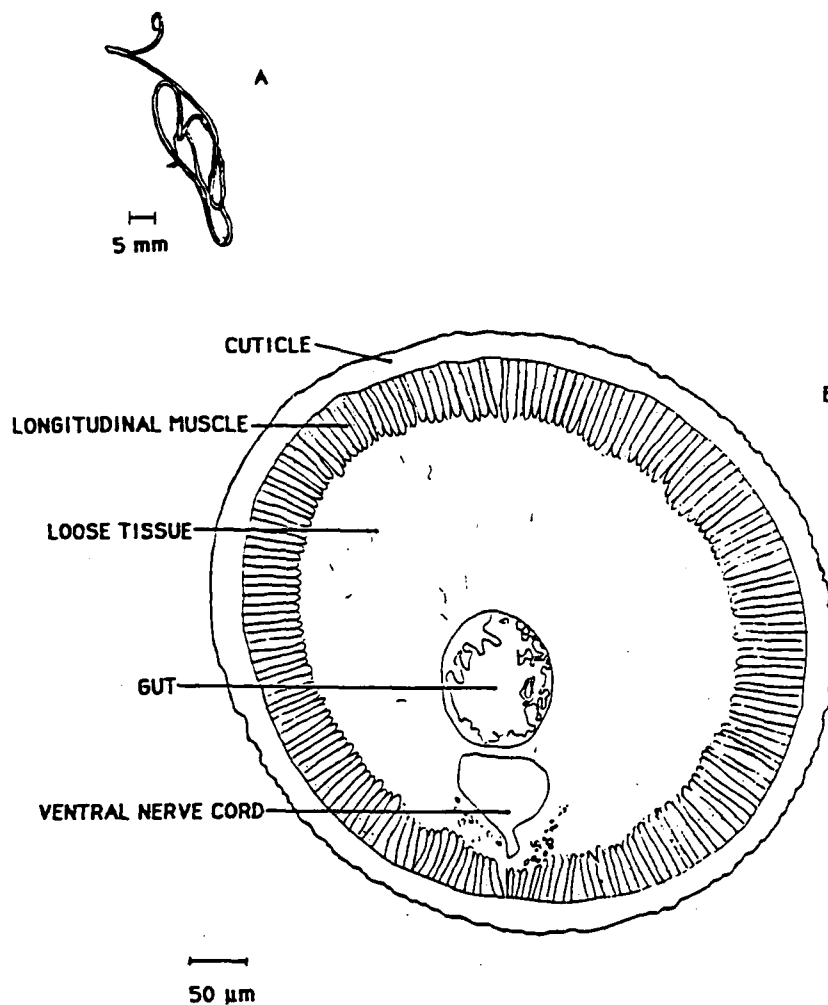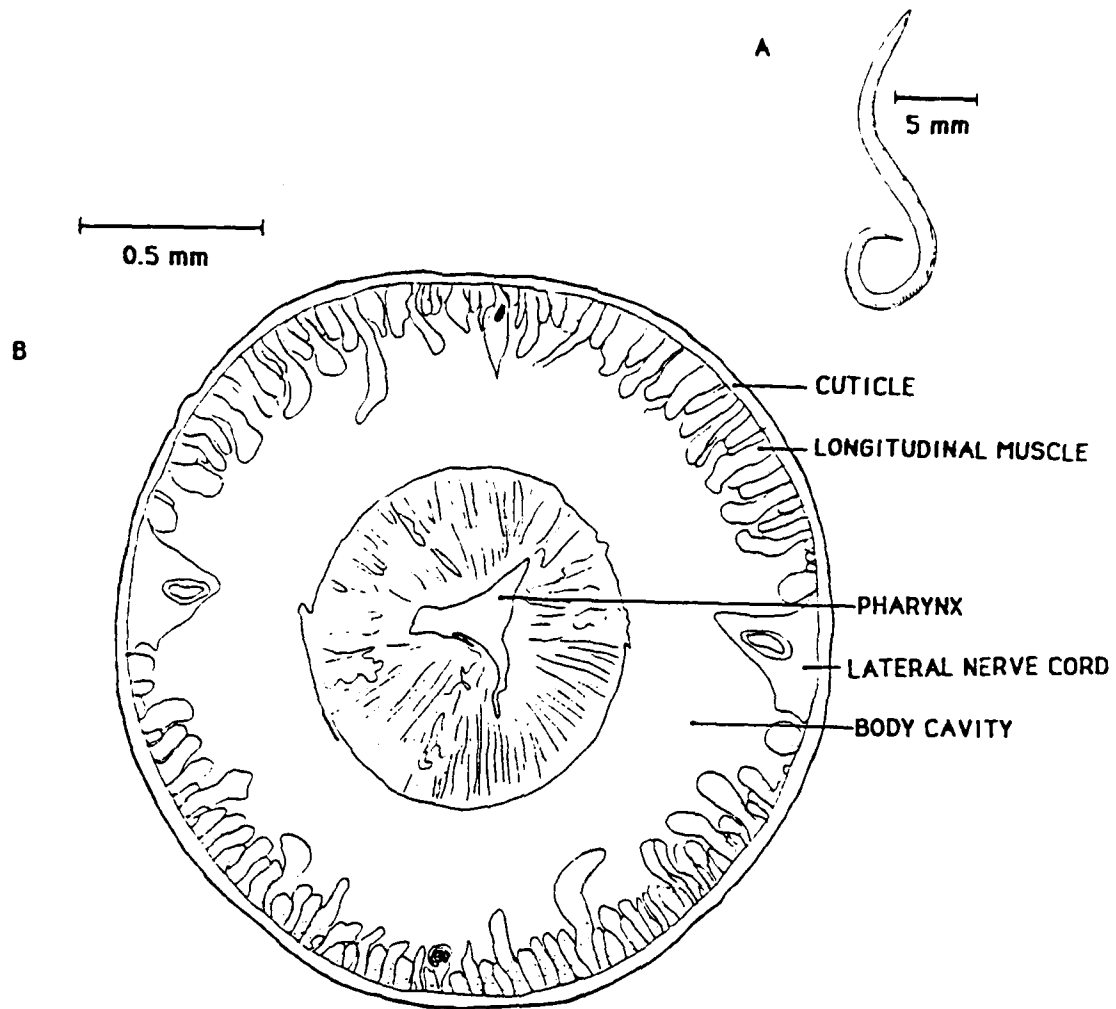
Figure 5. The Nematode worm *Ascaris*. a) External view of whole animal.
   Adapted from Riedl, 1983. b) Cross-section. Adapted from Freeman
   and Bracegirdle, 1971.

shortening, and bending. The structures I will discuss in relation to this musculature are the tongues of pangolins (*Manis*), lizards (*Varanus*), and domestic cats (*Felis*), and the bodies of leeches (*Hirudo*), earthworms (*Lumbricus*), and one polychaete (*Nephtys*).

Hirudo, Lumbricus, and *Nephtys* are all segmented worms of the phylum Annelida. Their bodies are divided into longitudinal sequences of segments separated from each other by transverse septa. This arrangement allows each segment to act as a little hydrostat independent of other segments.

Clark and Clark (1960) investigated the musculature of *Nephtys*, a worm which burrows and swims by means of undulatory waves of its body. Figure 6 is a drawing of two cross-sections of *Nephtys*. Figure 6A shows the musculature seen within a segment, and Figure 6B shows the musculature seen in a septum. The longitudinal muscles are clearly antagonized by the dorso-ventral transverse muscles within a segment; these muscles prevent an increase in height of a segment when longitudinal muscles contract to produce bending. It is less clear what muscles or structures prevent an increase in segmental width, although Clark and Clark found no increase in width during locomotion. *Nephtys* does not shorten and elongate noticeably (personal observation). Certainly there is not an abundance of transverse muscle to produce elongation.

Hirudo (Figure 7) and *Lumbricus* (Figure 8) are capable of bending, shortening, and elongating to incredible extents. They can also move via peristalsis. The longitudinal and circular muscles of their body walls are sufficient to produce these movements, as described above. Segmentation allows for the independent action of individual body segments, and this allows for peristalsis.

Vertebrate tongues are generally capable of shortening, elongating, and bending. They are often, though not exclusively, used to gather food and prey, and may sometimes be required to maneuver both quickly and forcefully. Pangolins (Figure 9) and lizards (Figure 10) are examples of vertebrates whose tongues have longitudinal muscles located both centrally and peripherally. Centrally located longitudinal muscle may function to increase the speed advantage of shortening, and peripherally located longitudinal muscle may function to increase the mechanical advantage of shortening.

Doran and Baggett (1971) classified mammalian tongues into two types: intra-oral and extra-oral. Intra-oral tongues are used to manipulate food inside the mouth, and are capable of less than 50% extension. Extra-oral tongues are used in addition to gather food outside of the mouth, and are capable of greater than 100% extension. Intra-oral

A

20 mm

B

LONGITUDINAL MUSCLE

GUT

TRANSVERSE (DORSO-
VENTRAL) MUSCLE

TRANSVERSE SEPTAL MUSCLE

PARAPODIUM

LONGITUDINAL MUSCLE

1mm

C

LONGITUDINAL MUSCLE

GUT

TRANSVERSE (DORSO-
VENTRAL) MUSCLE

GUT-SUSPENSION MUSCLE

LONGITUDINAL MUSCLE

BODY CAVITY

Figure 6. The polychaete worm *Nephtys.* a) External view of whole
animal. Adapted from Morris, Abbot, and Haderlie, 1980.
b) Cross-section showing musculature of septum. c) Cross-section
showing musculature of segment. b and c adapted from Clark and
Clark, 1960.

A

10 mm

B

EPITHELIUM

CIRCULAR MUSCLE

LONGITUDINAL MUSCLE

SINUS

LOOSE TISSUE

OESOPHAGUS

SINUS

SUBOESOPHAGEAL GANGLIA

SINUS

1 mm

C

EPITHELIUM

CIRCULAR MUSCLE

LONGITUDINAL MUSCLE

LOOSE TISSUE

SINUS

CROP

CROP

VENTRAL NERVE CORD

SINUS
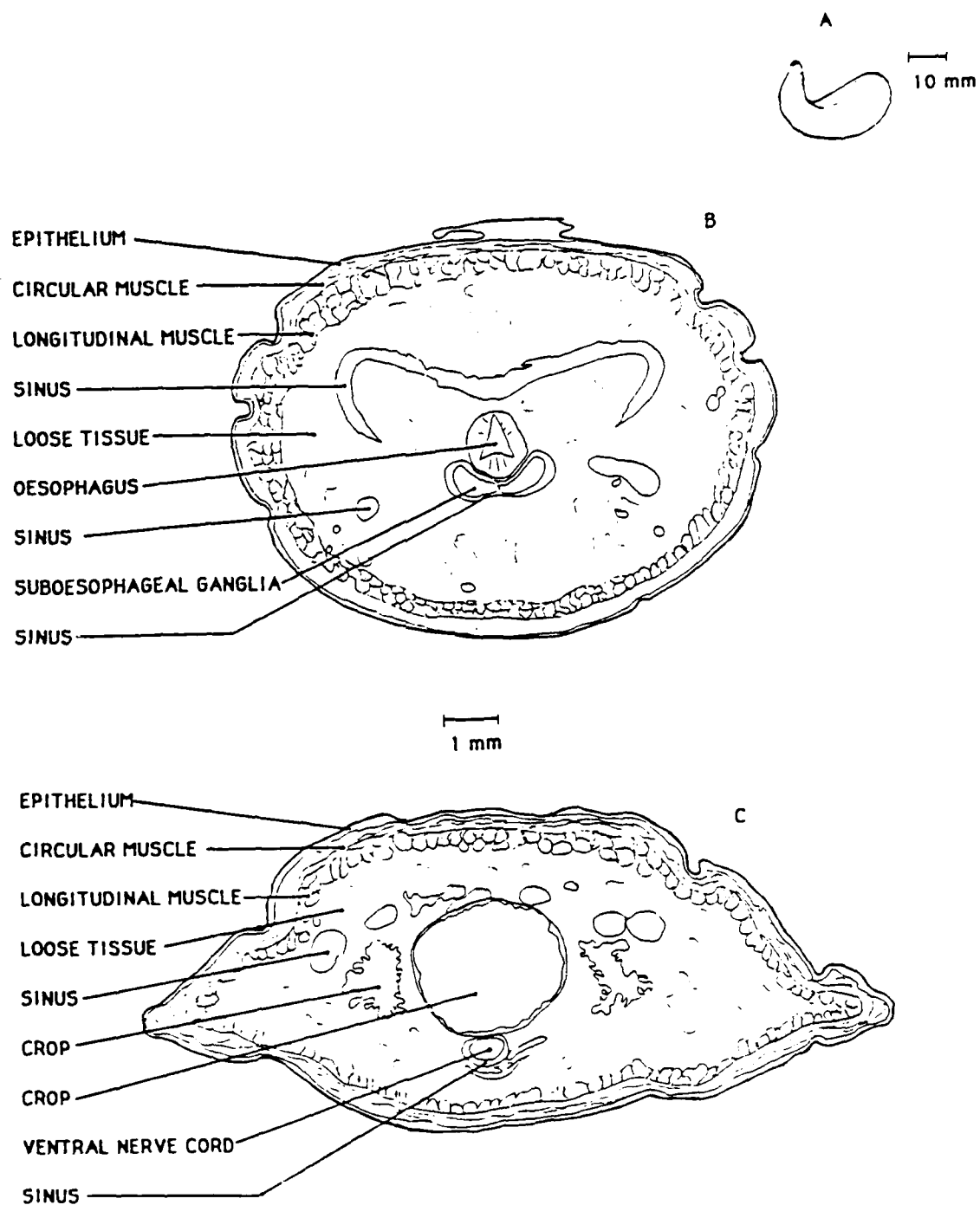
Figure 7. The leech *Hirudo.* a) External view of whole animal. Adapted
from Barnes, 1980. b) Cross-section of oesophageal region.
c) Cross-section of mid-gut region. b and c adapted from Freeman
and Bracegirdle, 1971.
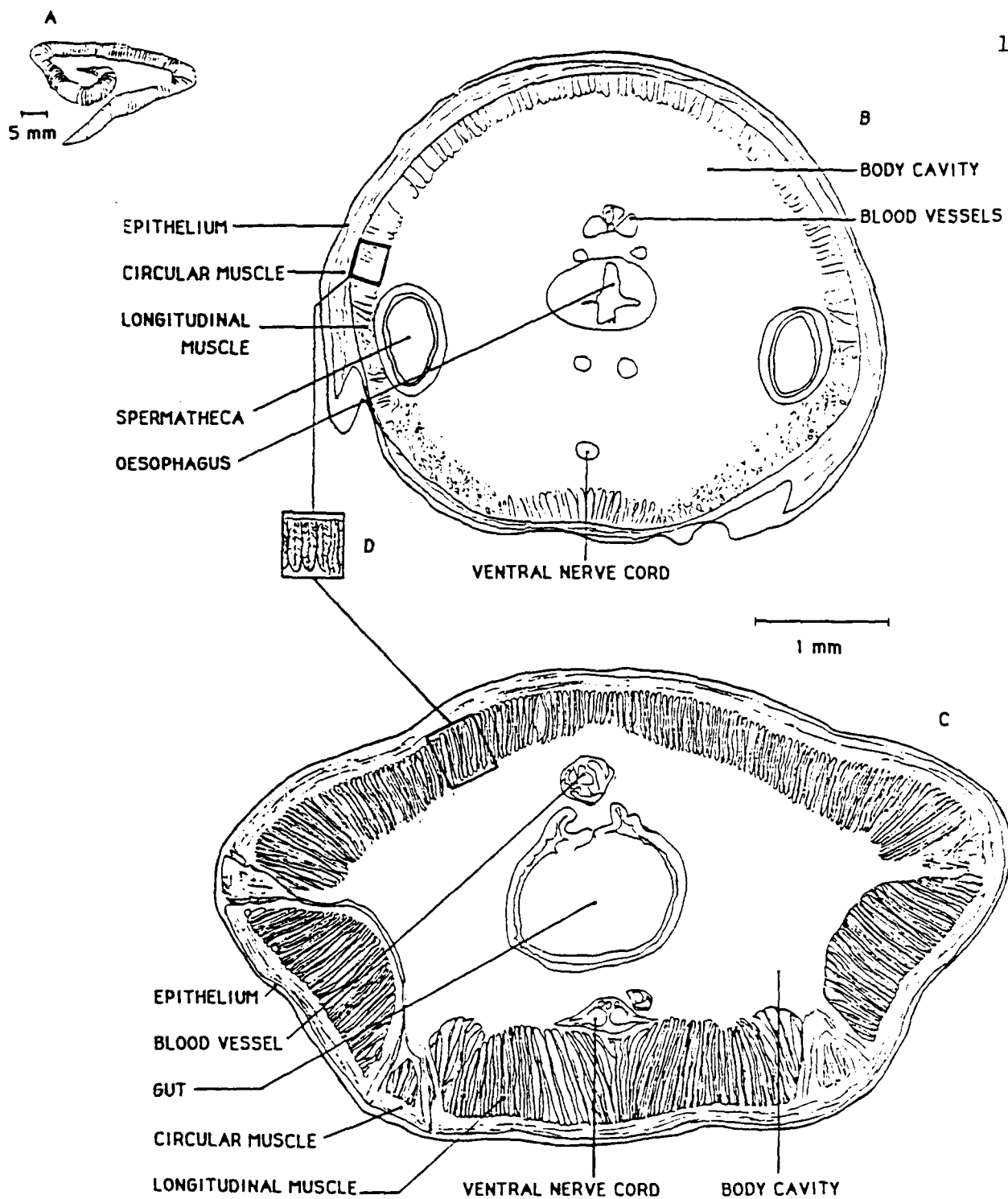
Figure 8. The Annelid earthworm *Lumbricus.* a) External view of whole
animal. Adapted from Wainwright et al, 1976. b) Cross-section of
oesophageal region. c) Cross-section of intestinal region. d) Detail
of longitudinal muscle bundles. b, c, and d adapted from Freeman
and Bracegirdle, 1971.

A

B

LONGITUDINAL MUSCLE

├─┤
1 mm

C

LONGITUDINAL MUSCLE

TRANSVERSE MUSCLE

D

LONGITUDINAL MUSCLE

CIRCULAR MUSCLE

├─┤
1 mm
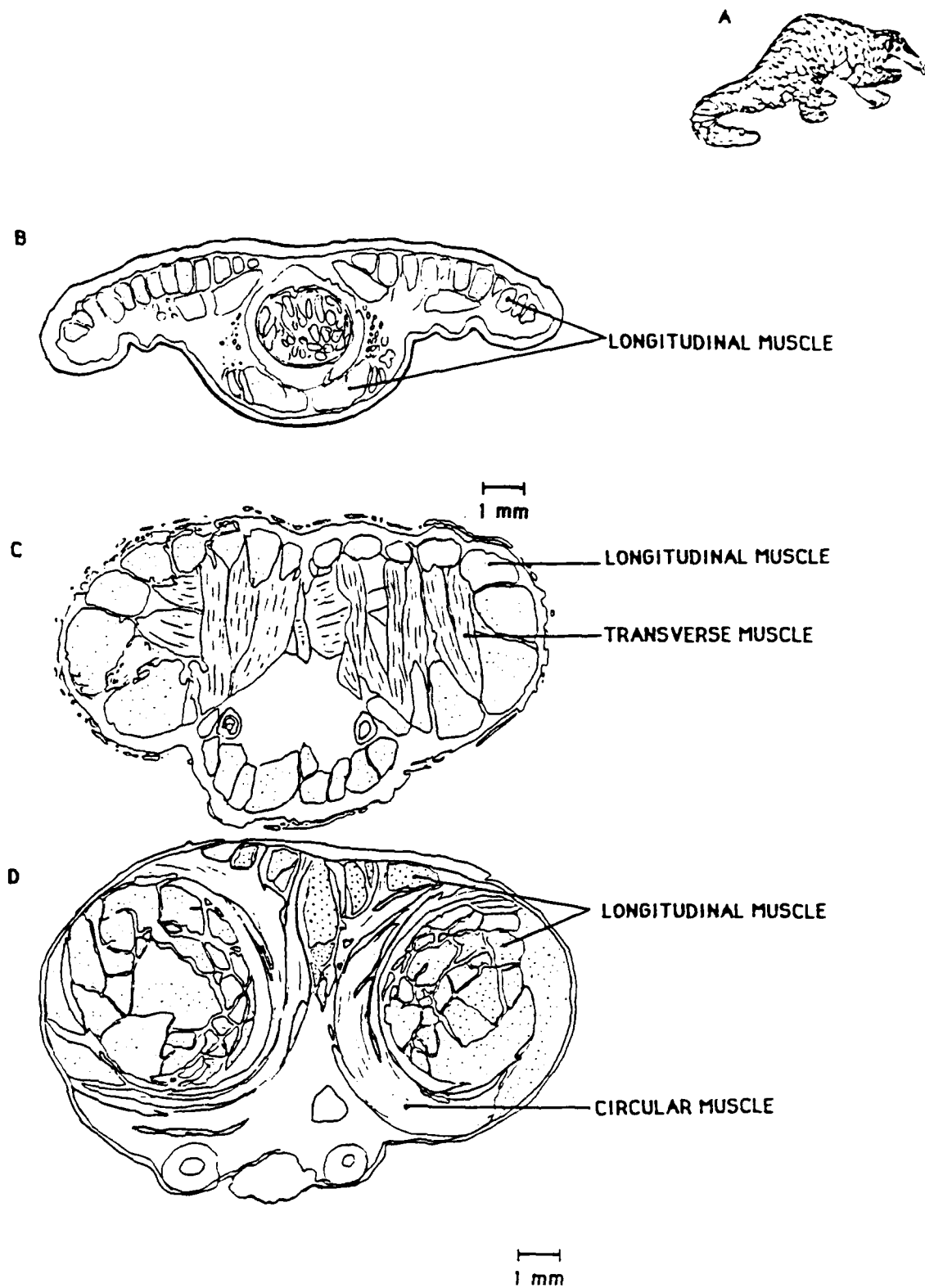
Figure 9. The African pangolin *Manis*. a) External view of whole animal. From Kingdon, 1971. b) Cross-section of rostral part of tongue. c) Cross-section of middle part of tongue. d) Cross-section of caudal part of tongue. b, c, and d adapted from Doran and Allbrook, 1973.

tongues have relatively low length/diameter ratios, while extra-oral tongues have relatively high length/diameter ratios.

An example of an extra-oral tongue is that of the pangolin (Figure 9). Pangolins are African mammals that use their tongues to dig for ants and then to manipulate ants into their mouths. A pangolin tongue has a high length/diameter ratio and is very extensible. The longitudinal muscles of the tongue originate far back in the body of the pangolin and stretch into the tip of the tongue. This may be a mechanism for enabling the longitudinal muscles to retract the tongue after extension, as discussed in the subsection "*Shortening*" above.

Although Doran and Baggett's classification was meant to apply to mammalian tongues, it can be extended to include many other vertebrates' tongues. Lizards with tongues very similar to that of the monitor lizard (*Varanus*) (Figure 10) have been shown to have extensible tongues with high length/diameter ratios (Kier and Smith, 1985; Smith, 1984).

An example of a mammalian intra-oral tongue is that of the domestic cat (*Felis*) (Figure 11). Cat tongues have a low length/diameter ratio and do not extend far out of the mouth.

Structures with Longitudinal Muscles; Transverse, Radial, or Circular Muscles; and Oblique Muscles

Structures with longitudinal muscles, their antagonists, and oblique muscles are the most versatile of the muscular hydrostats. They may be capable of shortening, extending, bending, and twisting. Such structures include the segmented polychaete worm *Nereis* (Figure 12), the Onychophoran worm *Peripatus* (Figure 13), the squid (*Loligo*) arms (Figure 14) and tentacles (Figure 15), the chambered *Nautilus* cirri (Figure 16), and the arms of *Octopus* (Figure 17).

The arrangement of muscles in these structures directly reflect the mechanical principles operating in the generalized cylindrical muscular hydrostat. Longitudinal and oblique muscles are located near the periphery of the structures to increase the mechanical advantage during bending and twisting. The cephalopod appendages also have longitudinal musculature located more centrally, implying that they are capable of bending and twisting with an increased velocity advantage also.
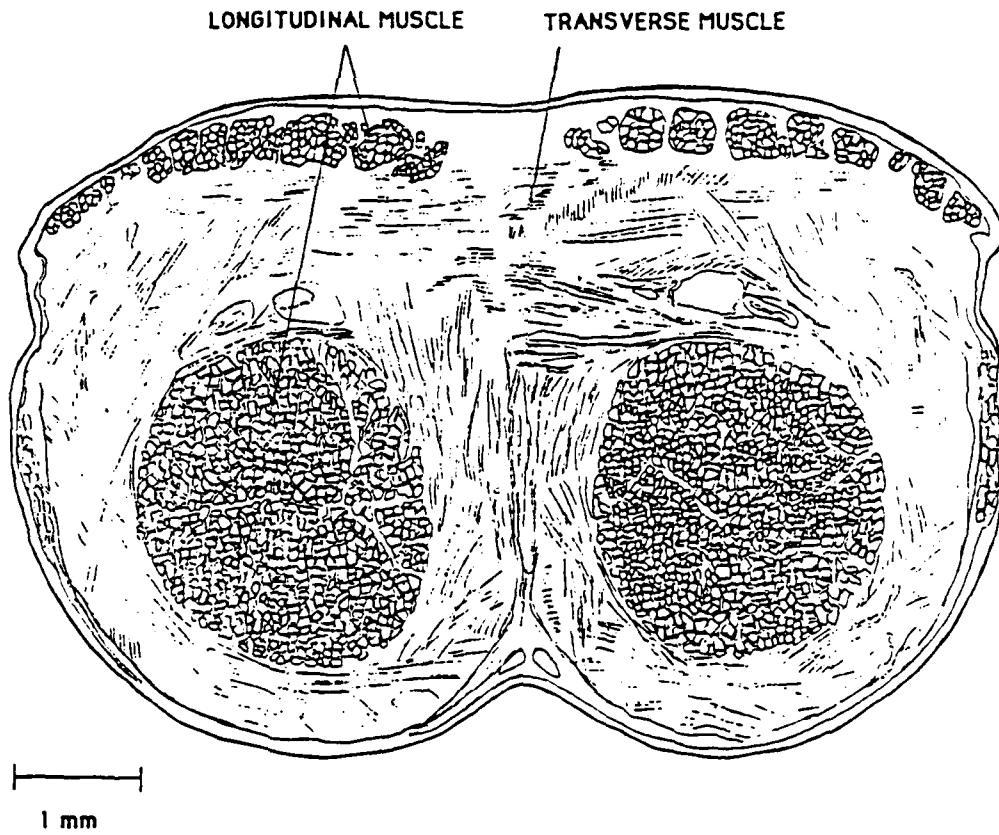
Figure 10. Cross-section of the tongue of the monitor lizard *Varanus*.
Adapted from Kier and Smith, 1985.

LONGITUDINAL MUSCLE TRANSVERSE MUSCLE

1 mm

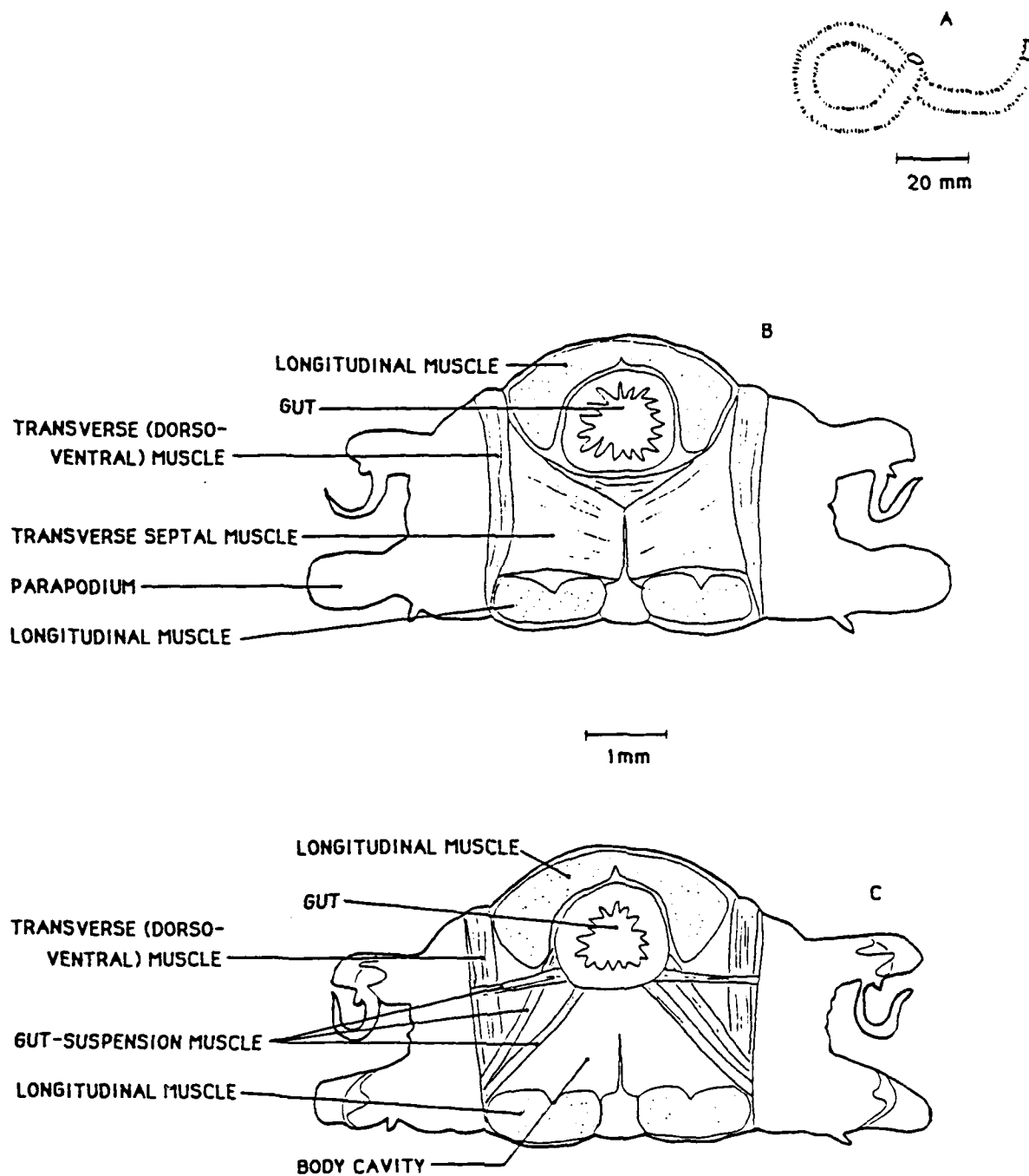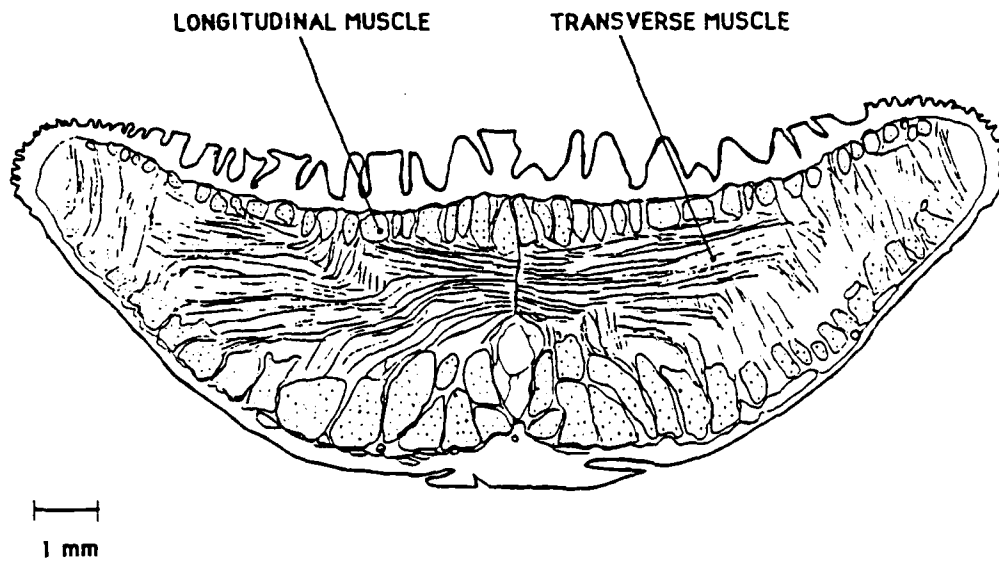Figure 11. Cross-section of the tongue of the domestic cat *Felis.* Adapted from Kier and Smith, 1985.
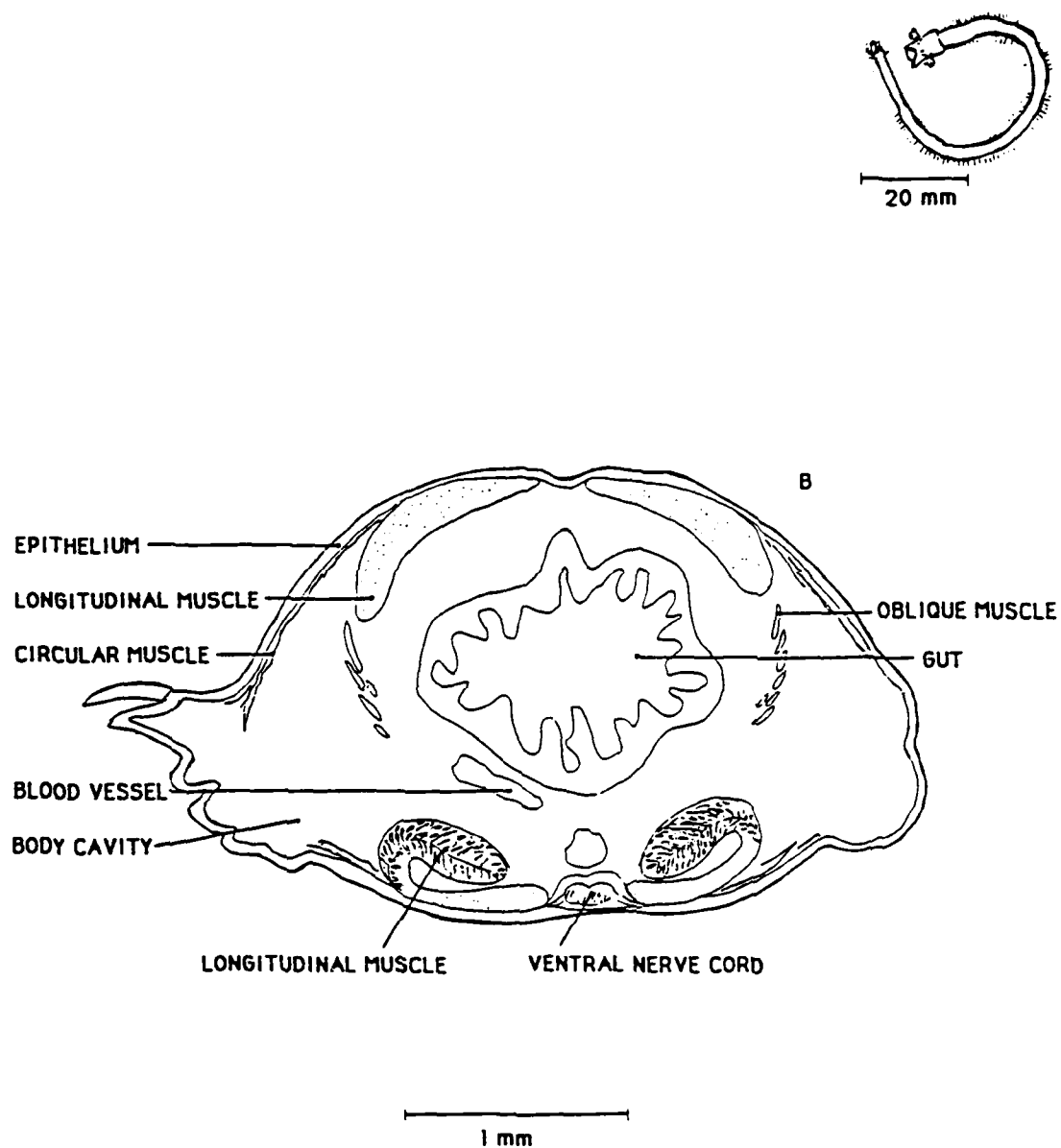
Figure 12. The polychaete worm *Nereis.* a) External view of whole
animal. Adapted from Morris, Abbot, and Haderlie, 1980.
b) Cross-section. Adapted from Freeman and Bracegirdle, 1971.
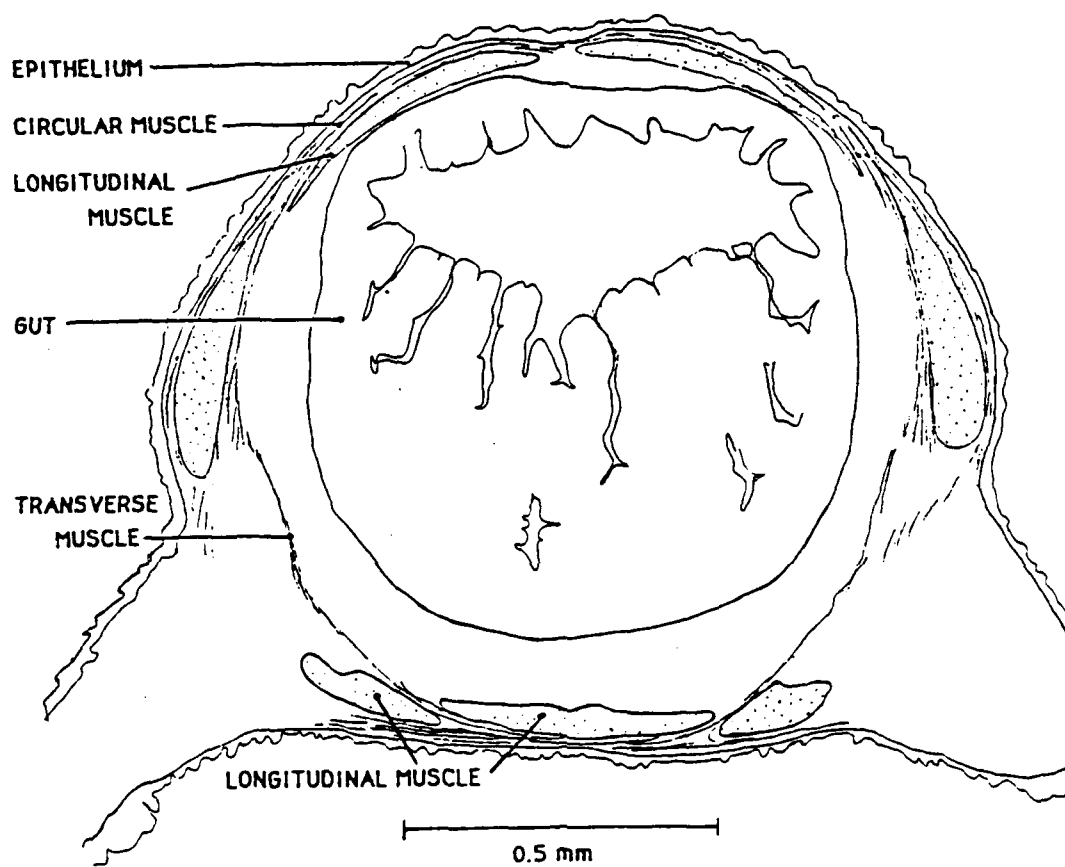
Figure 13. Cross-section of the onychophoran worm *Peripatus.* Adapted

from Freeman and Bracegirdle, 1971.

A

1mm

LONGITUDINAL MUSCLE

LEFT-HANDED OBLIQUE MUSCLE

RIGHT-HANDED OBLIQUE
MUSCLE

LONGITUDINAL MUSCLE

TRANSVERSE MUSCLE

B
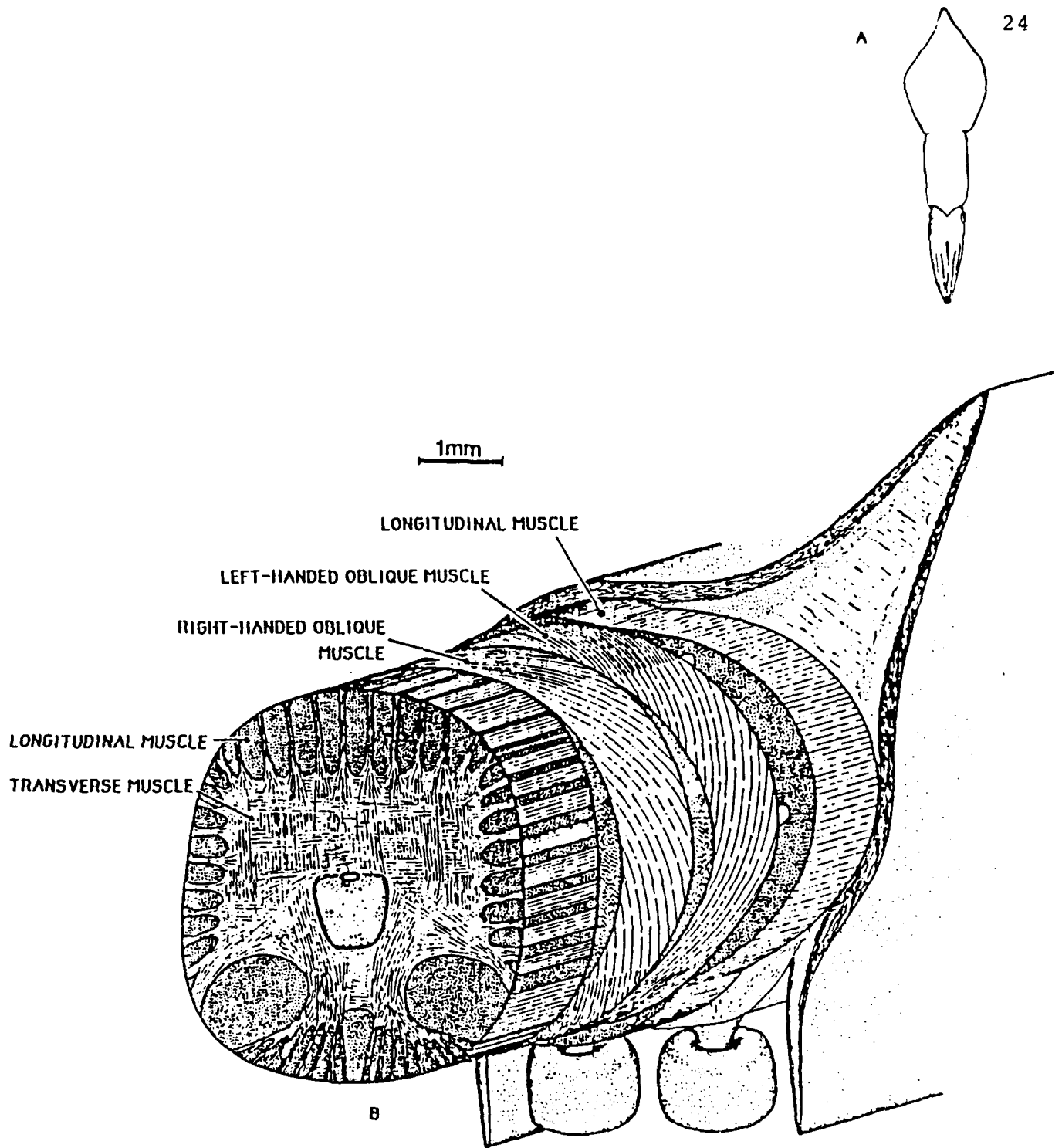
Figure 14. The squid *Loligo*. a) External view of whole animal. Adapted
from Barnes, 1980. b) Cut-away view of arm, showing musculature.
From Kier, 1983.

A

SUPERFICIAL LONGITUDINAL MUSCLE

LEFT-HANDED OBLIQUE MUSCLE

RIGHT-HANDED OBLIQUE MUSCLE

CIRCULAR MUSCLE

LONGITUDINAL MUSCLE

TRANSVERSE MUSCLE

B

1 mm
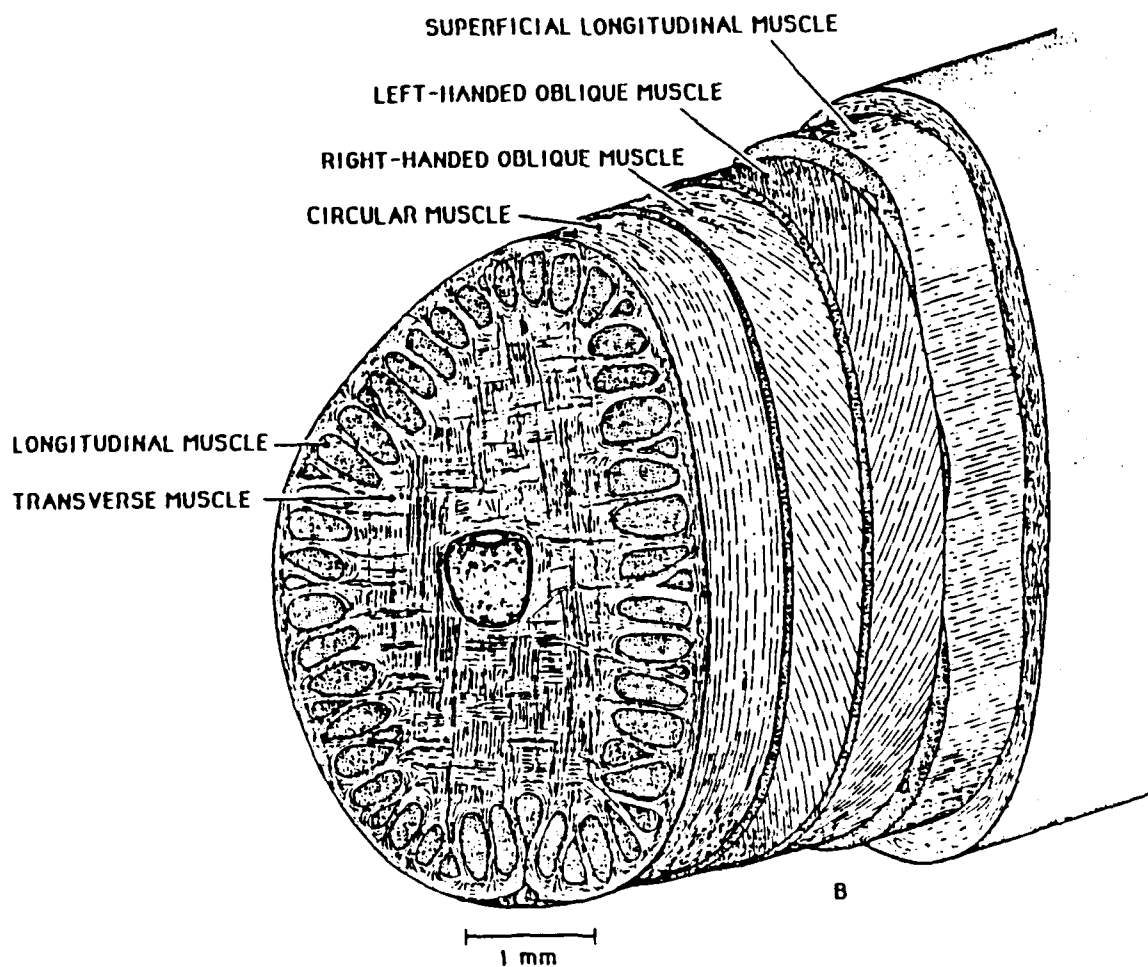
Figure 15. The squid *Loligo*. a) External view of whole animal with
tentacles extended. Adapted from Barnes, 1980. b) Cut-away view
of tentacle, showing musculature. From Kier, 1983.

CROSSED OBLIQUE MUSCLE

LONGITUDINAL MUSCLE

OBLIQUE MUSCLE

LONGITUDINAL MUSCLE

RADIAL MUSCLE

A

B

1 mm
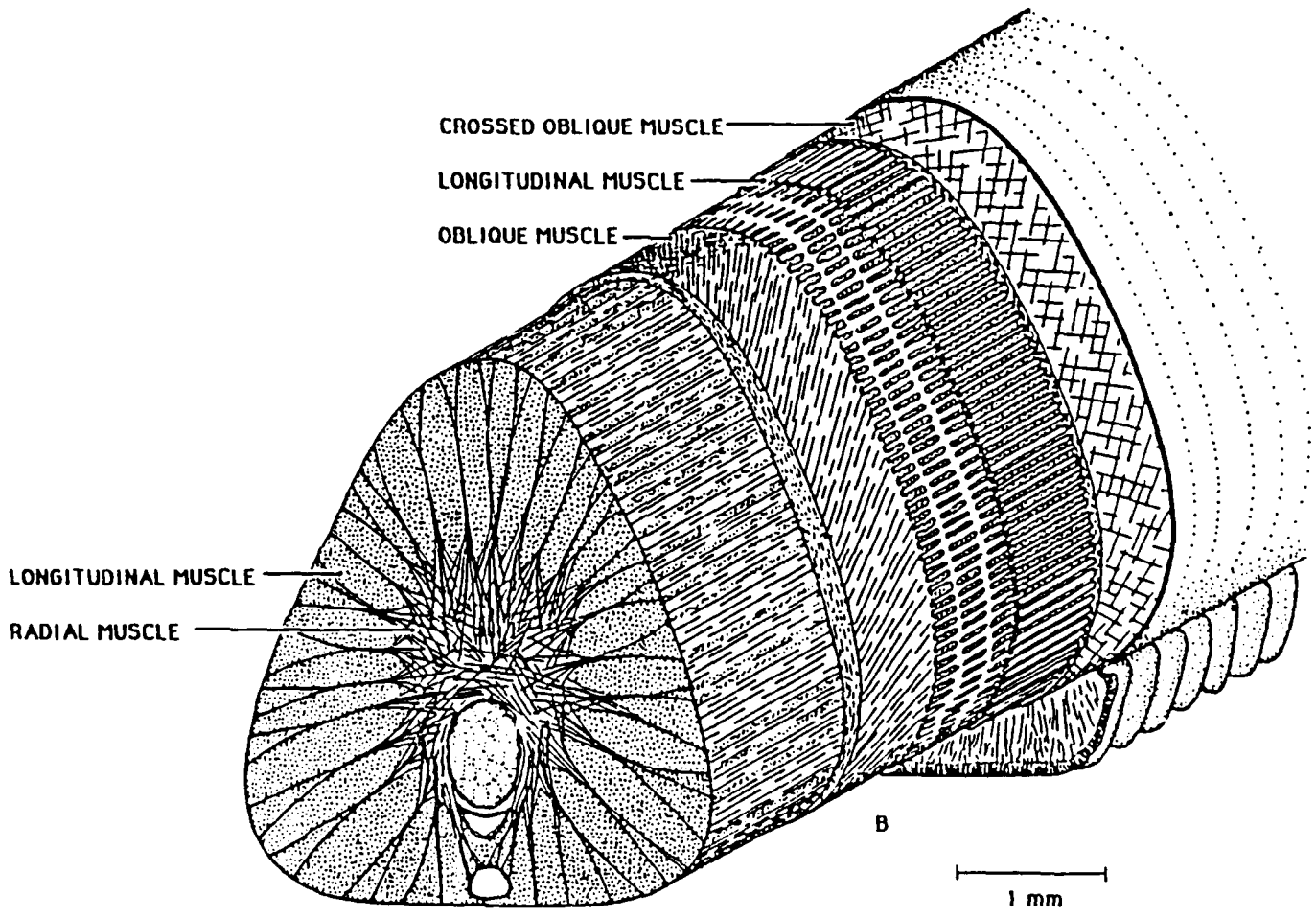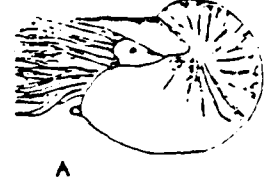
Figure 16. The chambered *Nautilus.* a) External view of whole animal.
Adapted from Barnes, 1980. b) Cut-away view of cirrus, showing
musculature. From Kier, 1983.

A

CIRCULAR MUSCLE

EXTERNAL LEFT-HANDED OBLIQUE MUSCLE

LONGITUDINAL MUSCLE

MEDIAL RIGHT-HANDED OBLIQUE MUSCLE

LONGITUDINAL MUSCLE

INTERNAL OBLIQUE MUSCLE

TRANSVERSE MUSCLE

B

|—————————|
1 mm
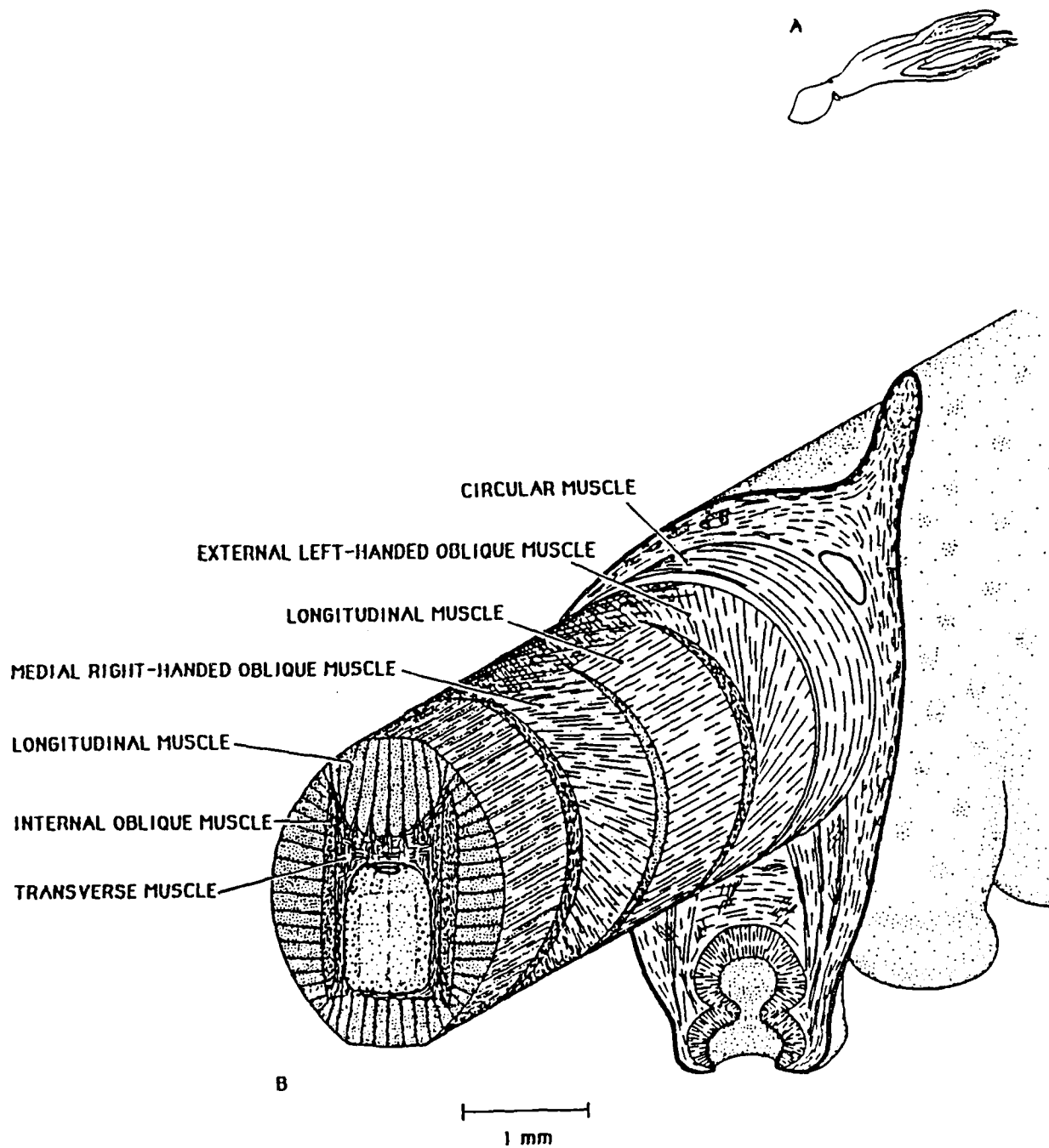
Figure 17. *Octopus*. a) External view of whole animal. b) Cut-away view
of arm, showing musculature. From Kier, 1983.

CLOSING THOUGHTS

In the analysis presented above, muscle has been considered in the conceptually simplest way possible--as tissue which shortens and thus exerts tension. Cross-sections of fourteen different deformable animal bodies, appendages, and tongues have been discussed in terms of several simple mechanical principles that must operate during motion of these structures.

Several questions about the mechanics of such structures remain unanswered. Is there, for example, a functional difference between radial, circular, and transverse muscle? In this chapter, these three types of muscle have been lumped into one category--musculature which is perpendicular to the longitudinal axis of a model cylinder. It is possible, however, that circular, radial, and transverse muscles differ in the amount of work, perpendicular to the long axis, they produce for a given contraction, and that the directions in which each of these muscles pull is functionally important.

To answer this question, detailed anatomical data is needed; at present, such data is lacking. For example, do single cells in circular muscle wrap all the way around a cylindrical muscular hydrostat in a circle, or do cells overlap so that no one cell goes all the way around although the muscle as a whole does? If the former, then, since the circumference varies directly with the radius of a circle, a 40% contraction of circular muscle cells would result in a 40 % decrease in the radius of the circle enclosed by the muscle; the area of the circle would vary with the square of the radius. If the latter, a 40% contraction would result in some smaller decrease in the circumference, the radius, and hence the cross-sectional area of the circle enclosed by the muscles. The same question arises when analysing the radial and transverse muscles, and it is evident that detailed anatomical studies must be performed, and generalizations and assumptions must be made.

To compare the radial and circular muscles of a right circular cylindrical muscular hydrostat, assume that circular muscle cells wrap completely around the circumference, radial muscle cells travel from the center to the edge of the circular cross-section, and the same number of cells of each type must contract to produce a given change in radius. Then, since the circumference of a circle varies directly with its radius, there is no difference between the decrease in cross-sectional area produced by a given contraction of the circular or radial muscles.

In addition, the change in area produced by a given contraction of radial or circular muscles will increase with the size of the circle

encompassed by the muscles. Therefore, circular muscles will produce a larger change in area if they are placed at the periphery of a cylindrical muscular hydrostat than they will if nearer the center, and radial muscles will produce a larger change in area if they stretch from the center to the periphery of the hydrostat than they will if they stretch only part way across the circular cross-section. In the animal structures presented in this chapter, circular muscles are always found near the periphery of the structures (Figures 7, 8, 9, 12, 13, 15, 17), and radial muscles send regular arrays of branches reaching as far to the periphery as possible (Figure 16).

Transverse muscle is a bit more difficult to analyze. Transverse muscle cells that pass near the center of the circular cross-section of a cylindrical muscular hydrostat probably act similarly to radial muscles. However, analysis of transverse muscle cells placed as chords across the cross-section nearer the periphery requires knowledge of anatomical detail which is not available. For example, the vertical and horizontal muscle bundles might act in perpendicular pairs to exert a diagonal force on the skin if both members of a pair are connected to the skin. It is difficult to compare the change in cross-sectional area produced by transverse muscles with that produced by radial and circular muscles without detailed anatomical information.

Another question of interest is whether the shape and arrangement of longitudinal muscle bundles is functionally significant. As shown in Figure 8D, the longitudinal muscles of the earthworm are arranged as many rows of oval bundles connected to connective tissue sheets which run longitudinally with the muscle. Many other animals have longitudinal muscle arranged seemingly randomly in dense arrays of parallel roughly cylindrical bundles. The significance of these arrangements has not been addressed in any literature of which I am aware.

How can the information presented in this chapter be used by designers of flexible robotic manipulators? To date, engineers involved in this project have designed inflatable plastic tubes whose walls are constructed so that the tubes bend, twist, elongate, or shorten when they are inflated. For example, an inextensible fiber oriented longitudinally in the wall will cause the tube to bend when inflated. Such tubes are not constant in volume, and they do not contain shortening elements; in these ways they are unlike muscular hydrostats. However, if one were to film a partially transparent muscular hydrostat as an opaque muscle bundle contracted, using a zoom lens so that the length of the muscle remained a constant in the field of view, the film would reveal something similar to an inflating tube with an inextensible fiber element. The muscle, filmed

so that it appears with a constant length, would play the part of the fiber element, and the rest of the structure, growing larger as the camera zooms to maintain the length of the muscle, would play the part of the inflating tube. In this way, inextensible fibers in the walls of inflatable plastic tubes play a similar role in the tubes to that played by muscles in muscular hydrostats. The orientation and placement of each determine the motion of the structure when the tube inflates or the muscle contracts. An insight to be gained from animal structure is that muscles (or inextensible fibers) in particular places and in particular orientations can result in particular motions when the structure (or tube) is activated. One can conceive of fabulous flexible tubes with fiber elements not only in the walls, but spanning the interior of the tubes, mimicking the muscular arrays and actions of animal structures.

Muscle can serve as an even richer source of ideas if the variety of muscle is considered. Although it is tempting to ignore this variety and conduct analyses with a generalized view of muscle contraction, the truth is that muscles are not the same from animal to animal and even from place to place within the same animal. Muscle contracts because an electrical impulse, usually via a nerve, sets into motion a sequence of events which activates the contractile elements in muscle. There is an infinite number of variations possible in this chain of events. Different patterns of nervous stimulation can give rise to muscle contractions which vary in strength and frequency. The manner in which an electrical impulse is conducted through a muscle cell can determine the time-course of a contraction. The arrangement of contractile elements in a muscle cell will determine the force and amount of contraction. The presence or absence of mitochondria in a muscle cell determines the source of energy for contraction, and thus affects characteristics of contraction. An engineer attempting to understand animal muscle structure would be well-advised to become familiar with these variations. Since it would require a small book to treat muscle variation even barely adequately, I refer the interested reader to McMahon (1984), Wilkie (1976), and Hoyle (1983). These authors treat the subject in detail, and their books may serve as sources of other relevant references. Consideration of the differences between muscles will lead to a more complete analysis of animal structures, and may aid in the choice of materials and method of control of robotic manipulators.

REFERENCES

Barnes, Robert D. (1980), *Invertebrate Zoology*, 4th edition, Saunders College/Holt, Rinehart, and Winston, Philadelphia.

Chapman, Garth (1958), The hydrostatic skeleton in the invertebrates, *Biological Reviews*, 33: 338-371.

Chapman, Garth (1975), Versatility of hydraulic systems, *Journal of Experimental Biology*, 194 #1: 249-270.

Clark, R.B. (1964), *Dynamics in Metazoan Evolution. The Origin of the Coelom and Segments*, Clarendon Press, Oxford.

Clark, R.B., and Clark, M.E. (1960), The ligamentary system and the segmental musculature of *Nephtys*, *Quarterly Journal of Microscopical Society*, 101, pt. 2: 149-176.

Doran, G.A., and Allbrook, D.B. (1973), The tongue and associated structures in two species of African pangolin, *Manis gigantea* and *Manis tricuspis*, *Journal of Mammalogy*, 54: 887-899.

Doran, G.A., and Baggett, H. (1971), A structural and functional classification of mammalian tongues, *Journal of Mammalogy*, 52: 427-429.

Eakin, Richard M., and Brandenburger, Jean L. (1974), Ultrastructural features of a gordian worm (Nematomorpha), *Journal of Ultrastructure Research*, 46: 351-374.

Freeman, W.H., and Bracegirdle, Brian (1971), *An Atlas of Invertebrate Structure*, Heinemann Educational Books Ltd., London.

Harris, J.E., and Crofton, H.D. (1957), Structure and function in the Nematodes: internal pressure and cuticular structure in *Ascaris*, *Journal of Experimental Biology*, 34 #1: 116-130.

Hoyle, Graham (1983), *Muscles and Their Neural Control*, John Wiley and Sons, Inc.

Kier, William M. (1983), *The Functional Morphology of the Musculature of the Arms and Tentacles of Cephalopods*, Unpublished, Ph.D. dissertation, Duke University, Durham, North Carolina.

Kier, William M., and Smith, Kathleen K. (1985), Tongues, tentacles, and trunks: the biomechanics of movement in muscular hydrostats, *Zoological Journal of the Linnaean Society*, 83: 307-324.

Kingdon, Jonathan (1971), *East African Mammals. An Atlas of Evolution in Africa. Volume I*, Academic Press, New York and London.

Lanzavecchia, G., and Arcidiacono, G. (1981), Contraction mechanisms of helical muscles: Experimental and theoretical analysis, *Journal of Submicroscopic Cytology,* 13:253-266.

McMahon, Thomas A. (1984), *Muscles, Reflexes, and Locomotion,* Princeton University Press, Princeton, New Jersey.

Morris, Robert H., Abbot, Donald P., and Haderlie, Eugene C. (1980), *Intertidal Invertebrates of California,* Stanford University Press, Stanford, California.

Rice, M.J. (1973), Supercontracting striated muscle in a vertebrate, *Nature, London,* 243: 238-240.

Riedl, Rupert (1983), *Fauna und Flora des Mittelmeeres,* Verlag Paul Parey, Hamburg and Berlin.

Russel-Hunter, W.D. (1979), *A Life of Invertebrates,* MacMillan Publishing Co., New York.

Sherman, Irwin W., and Sherman, Vilia G. (1976), *The Invertebrates: Function and Form. A Laboratory Guide,* 2nd edition, MacMillan Publishing Co., New York.

Smith, Kathleen K. (1984), The use of the tongue and hyoid apparatus during feeding in lizards (*Ctenosaura similis* and *Tupinambis nigropunctatus*), *Journal of Zoology, London,* 202: 115-143.

Wainwright, Stephen A. (1982), Structural systems: hydrostats and frameworks, in *A Companion to Animal Physiology,* ed. Taylor, Johansen, and Bolis, pp. 325-338.

Wainwright, Stephen A., Biggs, W.D., Currey, J.D., and Gosline, J.M. (1976), *Mechanical Design in Organisms,* Edward Arnold (Publishers) Ltd., London.

Wilkie, D.R. (1976), *Muscle,* 2nd edition, Edward Arnold (Publishers) Ltd., London.

Chapter II

FINITE DEFORMATIONS OF NONLINEAR,

ORTHOTROPIC CYLINDRICAL SHELLS

Gary Orgill and James F. Wilson

INTRODUCTION

The behavior of cylindrical shells under a variety of loading
combinations and boundary conditions has been the subject of intense study.
The literature is replete with classical and numerical solutions involving
stress, deformation and buckling mechanisms. Most of the work to date,
however, involves isotropic, linear, elastic materials where deformations are
assumed to be small. Wilson and Orgill (1985) presented numerical results for
small deformations of an orthotropic thin-wall right cylinder made of a
linear, elastic material. Verma and Rana (1983) investigated displacements of
a rotating concrete cylinder with steel reinforcing rods wound around the
cylinder as helices. Reissner (1970) calculated the general expressions for
stress and strain in anisotropic, thin walled cylinders and Lekhnitskii (1963)
solved several problems involving linear elastic orthotropic solids. However,
the work involving finite deformations of cylindrical shells, even for linear
elastic isotropic materials, is sparse. The classical text of Green and
Adkins (1970), discusses finite deformation analysis for shells from a general
viewpoint. Leonard (1967) solved the particular problem of large deformations
resulting from inflating a flexible isotropic shell of revolution. Presently
there are several commercial computer codes employing numerical techniques to
solve finite deformation, cylindrical shell problems.

As the use of rubber and other polymeric materials become increasingly
popular in structural design, an analysis is needed that accounts for both

geometric nonlinearities arising from finite deformations and material nonlinearities. In applications using such materials, it may be desirable to incorporate helical reinforcement in the cylindrical shell or to model helical corrugations as orthotropy of a continuum. A procedure that accounts for such material and geometric nonlinearities, as well as material orthotropy along parallel helices oriented at a constant angle to the cylinder's longitudinal axis, is developed herein. See Fig. 1. Parametric studies show how the selection of the orthotropic properties will affect the deformation patterns and how proper selection of such properties can result in an optimal deformation or load-carrying capacity. First, the problem of axially homogeneous stress and strain is considered. These results are then extended to include non-axially homogeneous stress and strain that arise due to end constraints. The assumption is made throughout this study that the stress and strain in the circumferential direction are homogeneous and that the cylinder maintains a circular cross-section as it deforms. Buckling loads and post-buckling behavior are not considered.

The loadings on the cylinder are internal pressure, an end load applied along the longitudinal axis of the cylinder, and a pure torque about the longitudinal axis of the cylinder, applied separately or in combination. An incremental analysis technique is used in which small increments of load are applied to the cylinder at each step and the incremental strain is computed by assuming linearity over that small range. The change in section properties such as wall thickness and radius are computed from the strain increments at each step, thus accounting for the geometric nonlinearities. In addition the material properties, assumed to be known functions of strain, are updated as well. After each increment of load is applied, the section properties and material properties are recomputed. The procedure continues in this fashion until the desired load level is attained.
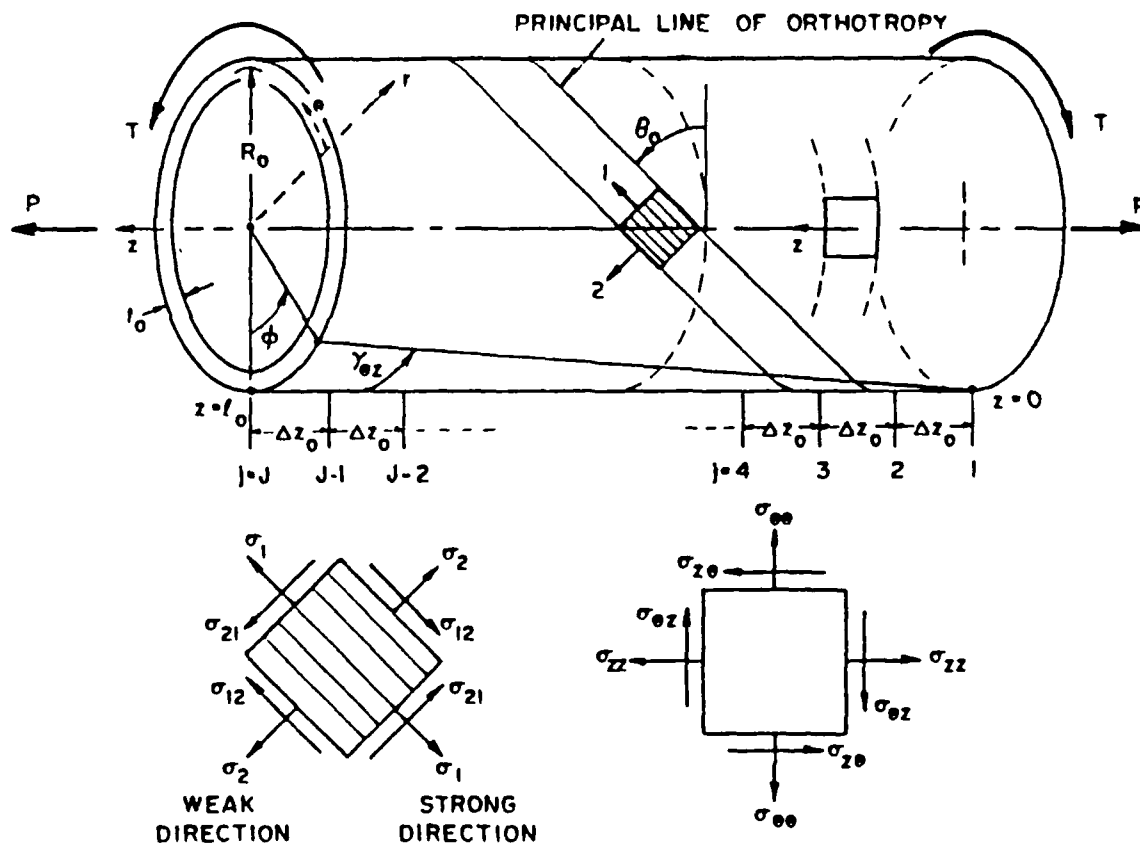
Fig. 1   Cylinder geometry, coordinates, and loading

PART I - AXIALLY HOMOGENEOUS STRESSES AND STRAINS

Incremental Stresses

The stresses and strains are assumed to be axially homogeneous, which is possible if both ends of the cylinder are capped with flexible membranes. For increments of internal pressure Δp, end load ΔP, and torque ΔT, the incremental stresses at load step n are derived from elementary theory. These are:

$$\Delta\sigma_{\theta\theta n} = \frac{\Delta p\ R_i}{t_i} \tag{1}$$

$$\Delta\sigma_{zzn} = \frac{\Delta p\ R_i}{2t_i} + \frac{\Delta P}{2\pi\ R_i\ t_i} \tag{2}$$

$$\Delta\sigma_{rrn} = 0 \tag{3}$$

$$\Delta\sigma_{\theta zn} = \frac{\Delta T}{2\pi R_i^2\ t_i} = \frac{\Delta T}{Z_i} \tag{4}$$

where $n = i + 1 = 1, 2, 3,\ldots$

Here Z_i is the polar section modulus, and R_i and t_i are respectively the mean radius and thickness of the cylinder at load step n. The radial stress $\Delta\sigma_{rrn}$ is vanishingly small, consistent with the thin wall assumption.

Constitutive Relationships and Strain Transformations

Consider the thin-walled right circular cylinder of Fig. 1, with the orthotropy defined by the constant helix angle θ_i. The initial condition $i = 0$ is the no load condition. At load step $n = i + 1$, the incremental strain vector $\Delta\varepsilon_n$ is related linearly to the incremental stress vector $\Delta\sigma_n$ through the 4x4 coefficient matrix A_i, assuming sufficiently small load increments. That is:

$$\Delta\varepsilon_n = A_i\ \Delta\sigma_n \qquad (i = n-1 = 0,1,2,\ldots) \tag{5}$$

where

$$\Delta \underset{\sim}{\epsilon}_n^T = [\Delta\epsilon_{\theta\theta} \quad \Delta\epsilon_{zz} \quad \Delta\epsilon_{rr} \quad \Delta\gamma_{\theta z}]_n \qquad (6)$$

$$\Delta \underset{\sim}{\sigma}_n^T = [\Delta\epsilon_{\theta\theta} \quad \Delta\sigma_{zz} \quad 0 \quad \Delta\sigma_{\theta z}]_n \qquad (7)$$

and T denotes transpose.

The general classical constitutive equations for $\underset{\sim}{A}_i$ as discussed by Lekhnitskii (1963) were reduced for the present problem by Wilson and Orgill (1985). The components of $\underset{\sim}{A}_i$ are as follows, where the subscripts denote, respectively, the row position, the column position and the load step.

$$a_{11_i} = \frac{\cos^4\theta_i}{E_i} + \left(\frac{1}{G_i} - \frac{2\nu}{E_i}\right)\sin^2\theta_i \,\cos^2\theta_i + \frac{\sin^4}{E_i'}\theta_i \qquad (8a)$$

$$a_{22_i} = \frac{\sin^4\theta_i}{E_i} + \left(\frac{1}{G_i} - \frac{2\nu}{E_i}\right)\sin^2\theta_i \,\cos^2\theta_i + \frac{\cos^4\theta_i}{E_i'} \qquad (8b)$$

$$a_{33_i} = \frac{1}{E_i} \qquad (8c)$$

$$a_{12_i} = a_{21_i} = \left(\frac{1}{E_i} + \frac{1}{E_i'} + \frac{2\nu}{E_i} - \frac{1}{G_i}\right)\cos^2\theta_i \,\sin^2\theta_i - \frac{\nu}{E_i} \qquad (8d)$$

$$a_{23_i} = a_{32_i} = a_{13_i} = a_{31_i} = -\frac{\nu}{E_i} \qquad (8e)$$

$$a_{44_i} = \left(\frac{4}{E_i} + \frac{4}{E_i'} + \frac{8\nu}{E_i} - \frac{4}{G_i}\right)\sin^2\theta_i \,\cos^2\theta_i + \frac{1}{G_i} \qquad (8f)$$

$$a_{14_i} = a_{41_i} = \left[-\frac{2}{E_i'}\sin^2\theta_i + \frac{2}{E_i}\cos^2\theta_i - \left(\frac{1}{G_i} - \frac{2\nu}{e_i}\right)(\cos^2\theta_i - \sin^2\theta_i)\right].$$

$$\cdot \sin\theta_i \, \cos\theta_i \qquad (8g)$$

$$a_{24_i} = a_{42_i} = \left[-\frac{2}{E_i'}\cos^2\theta_i + \frac{2}{E_i}\sin^2\theta_i + \left(\frac{1}{G_i} - \frac{2}{E_i}\right)(\cos^2\theta_i - \sin^2\theta_i)\right].$$

$$\cdot \sin\theta_i \, \cos\theta_i \qquad (8h)$$

$$a_{34_i} = a_{43_i} = 0 \qquad (8i)$$

In Equations (8), E_i and E_i' are the tangent moduli measured in simple tensile tests and correspond to the slopes of the stress-strain curves for principal strains ε_{11i} and ε_{22i} in the 1 and 2 directions, respectively. Similarly, G_i is the tangent modulus for a simple shear test at the principal shear strain γ_{12i}. Poisson's ratio ν is taken as invarient with respect to strain levels ε_{11i} and ε_{22i} as observed experimentally for rubber by Goodyear (1949). As shown later, the angle of orthotropy θ_i changes with load increment.

The uniaxial stress-strain behavior with respect to the principle directions of orthotropy is assumed in the following form:

$$\sigma_{11} = E_o \, \varepsilon_{11} + B \, \varepsilon_{11}^3 + C \, \varepsilon_{11}^5 \qquad (9)$$

$$\sigma_{22} = E_0' \, \varepsilon_{22} + B' \, \varepsilon_{22}^3 + C' \, \varepsilon_{22}^5 \qquad (10)$$

and the behavior in simple shear with respect to these principal directions is of the same form, or

$$\sigma_{12} = G_0' \, \gamma_{12} + B_g \, \gamma_{12}^3 + C_g \, \gamma_{12}^5 \qquad (11)$$

where the coefficients of the strain are measured constants. The tangent moduli with respect to the strains at level i in this 1-2 coordinate system, found by differentiating Equations (9)-(11), are:

$$E_i = E_o + 3B \, \varepsilon_{11i}^2 + 5C \, \varepsilon_{11i}^4 \qquad (12)$$

$$E_i' = E_o' + 3B' \, \varepsilon_{22i}^2 + 5C' \, \varepsilon_{22i}^4 \qquad (13)$$

$$G_i = G_0' + 3B_g \, \gamma_{12i}^2 + 5C_g \, \gamma_{12i}^4 \qquad (14)$$

These tangent moduli are used to compute the elements of $\underset{\sim}{A}_i$ given by Equations (8) for orientation θ_i.

The principal strains of Equations (12)-(14) are related to the strains at load level i in the cylindrical system through the well-known

transformation equations (Popov, 1981) given by:

$$2\epsilon_{11i} = \epsilon_{\theta\theta i} + \epsilon_{zzi} + (\epsilon_{\theta\theta i} - \epsilon_{zzi})\cos2\theta_i + \gamma_{\theta zi}\sin2\theta_i \qquad (15a)$$

$$2\epsilon_{22i} = \epsilon_{\theta\theta i} + \epsilon_{zzi} + (\epsilon_{zzi} - \epsilon_{\theta\theta i})\cos2\theta_i - \gamma_{\theta zi}\sin2\theta_i \qquad (15b)$$

$$\gamma_{12i} = (\epsilon_{zzi} + \epsilon_{\theta\theta i})\sin2\theta_i + \gamma_{\theta zi}\cos2\theta_i \qquad (15c)$$

Geometric Nonlinearities

If the initial wall thickness is t_0, then after the first load increment is applied there will be a corresponding incremental radial strain $\Delta\epsilon_{rr1}$. The updated wall thickness after the first load increment

$$t_1 = t_0(1 + \Delta\epsilon_{rr1}) \qquad (16)$$

Similarly, after the second load increment, the updated wall thickness is:

$$t_2 = t_1(1 + \Delta\epsilon_{rr2}) \qquad (17)$$

Between two successive load increments, it follows that the updated wall thickness is:

$$t_i = t_{i-1}(1 + \Delta\epsilon_{rri}) \qquad (18)$$

In terms of the initial wall thickness t_0, Equation (18) becomes:

$$t_i = t_0 \prod_{k=1}^{i} (1 + \Delta\epsilon_{rrk}) \equiv t_0 F_{ti} \qquad (19)$$

The factor F_{ti} represents the deviation of t_i from t_0 after load step i. The closer F_{ti} is to unity, the less the solution is affected by geometric nonlinearity.

A similar argument is made for changes in the mean radius. Equation (18), rewritten in terms of the mean radius and the incremental circumferential strain, is

$$R_i = R_{i-1}(1 + \Delta\epsilon_{\theta\theta i}) \qquad (20)$$

Likewise, R_i can be expressed in terms of R_0, the mean radius of the cylinder under zero load, or

$$R_i = R_0 \prod_{k=1}^{i} (1 + \Delta\varepsilon_{\theta\theta k}) \equiv R_0 F_{ri} \tag{21}$$

Here, F_{ri} represents the deviation of R_i from R_0 after load step i.

Based on the cross-sectional area of a thin ring given by $A_i = 2\pi R_i t_i$, the updated expressions for the area become:

$$A_i = A_{i-1} (1 + \Delta\varepsilon_{\theta\theta i})(1 + \Delta\varepsilon_{rri}) \tag{22}$$

$$A_i = 2\pi R_0 t_0 \prod_{k=1}^{i} (1 + \Delta\varepsilon_{\theta\theta k})(1 + \Delta\varepsilon_{rrk}) \equiv 2\pi R_0 t_0 F_{ai} \tag{23}$$

Likewise, the updated values of the polar section modulus, initially given by $Z_0 = 2\pi R_0^2 t_0$, are:

$$Z_i = Z_{i-1}(1 + \Delta\varepsilon_{\theta\theta i})^2(1 + \Delta\varepsilon_{rri}) \tag{24}$$

$$Z_i = 2\pi R_0^2 t_0 \prod_{k=1}^{i} (1 + \Delta\varepsilon_{\theta\theta k})^2(1 + \Delta\varepsilon_{rrk}) \equiv 2\pi R_0^2 t_0 F_{pi} \tag{25}$$

The corresponding expressions for changes in length of the cylinder are:

$$\ell_i = \ell_{i-1}(1 + \Delta\varepsilon_{zzi}) \tag{26}$$

$$\ell_i = \ell_0 \prod_{k=1}^{i} (1 + \Delta\varepsilon_{zzi}) \equiv \ell_0 F_{zi} \tag{27}$$

Computation of Strains

The total strains are needed in order to update values of the material properties E_i, E_i', and G_i and to compute cylinder displacements. Expressions for these strains are now deduced. Consider the relationship between the wall thicknesses t_1 and t_0 given in Equation (16). The total radial strain after the first load increment is:

$$\varepsilon_{rr1} = \frac{t_1 - t_0}{t_0} = \frac{t_0(1 + \Delta\varepsilon_{rr1})}{t_0} = \Delta\varepsilon_{rr1} \tag{28}$$

and after the second load increment is:

$$\epsilon_{rr2} = \frac{t_2 - t_o}{t_o} = \frac{t_o(1 + \Delta\epsilon_{rr1})(1 + \Delta\epsilon_{rr2}) - t_o}{t_o} = (1 + \Delta\epsilon_{rr1})(1 + \Delta\epsilon_{rr2}) - 1 \tag{29}$$

After i increments of load it follows that

$$\epsilon_{rri} = \frac{t_o \prod_{k=1}^{i} (1 + \Delta\epsilon_{rrk}) - t_o}{t_o} = F_{ti} - 1 \tag{30}$$

The total strains in the circumferential and longitudinal directions, obtained in a similar manner, are given by:

$$\epsilon_{\theta\theta i} = F_{ri} - 1 \tag{31}$$

$$\epsilon_{zzi} = F_{zi} - 1 \tag{32}$$

The total shearing strain $\gamma_{\theta zi}$ is simply the sum of the incremental shear strains, as there are no length changes involved. After i increments of load, this is

$$\gamma_{\theta zi} = \sum_{k=1}^{i} \Delta\gamma_{\theta zk} \tag{33}$$

The end rotation ϕ_i of the cylinder may be expressed in terms of shear strain. For the first and second load increments, the respective rotations are

$$\phi_1 = \Delta\phi_1 = \frac{\ell_o}{R_o} \Delta\gamma_{\theta z1} \tag{34}$$

$$\Delta\phi_2 = \frac{\ell_1}{R_1} \Delta\gamma_{\theta z2} \tag{35}$$

The total rotation after two increments of load is the sum of Equations (34) and (35), or

$$\phi_2 = \frac{\ell_o}{R_o} \Delta\gamma_{\theta z1} + \frac{\ell_1}{R_1} \Delta\gamma_{\theta z2} = \frac{\ell_o}{R_o} \left(\Delta\gamma_{\theta z1} + \frac{(1 + \Delta\epsilon_{zz1})}{(1 + \Delta\epsilon_{\theta\theta 1})} \Delta\gamma_{\theta z2} \right) \tag{36}$$

Extending Equation (36) to i increments of load leads to:

$$\phi_i = \frac{\ell_0}{R_0} \left(\sum_{k=1}^{i} \Delta\gamma_{\theta zk} \prod_{m=1}^{i-1} \left(\frac{1 + \Delta\epsilon_{zzm}}{1 + \Delta\epsilon_{\theta\theta m}} \right) \right) = \frac{\ell_0}{R_0} \cdot \frac{F_{z(i-1)}}{F_{r(i-1)}} \sum_{k=1}^{i} \Delta\gamma_{\theta zk} \tag{37}$$

Deformations for Single-Turn Orthotropy

Consider the segment of an unloaded cylinder with radius R_0 and length ℓ_0'. The length is selected such that a line parallel with the principal direction of orthotropy makes exactly one turn about the cylinder as shown in Fig. 2. This condition is expressed as:

$$\ell_0' = 2\pi R_0 \tan \theta_0 \tag{38}$$

After the first load increment, ℓ_0', R_0 and θ_0 change. The resulting change in geometry is given by Equations (20), (26), (34) and (38), or

$$\ell_1' = (2\pi + \phi_1) R_1 \tan \theta_1 = \ell_0' (1 + \Delta\epsilon_{zz1}) = (2\pi + \frac{\ell_0'}{R_0'} \Delta\gamma_{\theta z1}) R_0 (1 + \Delta\epsilon_{\theta\theta 1}) \tan\theta_1 \tag{39}$$

It follows that the length for steps $i-1$ and i are given as:

$$\ell_{i-1}' = (2\pi + \phi_{i-1}) R_{i-1} \tan \theta_{i-1} \tag{40}$$

$$\ell_i' = (2\pi + \phi_i) R_i \tan \theta_i = (2\pi + \phi_{i-1} + \frac{\ell_{i-1}}{R_{i-1}} \Delta\gamma_{\theta zi}) R_i \tan \theta_i \tag{41}$$

Using Equations (40) and (41), a recursion relationship to compute θ_i is deduced as:

$$\theta_i = \tan^{-1} \left(\frac{1 + \Delta\epsilon_{zzi}}{1 + \Delta\epsilon_{\theta\theta i}} \cdot \frac{1}{\cot \theta_{i-1} + \Delta\gamma_{\theta zi}} \right) \tag{42}$$

Increment Selection and Convergence

The selection of the appropriate load increment will depend on the initial angle θ_0, the ratio of the elastic moduli E_i/E_i' and E_i/G_i, the magnitude of the load, and the type of loading. As the load increment is
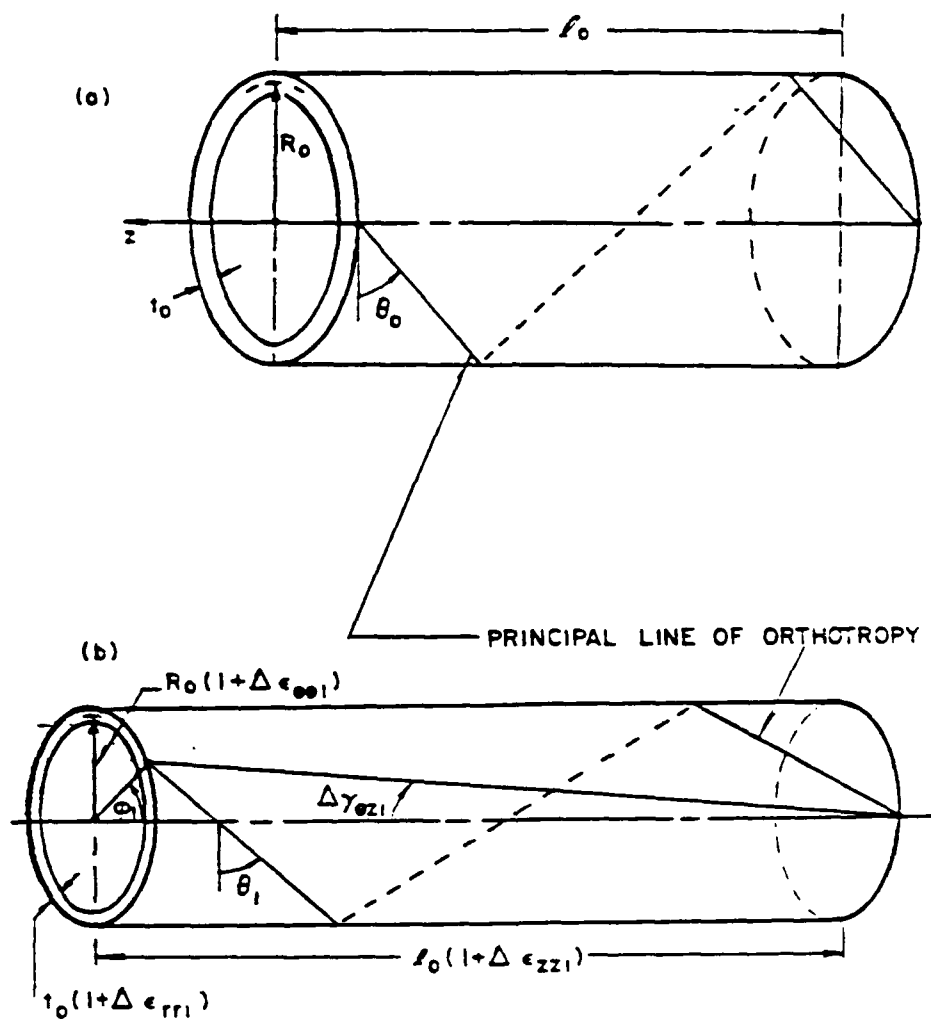
Fig. 2   Cylinder with a single turn helix: before loading (a), and after one load step (b)

increased, the computational effort is decreased, but the solution error is increased. The solution error after loading step i is defined as

$$\% \text{ Error} = \frac{100||\underset{\sim}{\varepsilon}_i - \underset{\sim}{\varepsilon}^*||_2}{||\underset{\sim}{\varepsilon}^*||_2} \tag{43}$$

where $\underset{\sim}{\varepsilon}_i$ is the total strain vector with components $\varepsilon_{\theta\theta i}$, ε_{zzi}, ε_{rri} and $\gamma_{\theta zi}$. The vector $\underset{\sim}{\varepsilon}^*$ is the exact total strain vector for the corresponding loading level containing the four strain components. The percent error is the Euclidean norm of the residual vector divided by the Euclidean norm of the exact solution. The exact solution is obtained by choosing increasingly smaller loading increments until the solution converges.

Typical results of such studies are shown in Table 1 which gives values of load increments that can be used over the range of angle $0 < \theta_0 < 90$ deg. These load increments were selected so that the percent error as defined never exceeds 5% if the values of the total nondimensional load parameters do not exceed their listed values. The maximum internal pressure, applied torque and longitudinal load are p, T and P, respectively. The material is linear for these cases, where the only nonzero constants of Equations (12)-(14) are E_0, E'_0 and G'_0.

PART II NON-AXIALLY HOMOGENEOUS STRESSES AND STRAINS

Certain edge constraints give rise to nonuniform stresses and strains in the loaded orthotropic cylinder. To account for such nonhomogenity along the length, the cylinder is divided into J-1 segments each of length Δz_0 given by

$$\Delta z_0 = \frac{\ell_0}{J-1} \tag{44}$$

The incremental and total stresses and strains are computed at each point

Table 1. Load Increments Required for a Solution Error of Less than 5% (Linear Material)

Maximum value of Load Parameter	E_i/E_i'	E_i/G_i	Increment in Load Parameter
$\dfrac{p\,R_o}{E_o t_o} = 0.08$	10	3	0.001
$= 0.01$	50	3	0.001
$\dfrac{T}{E_o t_o R_o^2} = 0.07$	10	3	0.005
$= 0.25$	50	3	0.002
$\dfrac{P}{E_o t_o R_o} = 0.40$	10	3	0.001
$= 0.16$	50	3	0.001

j=1,2,...J as shown in Fig. 1. The boundary conditions are incorporated when the strains are integrated numerically for the deformations. The computational procedure follows closely that of the axially homogeneous case of Part I. However, quantities such as $\Delta\epsilon_{\theta\theta i}$, F_{ti}, etc., are now vector quantities of dimension J with components $\Delta\epsilon_{\theta\theta ij}$, F_{tij}, etc. The added index j denotes the length from the coordinate origin as shown in Fig. 1.

Incremental Stresses

The equation of equilibrium for an element of a thin-wall shell of revolution at location j and after loading step i, deduced by Timoshenko and Woinowsky-Kreiger (1959), is

$$\frac{\sigma_{\theta\theta ij}}{R_{ij}} + \frac{\sigma_{\psi\psi ij}}{\rho_{ij}} = \frac{p_i}{t_{ij}} \tag{45}$$

Here $\sigma_{\psi\psi ij}$ is the meridional stress in the shell, ρ_{ij} is the radius of curvature in the meridional direction, $\sigma_{\theta\theta ij}$ is the circumferential stress in the shell, R_{ij} is the shell radius, p_i is the total internal pressure, and t_{ij} is the wall thickness. If the load increment is sufficiently small, Equation (45) can be rewritten in terms of the section properties of the previous step, or

$$\frac{\sigma_{\theta\theta ij}}{R_{(i-1)j}} + \frac{\sigma_{\psi\psi ij}}{\rho_{(i-1)j}} \approx \frac{p_i}{t_{(i-1)j}} \tag{46}$$

The meridional stress (Timoshenko and Woinkowski-Kreiger, 1959) is

$$\sigma_{\psi\psi ij} = \frac{p_i \pi R^2_{(i-1)j}}{2\pi R_{(i-1)j} t_{(i-1)j}} = \frac{p_i R_{(i-1)j}}{2t_{(i-1)j}} \tag{47}$$

By combining Equations (46) and (47), the circumferential stress becomes

$$\sigma_{\theta\theta ij} = \frac{p_i R_{(i-1)j}}{t_{i-1}} (1 - \frac{R_{(i-1)j}}{2\rho_{(i-1)j}}) \tag{48}$$

Expressions for the incremental stresses for load step i-1 follow from
Equations (47) and (48), or

$$\Delta\sigma_{\psi\psi ij} = \frac{\Delta p \; R_{(i-1)j}}{2t_{(i-1)j}} \tag{49}$$

$$\Delta\sigma_{\theta\theta ij} = \frac{\Delta p \; R_{(i-1)j}}{t_{(i-1)j}} \left(1 - \frac{R_{(i-1)j}}{2\rho_{(i-1)j}}\right) \tag{50}$$

Equations (49) and (50) are similar to the internal pressure components of
stress given for the axially homogeneous case in Equations (1) and (2). Note
that for the homogeneous stress case, $\rho_{(i-1)j} \to \infty$ and $\sigma_{\psi\psi ij} = \sigma_{\theta\theta ij}/2$.

To compute strains and deformations in the cylindrical coordinate system,
it is necessary to transform $\sigma_{\psi\psi ij}$ to that coordinate system. Using the
stress-transformation equations (Popov, 1981) yields

$$\sigma_{zz ij} = \sigma_{\psi\psi ij} \left[\frac{1}{2} - \frac{\cos 2\alpha_{(i-1)j}}{2}\right] \tag{51}$$

where $\alpha_{(i-1)j}$, the angle that the wall of the cylinder makes with the
longitudinal axis, is defined as the gradient of the radial deformation, or

$$\tan \alpha_{(i-1)j} = \frac{\partial u_{r(i-1)j}}{\partial z} \tag{52}$$

In employing the stress transformation of Equation (51), it is assumed that
alpha is sufficiently small so that the radial stresses in the cylindrical
coordinate system are small, contributing a negligible amount to the cylinder
deformation.

While the discussion in this section has dealt only with stress and
deformation due to internal pressure, results can be developed analogously for
end load and pure torque, as well as for various combinations of these three
types of loads.

Constitutive Relationships, Material and Geometric Nonlinearity

The incremental constitutive law given by Equations (5)-(8), along with the material nonlinearity of Equations (12)-(14) and the transformations of Equations (15), are assumed to be valid not only at each load step i but also at each length location j. With this notation, Equations (5)-(8) become

$$
\begin{bmatrix} \Delta\varepsilon_{\theta\theta nj} \\[1em] \Delta\varepsilon_{zznj} \\[1em] \Delta\varepsilon_{rrnj} \\[1em] \Delta\varepsilon_{\theta znj} \end{bmatrix} = \begin{bmatrix} a_{11ij} & a_{12ij} & a_{13ij} & a_{14ij} \\[1em] a_{21ij} & a_{22ij} & a_{23ij} & a_{24ij} \\[1em] a_{31ij} & a_{32ij} & a_{33ij} & a_{34ij} \\[1em] a_{41ij} & a_{42ij} & a_{43ij} & a_{44ij} \end{bmatrix} \begin{bmatrix} \Delta\sigma_{\theta\theta nj} \\[1em] \Delta\sigma_{zznj} \\[1em] \Delta\sigma_{rrnj} \\[1em] \Delta\sigma_{\theta znj} \end{bmatrix}
\tag{53}
$$

$$n = i + 1 = 1,2,3,\ldots$$
$$j = 1,2,3,\ldots J$$

Note the components of the coefficient matrix of Equation (53) are still given by Equations (8) where each parameter with the subscript i now has the added subscript j. In Equations (12)-(15), the single subscript i is also replaced by ij.

The geometric properties, except for length change, are deduced from Equations (19), (21), (23) and (25), i being replaced by ij. The change in length along the longitudinal axis for a segment bounded by points j and j+1 is given by

$$\Delta z_{ij} = \Delta z_0 + u_{zi(j+1)} - u_{zij} \equiv \Delta z_0\, F_{zij} \tag{54}$$

where Δz_0 is given by Equation (44) and where $u_{zi(j+1)}$ amd u_{zij} are the total displacements measured relative to the initial points j and j+1 when the cylinder is without load (i=0).

Computation of Strain, Rotation and Orthotropy Angle

The total strains can be computed either from the incremental strains or from the displacements. The radial, circumferential and shear strain at load level i and position j, expressed as ϵ_{rrij}, $\epsilon_{\theta\theta ij}$, and $\gamma_{\theta zij}$ respectively, are given explicitly by Equations (30), (31) and (33), where ij replaces i.

An efficient method for calculating ϵ_{zzij}, the longitudinal strain, is by the finite difference method used by Utku (1981). If u_{zij} denotes a segment displacement, then

$$\epsilon_{zzij} = \frac{u_{zi(j+1)} - u_{zi(j-1)}}{\Delta z_{i(j-1)} + \Delta z_{ij}} \qquad (55)$$

The average longitudinal strain for the whole cylinder of initial length ℓ_0 is

$$\bar{\epsilon}_{zzij} = \frac{1}{\ell_0} (u_{ziJ} - u_{zi1}) \qquad (56)$$

where J-1 is the number of length segments.

Tne end rotation φ_{ij} of the cylinder segment between locations j and j+1 can be computed from Equation (37), after the subscript j is added where appropriate; or from tne expression involving the incremental circumferential displacement $\Delta u_{\theta ij}$ given by

$$\phi_{ij} = \phi_{(i-1)j} + \frac{\Delta u_{\theta ij}}{R_{(i-1)j}} \qquad (57)$$

The angle of orthotropy θ_{ij} in each of the J-1 longitudinal segments is given by Equation (42) where each subscript i or (i-1) is replaced by ij or (i-1)j, respectively.

Computation of Displacements and Curvature

The computation of displacements u_r, u_z and u_θ in the case of axially nomogeneous strain is a straightforward application of the strain-displacement equations (Wilson and Orgill, 1985). However, when the strains are axially

nonhomogeneous, displacements are more difficult to compute and in general
must be obtained numerically. The results that follow will be based on the
finite difference method discussed by Utku (1981) and Carnahan, et al (1964).

From the strain-displacement equations given by Sokolnikoff (1956), the
incremental radial displacement becomes

$$\Delta u_{rij} = R_{(i-1)j}\ \Delta\epsilon_{\theta\theta ij} \tag{58}$$

The incremental displacement is then added to the total displacement from the
previous load step to obtain the total radial displacement at step i for
segment j, or

$$u_{rij} = u_{r(i-1)j} + \Delta u_{rij} \tag{59}$$

Computation of the incremental longitudinal displacement is obtained from
the strain-displacement equations by integrating the incremental longitudinal
strain given by

$$\Delta u_{zi(j+1)} - \Delta u_{zi(j-1)} = [\Delta z_{(i-1)j} + \Delta z_{(i-1)(j-1)}]\ \Delta\epsilon_{zzij} \tag{60}$$

As j varies from 1 to J in Equation (60), a tridiagonal system of linear
equations is found. These equations are solved simultaneously for the
incremental displacements Δu_{zij}. The total longitudinal displacement at step
i is once again computed by adding the incremental displacement to the total
longitudinal displacement at the previous step.

$$u_{zij} = u_{z(i-1)j} + \Delta u_{zij} \tag{61}$$

The computation of the circumferential displacement is obtained from the
strain-displacement equations by integrating the incremental shear strain.
The integration results in expressions similar to Equations (60) and (61) for
the longitudinal displacement. The incremental circumferential displacement
and total circumferential displacement are, respectively:

$$\Delta u_{\theta i(j+1)} - \Delta u_{\theta i(j-1)} = [\Delta z_{(i-1)j} + \Delta z_{(i-1)(j-1)}]\ \Delta\gamma_{\theta z ij} \tag{62}$$

$$u_{\theta ij} = u_{\theta(i-1)j} + \Delta u_{\theta ij} \tag{63}$$

With these displacements it is possible to compute α_{ij}, the angle between the meridional direction and the longitudinal axis of the cylinder; and ρ_{ij}, the radius of curvature in the meridional direction. The angle α_{ij} is used in transforming stress from the meridional direction to the longitudinal direction as given in Equation (51). Equation (52) expresses α_{ij} in terms of the derivative of u_{rij} in the z-direction. In finite difference form, the first and second derivatives of this displacement are as follows.

$$\frac{\partial u_{rij}}{\partial z} = \frac{-u_{ri(j-1)} + u_{ri(j+1)}}{\Delta z_{(i-1)j} + \Delta z_{(i-1)(j-1)}} = \tan \alpha_{ij} \tag{64}$$

$$\frac{\partial^2 u_{rij}}{\partial z^2} = \frac{2[u_{ri(j-1)} + u_{ri(j+1)} - 2u_{rij} + \frac{\partial u_{rij}}{\partial z}(\Delta z_{(i-1)(j-1)} - \Delta z_{(i-1)j})]}{\Delta z^2_{(i-1)(j-1)} + \Delta z^2_{(i-1)j}} \tag{65}$$

The radius of curvature is computed from the following familiar form, together with Equations (64) and (65).

$$\rho_{ij} = \frac{[1 + (\frac{\partial u_{rij}}{\partial z})^2]^{3/2}}{\frac{\partial^2 u_{rij}}{\partial z^2}} \tag{66}$$

A comprehensive treatment of the finite difference representation of displacement boundary conditions that satisfy various end restraints at $j=1$ and J is given by Carnahan, et al (1964). A particular example is presented below.

For suitable convergence, it is important to select a sufficient number of cylindrical segments J-1 to accurately represent the cylinder's overall shape. As Equations (60) and (61) are integrated to yield the displacement, the error in the result will decrease as J is increased. However, if J is too large, the accuracy of the derivatives computed by Equations (64) and (65) may

actually decrease. It was found that the selection of the number J is tempered by the initial cylinder geometry, the orthotropy angle θ_0, the material constants, the type and magnitude of loading, and the computational effort.

PARAMETRIC STUDIES

A Fortran IV computer code was written to carry out the calculations for the finite deformation behavior of both the homogeneous and nonhomogeneous types of cylinders. Selected parametric studies for both types are now presented. For cases where the material is linear and only one of the three loads is present (longitudinal load P, internal pressure p, or pure torque T), the deformations depend on the following appropriate independent nondimensional load parameters and three geometric parameters.

$$\bar{P} = \frac{P}{E_0 R_0 t_0} \quad ; \quad \bar{p} = \frac{pR_0}{E_0 t_0} \quad ; \quad \bar{T} = \frac{T}{E_0 R_0^2 t_0} \quad ; \quad \theta_0 \quad ; \quad \frac{R_0}{t_0} \quad ; \quad \frac{\ell_0}{R_0} \quad (67)$$

In the selected examples, the deformations were found to be very sensitive to tne independent parameter θ_0, tne initial angle of orthotropy. Thus θ_0 was taken as the abscissa in the presentation of the graphical results. The last two geometric parameters of (67) affect deformations only in axial nonhomogeneous problems.

The first type of cylinder has axially homogeneous stresses and strains and is made of an orthotropic, linear elastic material with the following properties:

$$E_i/E_i' = E_0/E_0' = 10 \quad ; \quad E_i/G_i = E_0/G_0 = 3$$
$$B = B' = B_g = C = C' = C_g = 0 \quad ; \quad \nu = 0.5 \quad (68)$$

The results for this cylinder are presented in Figs. 3-8.

Figures 3, 4 and 5 show the behavior of the finite longitudinal strain ϵ_{zz} with the loading P, p, and T respectively. For longitudinal loading, it is deduced from Fig. 3 that for $\theta_0 = 27$ deg and $\theta_0 > 60$ deg, the curves coalesce and ϵ_{zz} is linear with P. For $0 < \theta_0 < 27$ deg, however, the cylinder acts as a "soft" spring in the axial direction, since as P increases, ϵ_{zz} becomes proportionally larger. For $27 < \theta_0 < 60$ deg, however, the reverse is true but is less pronounced, where the cylinder behaves as a "hard" spring. However, for internal pressure loading, Fig. 4, linear behavior is found for $\theta_0 = 52$ deg, with soft spring behavior for smaller values and hard spring behavior (but less pronounced) for larger values of θ_0. Except near the extreme values of θ_0, the behavior of axial strain with pure torque is more complex, as shown in Fig. 5. For θ_0 up to 3 deg, the behavior is linear; and from that point to 30 deg the cylinder "winds together" where, as T increases, changes in ϵ_{zz} are proportionally smaller. However, for θ_0 near 80 deg, as T increases, ϵ_{zz} becomes proportionally larger, and the cylinder winds together more and more easily, within small changes for θ_i. It is noted that θ_i decreases as the cylinder winds together.

Figures 6, 7 and 8 show the behavior of ϕ, the finite angle of rotation about the longitudinal axis of the cylinder, with loading P, p, and T respectively. The negative ordinate in Figs. 6 and 7 indicates that the cylinder unwinds with the application of load. The change from a soft or flexible configuration to a hard one at $\theta_0 = 30$ deg is apparent in Fig. 6; but for pressure loading this change is less distinct and occurs when θ_0 is between 50 and 60 deg, as shown in Fig. 7. The effect of pure torque on ϕ for θ_0 up to about 30 deg is clear from Fig. 8: as T increases, ϕ becomes proportionally larger, and the cylinder winds together and becomes shorter.

Fig. 3   Effect of axial load and orthotropy on axial strain (axially homogeneous case)
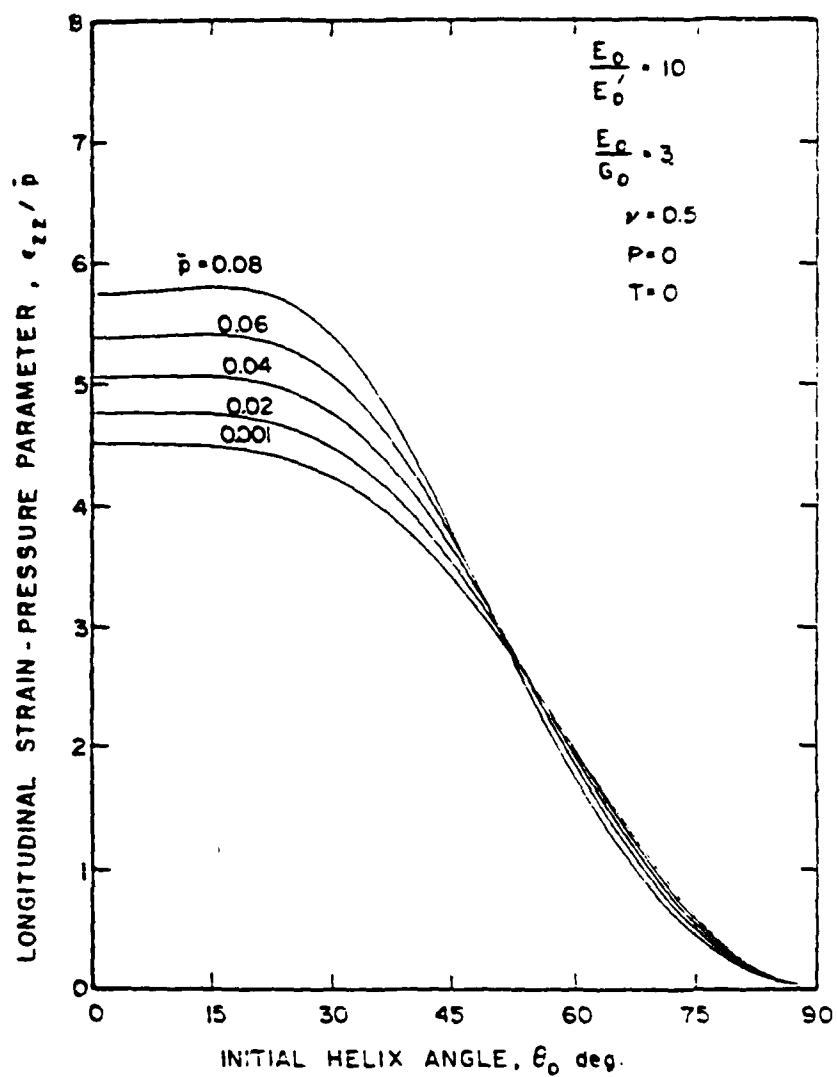
Fig. 4   Effect of internal pressure and orthotropy on axial strain (axially homogeneous case)
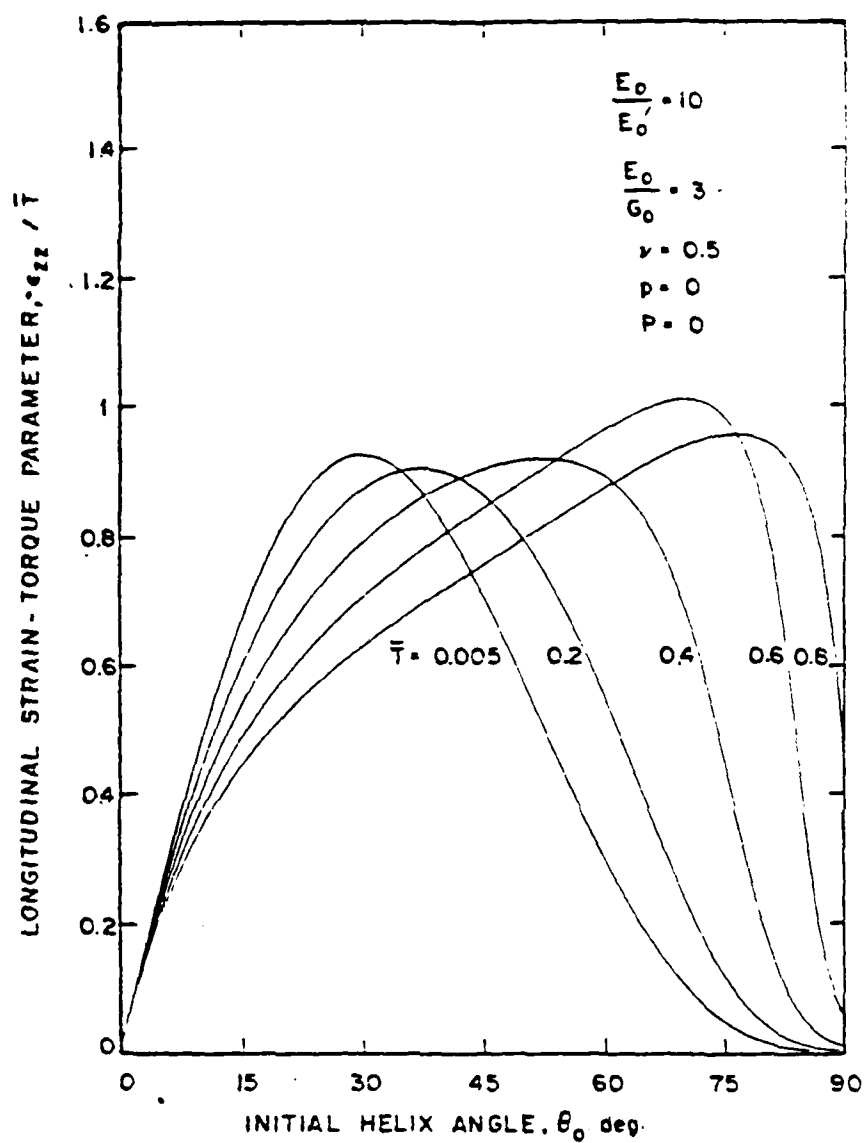
Fig. 5   Effect of pure torque and orthotropy on axial strain (axially
          homogeneous case)
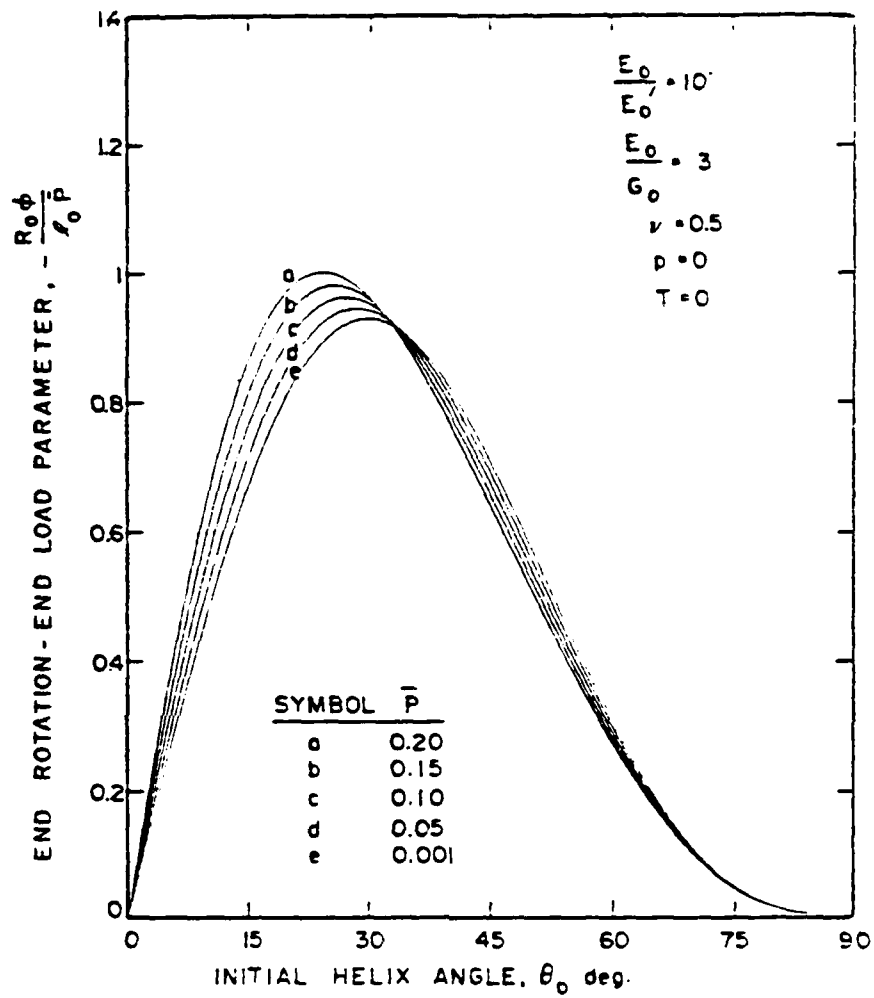
Fig. 6   Effect of axial load and orthotropy on end rotation (axially homogeneous case)
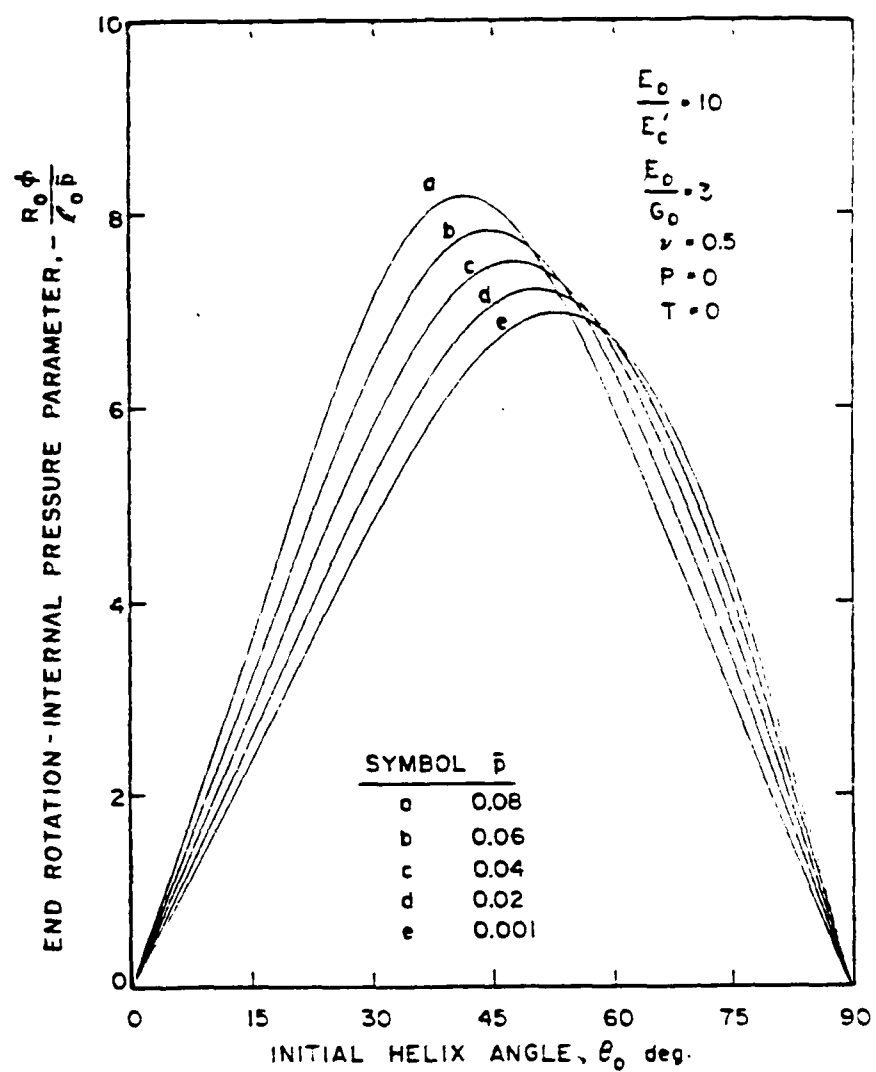
Fig. 7   Effect of internal pressure and orthotropy on end rotation (axially homogeneous case)

The second type of cylinder selected for study has axially nonhomogeneous stresses and strains, but has the same material constants as for the study just completed. That is, the material is orthotropic, linear and elastic with the properties defined by Equations (68). For axial nonhomogeneity, the initial geometry (ℓ_0, R_0, t_0) and number of points J along the length affect the deformation patterns. These particular quantities were chosen as follows:

$$\ell_0/R_0 = 10 \quad ; \quad R_0/t_0 = 10 \quad ; \quad J = 11 \tag{69}$$

The boundary conditions for the second type of cylinder were chosen to simulate a fully clamped condition at one end, j=1, and zero radial displacement at the other end, $J = 11$. However, the longitudinal displacement and twisting angle were chosen to be unrestrained at $J = 11$. These conditions are:

$$u_{z1} = u_{\theta 1} = u_{r1} = u_{rJ} = 0 \tag{70}$$

The results for this second type of cylinder are presented in Figs. 9, 10 and 11 in which the only loading is internal pressure. For the range of $\bar{p}$ that overlaps ($0.001 < \bar{p} < 0.02$), it is observed that the curves of Fig. 9 for the average longitudinal strain $\bar{\epsilon}_{zz}$ are identical to those of Fig. 4 for the homogeneous strain ϵ_{zz}. For this range, then, the end boundary constraints have a negligible effect on the total longitudinal deformation. However, for the range of $\bar{p}$ that overlaps ($0.001 < \bar{p} < 0.02$), the total end rotations ϕ of Fig. 10 differ from the counterpart results of Fig. 7 (boundaries uncon-strained), where these rotations become more dissimilar as θ_0 is increased beyond 15 deg. Compared to the constrained case, the geometric changes along the length of an unconstrained cylinder are always more pronounced. The last study, Fig. 11, shows the nonlinear variation in midlength radius R_M, with internal pressure. Such calculations are of particular importance for axially
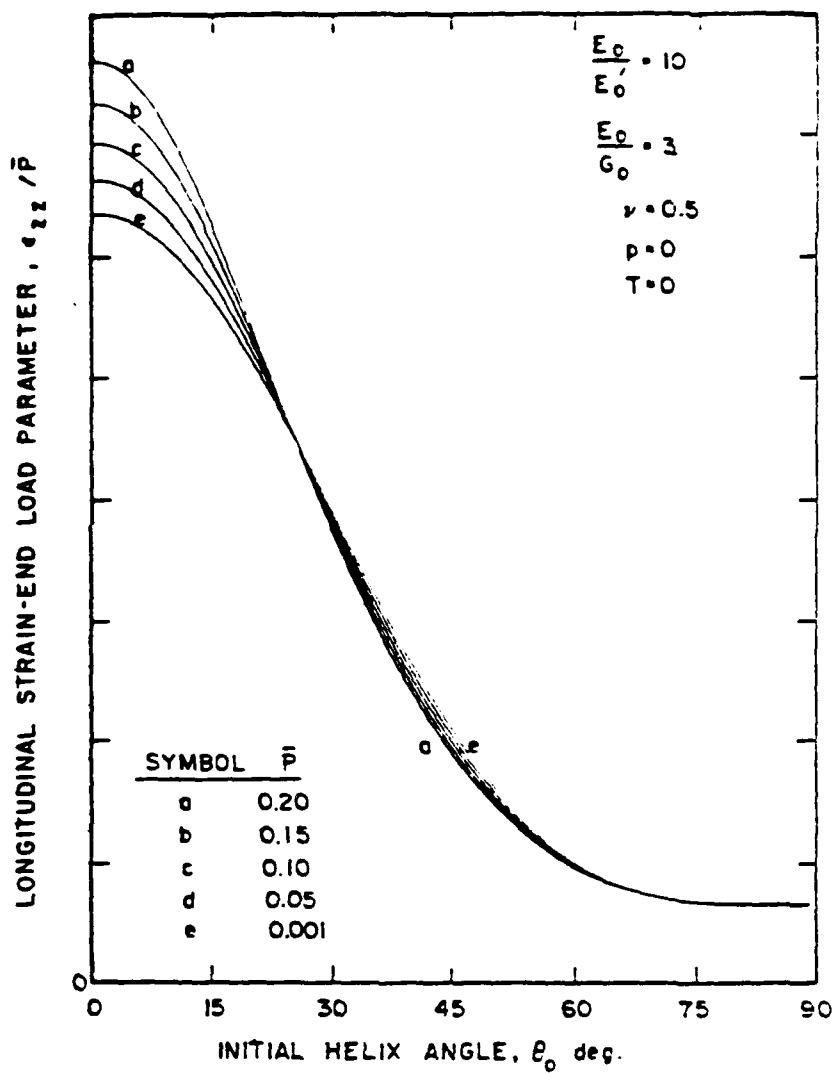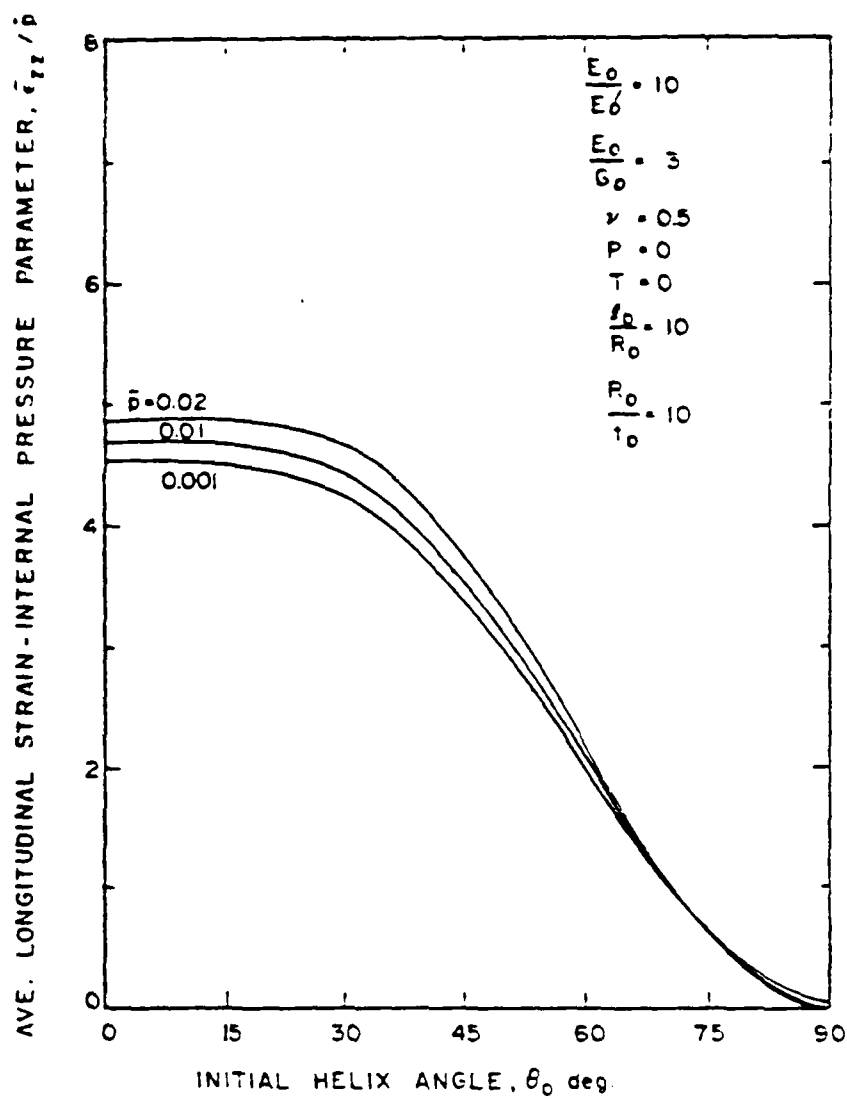
Fig. 9   Effect of internal pressure and orthotropy on axial strain (axially nonhomogeneous case)
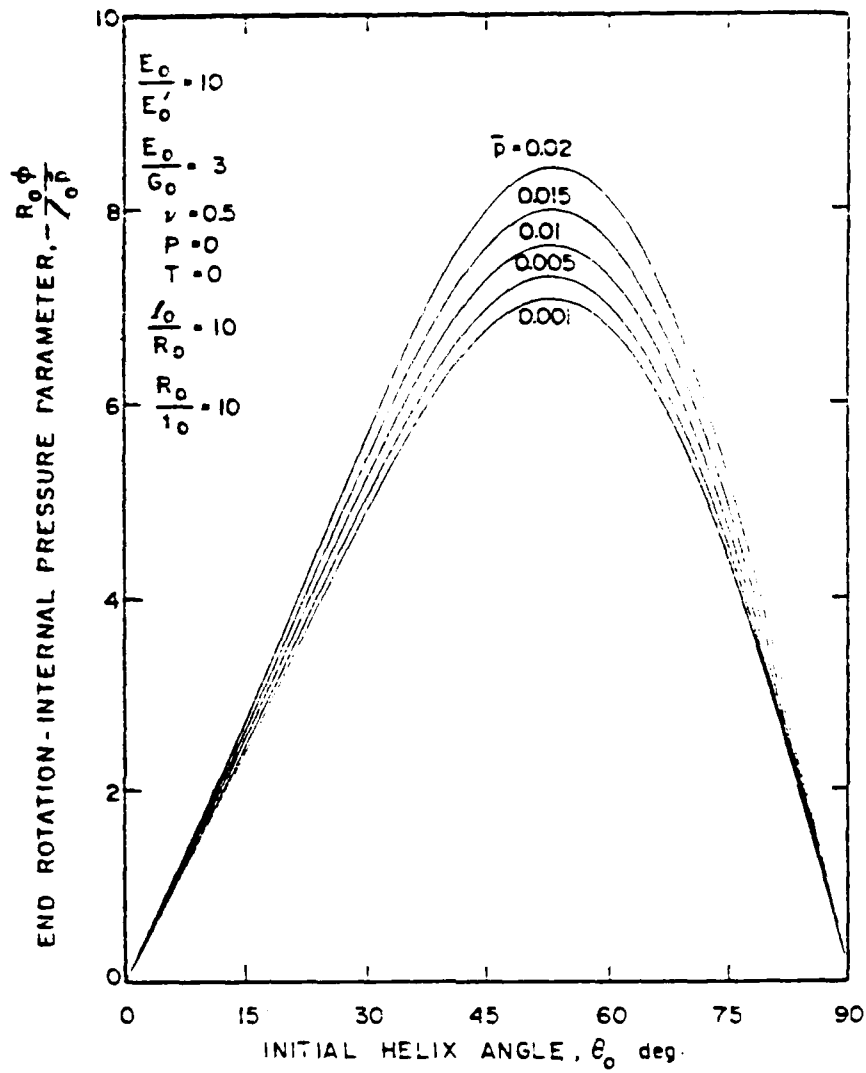
Fig. 10   Effect of internal pressure and orthotropy on end rotation (axially
nonhomogeneous case)
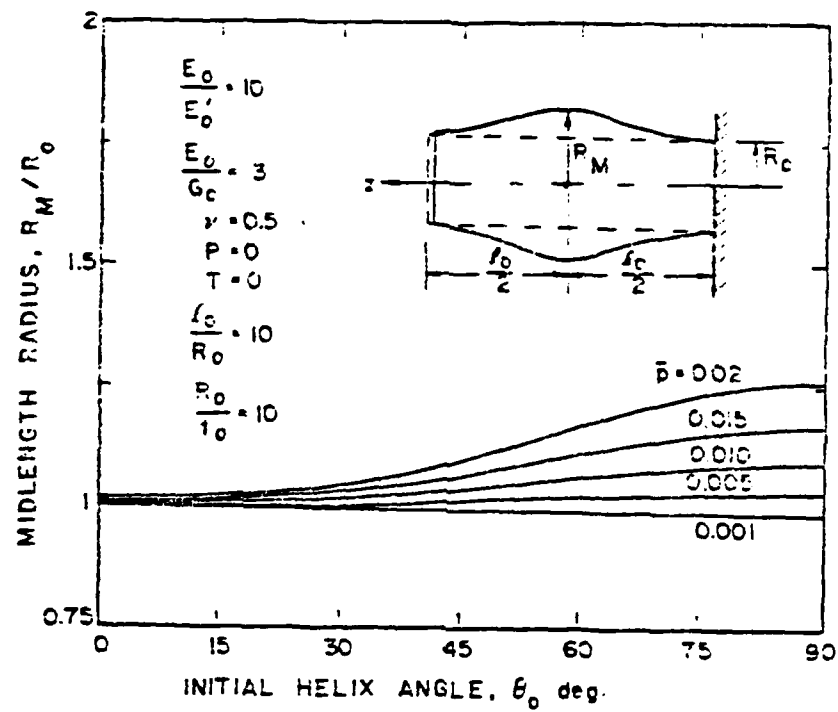
Fig. 11   Effect of internal pressure and orthotropy on midlength radial

expansion (axially nonhomogeneous case)

nonhomogeneous deformations because they serve as a way to check the limits of validity of the present analysis. That is, since out-of-plane stresses, strains, and deformations were ignored, then the angle α_{ij} needs to be sufficiently small for the results of Figs. 9, 10 and 11 to be valid, or cos $\alpha_{ij} \approx 1$, $\sin \alpha_{ij} \approx \alpha_{ij}$. For instance, if $\bar{p} = 0.02$ and $\theta_0 = 75$ deg, then $R_M/R_0 = 1.25$ from Fig. 11. Let α_{ij} be approximated from Equation (52) as follows.

$$\alpha_{ij} \approx \tan^{-1}\left(\frac{\Delta u_r}{\Delta z}\right) = \tan^{-1}\left(\frac{R_M - R_0}{0.5\,\ell_0}\right)$$

$$= \tan^{-1}\left(\frac{1.25\,R_0 - R_0}{5\,R_0}\right) \approx 2.86 \text{ deg} \tag{71}$$

Thus, α_{ij} is sufficiently small to justify the present analysis of Part 2.

References

Carnahan, B., Luther, H. A. and Wilkes, J. O., 1964, _Applied Numerical Methods_, John Wiley, New York.

Goodyear Tire and Rubber Co., 1949, _Handbook of Molded and Extruded Rubber_, 1st ed., Akron, Ohio.

Green, A. E. and Adkins, J. E., 1970, _Large Elastic Deformations_, 2nd Edition, Clarendon Press, Oxford, U.K.

Lekhnitskii, S. G., 1963, _Theory of Elasticity of an Anisotropic Body_, translated from Russian by P. Fern, Holden-Day Inc., San Francisco.

Leonard, J. W., 1967, "Inflatable Shells: In-service Phase," _Journal of Engineering Mechanics_, ASCE Vol. 93.

Popov, E. P., 1981, _Mechanics of Materials_, 2nd ed., Prentice-Hall, New York.

Reissner, E., 1970, "On Uniform Stress and Strain in Axially Homogeneous Cylindrical Shells," _International Journal of Solids and Structures_, Vol. 6, pp. 133-138.

Sokolnikoff, I. S., 1956, _Mathematical Theory of Elasticity_, 2nd Edition, McGraw-Hill, New York.

Timoshenko, S. P. and Woinowsky-Kreiger, S., 1959, _Theory of Plates and Shells_, 2nd Edition, McGraw-Hill, New York.

Utku, S., 1981, _Numerical Solutions of Partial Differential Equations_, Dept. of Civil Engineering and Dept. of Computer Science, Duke University, Durham, NC.

Verma, P. D. S. and Rana, O. K., 1983, "Rotation of a Circular Cylindrical Tube Reinforced by Fibres Lying Along Helices," _Mechanics of Materials_, Vol. 2, pp. 353-359.

Wilson, J. F. and Orgill, G., 1985, "Linear Analysis of Uniformly Stressed, Orthotropic Cylindrical Shells," (in review).

CHAPTER III

LARGE DEFLECTIONS OF CONTINUOUS ELASTIC STRUCTURES

Murugappan Palaniappan and James F. Wilson

1. INTRODUCTION

A robot is a reprogrammable, multifunctional manipulator designed to
perform a variety of tasks. Examples of robot functions are material
handling, spray painting and aligning of screws in assembly line operations
(Critchlow, 1985). The present state of robot technology is that the arm
moves around accurately but not efficiently. Most of the robotic arms in use
today consist of rigid elements connected by hinged or pivoted joints. The
movement of these arms is slow because of their high weight and inertia, and
the time needed to compute and control the coordinates of their elements or
arm segments.

A different approach to arm design is based on the motion of a
flexible elephant trunk (Mahajan, 1985). The flexible arm is made of
lightweight, polymeric material and may handle comparatively heavy payloads at
higher speeds than most rigid arm designs. These flexible arms are based on
the action of corrugated tube elements (Wilson, 1984-a) that bend when
pressurized.

Three distinct aspects of flexible arm design are analyzed in this
thesis: the equivalent or reduced modulus E' for the corrugated portion of a
bending element; the single, elastic bending element treated as a composite,
reinforced, elastic cantilevered beam; and the whole arm deflection analysis,
treated as bending elements in series. In this analysis, self weight is

neglected since the payloads are expected to be at least an order of magnitude higher than the arm weight.

Section 2 deals with the computation of reduced modulus E' of a rectangular corrugation in which the static load responses of bellows type arms with Young's modulus E, using classical theory of plates and shells are derived. In his classic paper, Donnell (1932) calculated the longitudinal flexibility for several types of corrugations and derived a reduced modulus of elasticity for these corrugated bellows as if they were smooth tubes. Calladine (1974) used energy methods to compute the flexibility of an axially symmetric elastic bellows subjected to axial loading. Haringx (1952) studied the instability of rectangular corrugation bellows when loaded by internal pressure. Wilson (1984-b) reviewed several mathematical models and the assumptions used to compute E' and to compare calculated and experimental values of E'. He also shows that the mean bellows radius is the appropriate dimension needed to convert internal pressure to an external load.

Section 3 deals with the plane, finite deflection analysis of a cantilever beam subjected to end loading. The exact differential equation is solved in terms of the slope of the elastic curve. Related work is summarized as follows: Scott, Carver (1953) presented an integral power series solution of the nonlinear beam equation in which the moment is expressed as a function of the distance x from the origin. Lewis, Monasa (1982) presented a large deflection analysis of thin cantilever beams of nonlinear materials subjected to a constant end moment. Theocaris, Panayotounakos (1982) solved the nonlinear differential equation of an elastic cantilever subjected to coplanar terminal loading, taking into account the influence of transverse shear deformations. Bisshop, Drucker (1945) presented a solution for large deflections of a cantilever beam subjected to a tip transverse load in terms

of an elliptic integral.

The solutions given by ([Scott, Carver], [Lewis, Monasa], [Theocaris, Panayotounakos]) are in terms of Cartesian coordinates. The solution presented herein involves solving iteratively a complete elliptic integral of the first kind for the maximum slope at the tip of an elastic cantilever subjected to general plane loading at the tip. This solution is a generalization of the elastica in which only longitudinal loads were considered (Timoshenko and Gere, 1961).

Section 4 deals with the deflection of the flexible arm in two dimensional space, where the arm is composed of end-to-end cantilevers. Each element of the arm is analyzed as an elastic cantilever, starting from the tip, with the fixed end at the tip of the previous element. Transformation equations are used to relate the tip of each element to the global coordinate system which is fixed at the root of the arm. Knowing the final destination of the payload at the tip of the arm, an iterative procedure is used to vary the pressure history in each corrugated tube element of the arm so that the payload may reach its destination.

In Section 5, conclusions of this study and recommendations for further research are presented. Different geometrical arrangement of the bellows is discussed to achieve out-of-plane motion. A systematic procedure is suggested to vary the pressure to achieve rapid convergence to the destination coordinate. A data base approach is suggested to overcome the numerous computation involved in the computation of the tip angle α.

All computer codes listed in the appendices were written by the author. They are used to compute the reduced modulus E', the shape of the elastic curve of the deformation behavior of a single cantilever and the equilibrium states of a manipulator arm.

2. ANALYSIS OF BELLOWS ELEMENT

A. Mathematical Model

Bellows are thin walled corrugated tubes designed for high flexibility when subjected to axial loads, internal pressure or bending moments. The present study is of a bellows corrugation model consisting of cylindrical shell sections connected by annular plates and subjected to axial load and internal pressure. These bellows are to be used as the structural section of the robotic manipulator. The desired motion of the bellows will be controlled by microcomputer and monitored through pressure gages. Figure (2.1) shows a longitudinal section through the bellows, which is subjected to internal pressure p and axial force F_0. The shaded section is a typical half corrugation used in the analysis.

Calculations for bellows extension, compression and transverse bending are made as if the bellows were an equivalent cylinder of the same mean radius, length and wall thickness. The equivalent cylinder has a reduced Young's modulus E' which is used to compute static load responses of the bellows with modulus E. Figure (2.2) shows the geometry of a half corrugation of the bellows together with the coordinate system for the inner and outer shells and plate. For a bellows of n corrugations of mean cross sectional

LINE OF LINE OF
SYMMETRY SYMMETRY
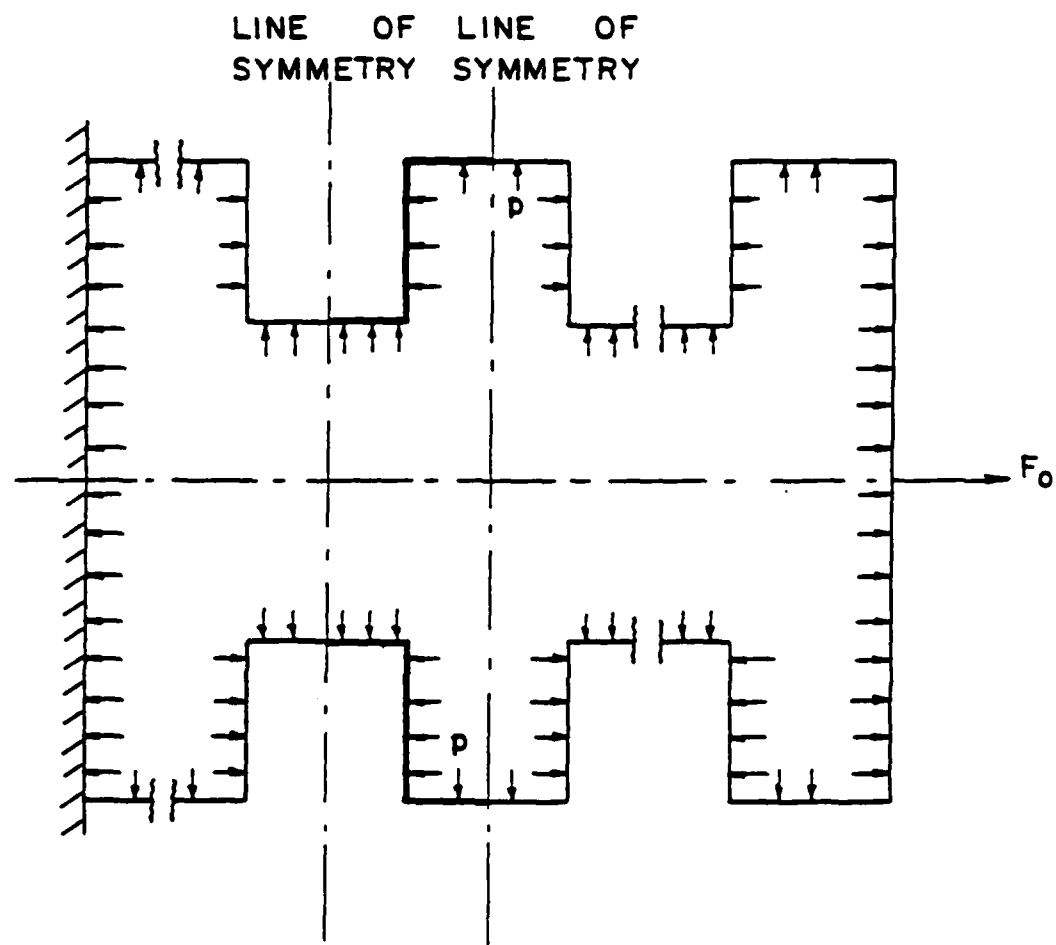
Figure 2.1 Longitudinal bellows section subjected to internal pressure p

and axial force F_o and a darkened typical half corrugation

used in analysis.
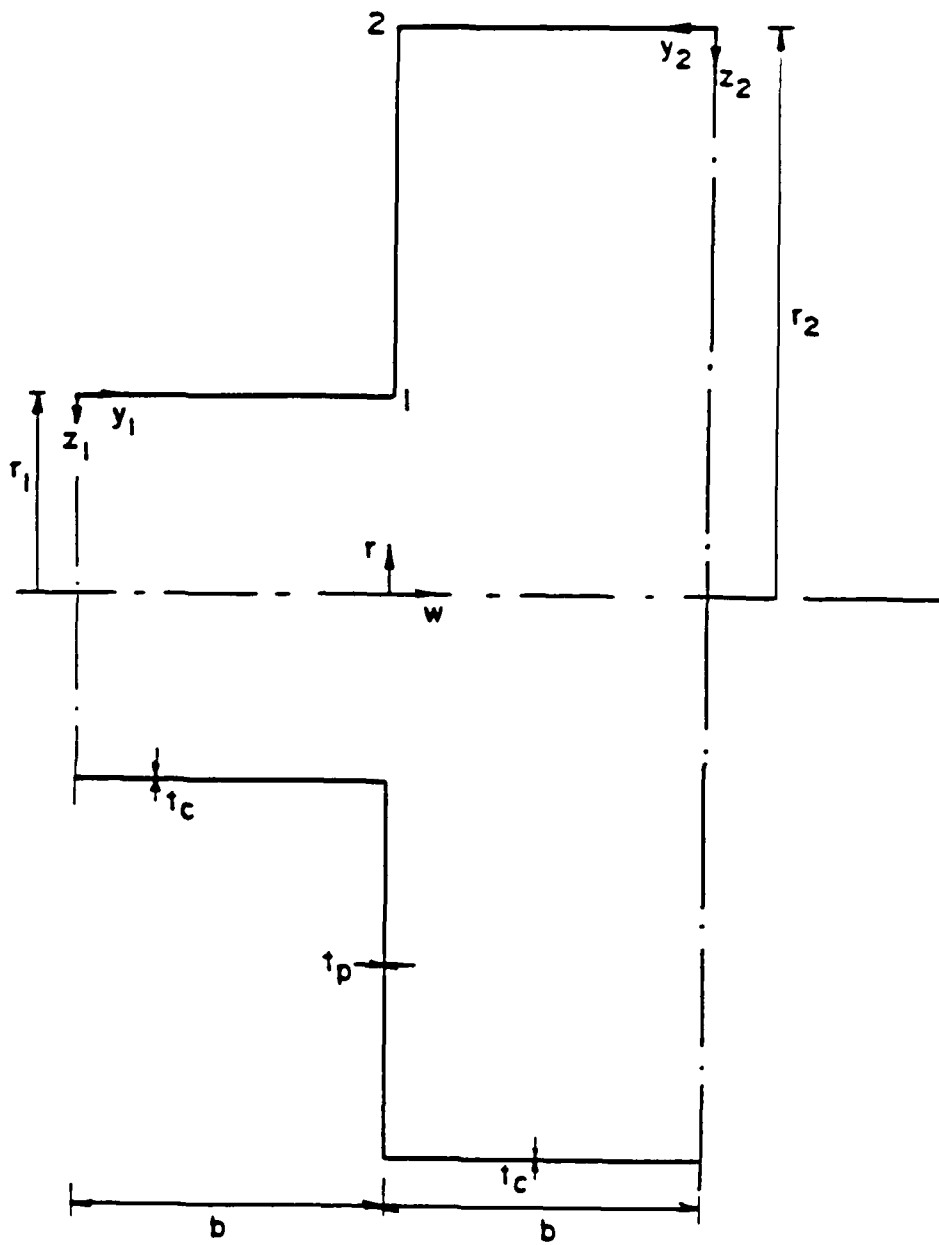
Figure 2.2 Geometry of half corrugation with local coordinate system.

area $2\pi Rt$, the axial extension from strength of materials is

$$\Delta_b = \frac{P}{E'} \frac{4nb}{2\pi Rt} = \frac{P}{E'} \frac{2nb}{\pi Rt} \qquad (2.1)$$

where

$$P = F_0 + \pi R^2 p$$

E' = modulus of equivalent cylinder

As the corrugation is symmetric transversely, we need to consider only one-half of the corrugation, of length 2b, to transform it into an equivalent cylinder, as shown in Figure (2.3). The axial extension of the equivalent cylinder is

$$\Delta = \frac{P}{E'} \frac{2b}{2\pi Rt} = \frac{P}{E'} \frac{b}{\pi Rt} \qquad (2.2)$$

or

$$E' = \frac{b}{\pi Rt} \left(\frac{P}{\Delta}\right) \qquad (2.2a)$$

First, the axial extension Δ of the corrugation is predicted from the theory of plates and shells. Equation (2.2a) is then used to compute the reduced modulus E' of the equivalent cylinder. Figure (2.4) shows a free body sketch of the corrugation together with its slope and moment compatibility at the junctions. Figure (2.5) shows the corrugation subjected to internal pressure p and axial force F_0 and its resulting deflected shape. Radial displacement of the plate is neglected.

The assumptions of the mathematical model are summarized below:

1) The inner and outer cylindrical shells restrain the radial displacement of the annular plate at junctions 1 and 2.

2) Right angles are maintained at junctions 1 and 2.

3) Axial forces in the cylindrical shells have negligible effect on the shell stiffnesses.
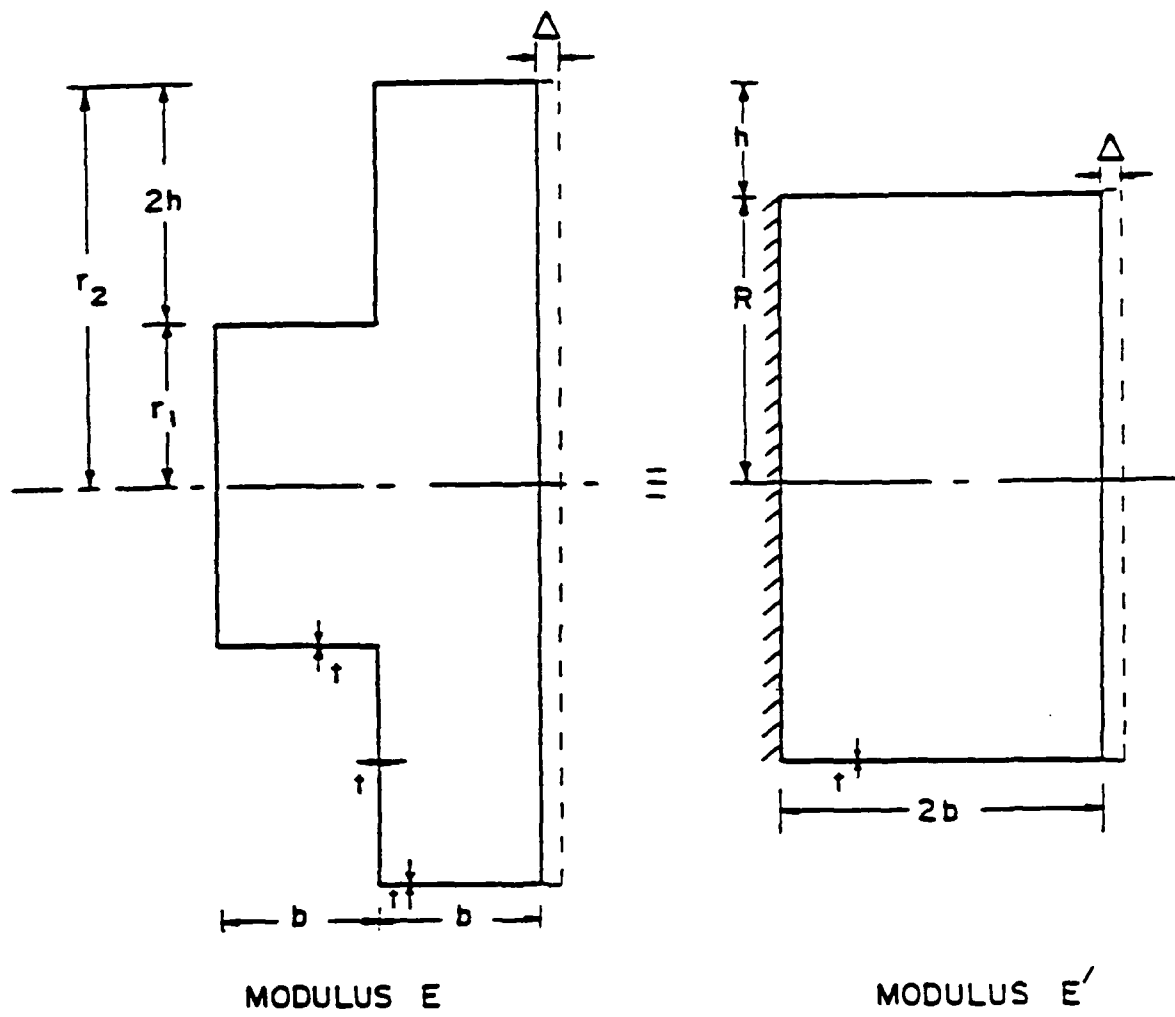
Figure 2.3 Half corrugation of modulus E with axial elongation Δ and its equivalent cylinder of modulus E' with same axial elongation Δ.
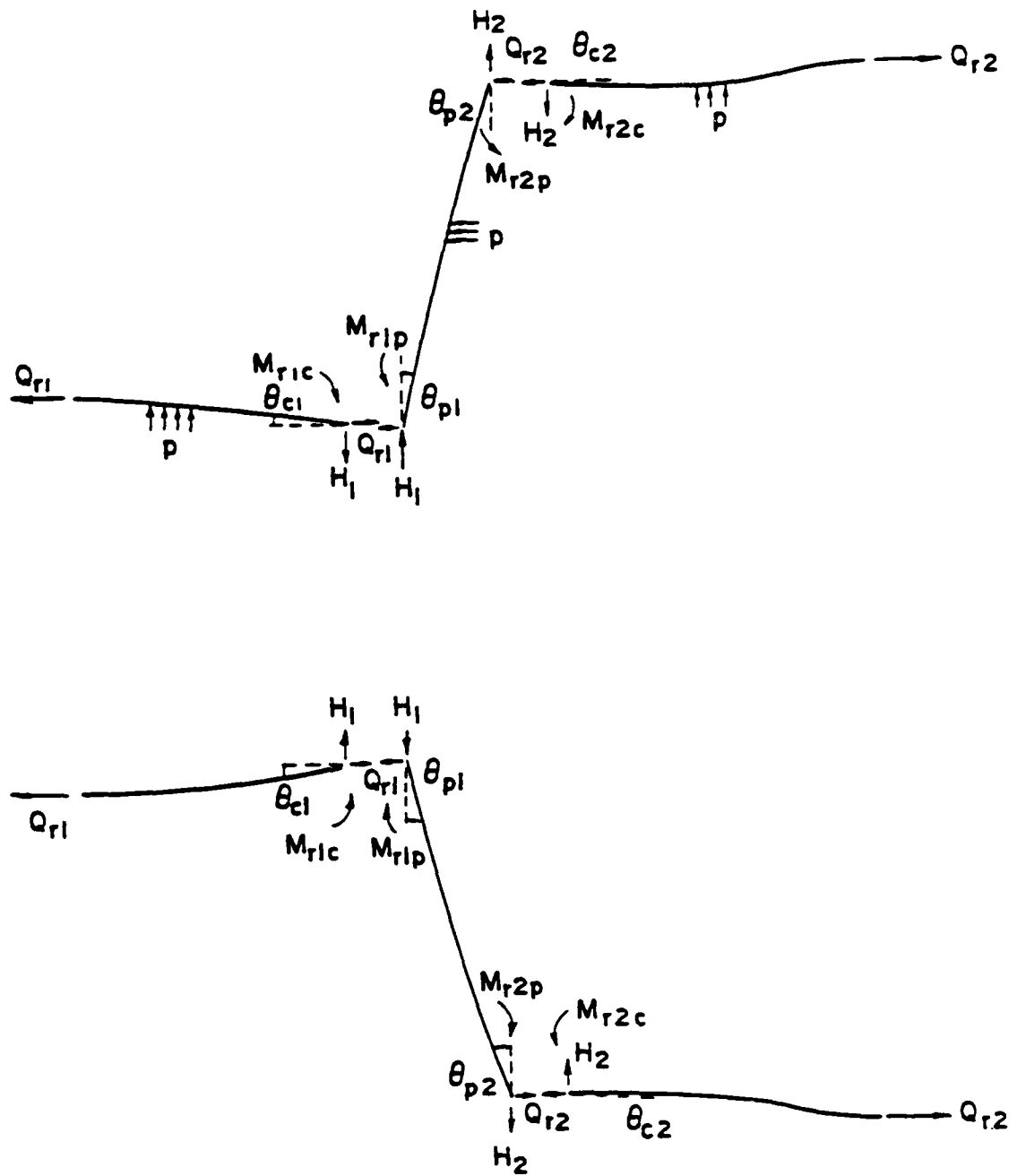
Figure 2.4 Free body sketch showing slope and moment compatibility.
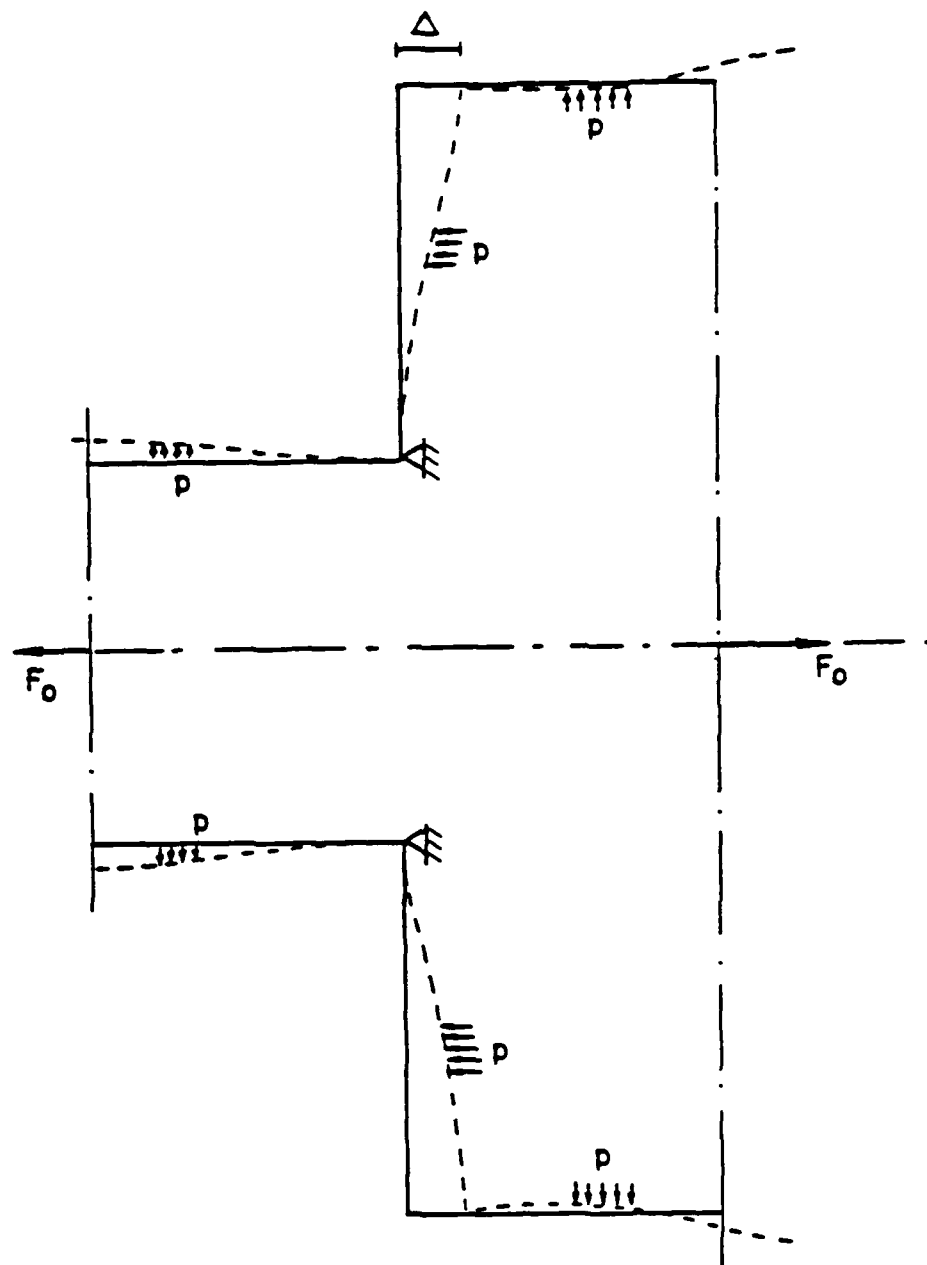
Figure 2.5 Half corrugation subjected to internal pressure p and axial

force F_o and its deflected shape.

4) The cylindrical shells contribute a negligible amount to the axial deflection under internal pressure p and axisymmetrical load F_0.

5) Plate bending accounts for all of the axial deflection under loads p and F_0.

6) In-plane (radial) loads on the plate have negligible effect on its stiffness and axial deflection.

7) Effects of rigid end plates on symmetrical deformation of a typical element are negligible.

8) Classical plate and shell theory govern the system behavior under loads p and F_0.

B. Plate Analysis

The governing 4th order plate equation is

$$\nabla^2 \nabla^2 w = -\frac{p}{D_p} \tag{2.3}$$

where

$$D_p = \frac{E t_p^3}{12(1 - \nu^2)}$$

$$\nabla^2 = \left(\frac{d^2}{dr^2} + \frac{1}{r}\frac{d}{dr}\right)$$

The pressure loading p is a non-negative quantity and the sign associated with p is negative as the direction of p is opposite to the direction of lateral deflection w. Here, r is the radial coordinate and D_p is the rigidity of the plate.

A more convenient form of Equation (2.3) is

$$\frac{1}{r}\frac{d}{dr}\left\{r\frac{d}{dr}\left[\frac{1}{r}\frac{d}{dr}\left(r\frac{dw}{dr}\right)\right]\right\} = -\frac{p}{D_p} \tag{2.4}$$

The moment and shear equations of a plate are

$$M_{rp} = -D_p\left(\frac{d^2w}{dr^2} + \frac{\nu}{r}\frac{dw}{dr}\right) \tag{2.5}$$

$$Q_{rp} = -D_p\frac{d}{dr}\left[\frac{1}{r}\frac{d}{dr}\left(r\frac{dw}{dr}\right)\right] \tag{2.6}$$

Integrating Equation (2.4) directly, we obtain

$$w = -\frac{r^4 p}{64D_p} + C_3\left(\frac{r}{r_1}\right)^2 \ln\left(\frac{r}{r_1}\right) + C_2\left(\frac{r}{r_1}\right)^2 + C_1\ln\left(\frac{r}{r_1}\right) + C_0 \tag{2.7}$$

where C_0, C_1, C_2 and C_3 are arbitrary constants of integration.

These four constants are written in terms of the following edge conditions.

$$w = 0 \text{ at } r = r_1 \tag{2.8}$$

$$M_{r_{1p}} = D_p\left(\frac{d^2w}{dr^2} + \frac{\nu}{r}\frac{dw}{dr}\right) \tag{2.9}$$

$$M_{r_{2p}} = -D_p\left(\frac{d^2w}{dr^2} + \frac{\nu}{r}\frac{dw}{dr}\right) \tag{2.10}$$

$$Q_{r_{2p}} = -D_p\frac{d}{dr}\left[\frac{1}{r}\frac{d}{dr}\left(r\frac{dw}{dr}\right)\right] \tag{2.11}$$

Apply Equation (2.8) to (2.4).

$$C_0 = \frac{r_1^4 p}{64D_p} - C_2 \tag{2.12}$$

Substitute C_0 in Equation (2.4).

$$w = -(r^4 - r_1^4)\frac{p}{64D_p} + C_3\left(\frac{r}{r_1}\right)^2 \ln\left(\frac{r}{r_1}\right) + C_2\left[\left(\frac{r}{r_1}\right)^2 - 1\right] + C_1\ln\left(\frac{r}{r_1}\right) \tag{2.13}$$

Use the derivatives of w in Equation (2.9) and evaluate the moment at $r = r_1$.

$$M_{r_{1p}} = D_p \left\{ -\frac{r_1^2 p}{16 D_p} (3 + \nu) + \frac{C_3}{r_1^2} (3 + \nu) + \frac{C_2}{r_1^2} 2(1 + \nu) - \frac{C_1}{r_1^2} (1 - \nu) \right\} \quad (2.14)$$

Use the derivatives of w in Equation (2.10) and evaluate the moment at r = r_2.

$$M_{r_{2p}} = -D_p \left\{ -\frac{r_2^2 p}{16 D_p} (3 + \nu) + \frac{C_3}{r_1^2} \left[3 + \nu + 2 \ln \left(\frac{r_2}{r_1} \right)(1 + \nu) \right] \right.$$

$$\left. + \frac{C_2}{r_1^2} 2(1 + \nu) - \frac{C_1}{r_2^2} (1 - \nu) \right\} \quad (2.15)$$

Use Equation (2.11) and evaluate the shear at r = r_2.

$$Q_{r_{2p}} = D_p \left(\frac{r_2 p}{2 D_p} - C_3 \frac{4}{r_1^2 r_2} \right) \quad (2.16)$$

or

$$C_3 = \frac{r_1^2 r_2^2 p}{8 D_p} - \frac{r_1^2 r_2}{4} \frac{Q_{r_2}}{D_p} \quad (2.16a)$$

Noting that Q_{r_2}, the axial force in the outer cylinder, can be evaluated from equilibrium, C_3 becomes a known constant.

The problem is now reduced to two unknown constants C_1 and C_2 which are given by Equations (2.14) – (2.15) in terms of the redundant moments $M_{r_{1p}}$ and $M_{r_{2p}}$.

C. Shell Analysis

Both the inner and outer shells have an identical coordinate system, pressure loading p, rigidity D_c and modulus E. Hence, the governing equation is developed for a typical shell with radius r.

The governing 4th order cylindrical shell equation, giving radial deflection z at axial position y is

$$\frac{d^4 z}{dy^4} + \frac{Et_c z}{r_c^2 D_c} = -\frac{p}{D_c} \qquad (2.17)$$

where

$$D_c = \frac{Et_c^3}{12(1 - v^2)}$$

The moment and shear equations for a cylindrical shell are

$$M_y = -D_c \frac{d^2 z}{dy^2} \qquad (2.18)$$

$$Q_y = -D_c \frac{d^3 z}{dy^3} \qquad (2.19)$$

The particular solution to Equation (2.17) is $z = -\frac{pr_c^2}{Et_c}$. Let $\beta^4 = \frac{Et_c}{4r_c^2 D_c}$ be a shell parameter. Then, Equation (2.17) reduces to

$$\frac{d^4 z}{dy^4} + 4\beta^4 z = -\frac{p}{D_c} \qquad (2.17a)$$

The solution to the homogeneous form of this equation is

$$z = e^{\beta y}(D_1 \cos \beta y + D_2 \sin \beta y) + e^{-\beta y}(D_3 \cos \beta y + D_4 \sin \beta y)$$

where D_1, D_2, D_3 and D_4 are arbitrary constants of integration.

Replacing the exponential functions with hyperbolic functions and adding a particular solution, the solution to Equation (2.17a) becomes

$$z = -\frac{pr_c^2}{Et_c} + D_1 \sin (\beta y) \sinh (\beta y) + D_2 \sin (\beta y) \cosh (\beta y)$$

$$+ D_3 \cos (\beta y) \sinh (\beta y) + D_4 \cos (\beta y) \cosh (\beta y) \qquad (2.20)$$

By symmetry, if y is changed to (-y), the solution must remain unchanged i.e. the odd functions of Equation (2.20) must vanish. Hence

$$D_2 = D_3 = 0 \qquad (2.21)$$

Subscript 1 refers to the inner shell while subscript 2 refers to the outer shell. The four constants, two from the inner and two from the outer shell, are written in terms of the redundant moments $M_{r_{1c}}$ and $M_{r_{2c}}$.

Use the second derivative of z and evaluate moments $M_{r_{1c}}$ at $r = r_1$ and $M_{r_{2c}}$ at $r = r_2$ and at $y = b$.

$$M_{r_{1c}} = D_c \frac{d^2 z}{dy^2}$$

$$= 2D_c \beta_1^2 [A_1 \cos(\beta_1 b)\cosh(\beta_1 b) - B_1 \sin(\beta_1 b)\sinh(\beta_1 b)] \qquad (2.22)$$

$$M_{r_{2c}} = - D_c \frac{d^2 z}{dy^2}$$

$$= - 2D_c \beta_2^2 [A_2 \cos(\beta_2 b)\cosh(\beta_2 b) - B_2 \sin(\beta_2 b)\sinh(\beta_2 b)] \qquad (2.23)$$

D. Compatibility

Referring to the free body sketch of Figure (2.4), we can write the compatibility conditions. The displacement compatibility is expressed as

$$z_1 = 0 \text{ at } y_1 = b \text{ and } r = r_1 \qquad (2.24)$$

$$z_2 = 0 \text{ at } y_2 = b \text{ and } r = r_2 \qquad (2.25)$$

The slope compatibility is given by

$$\theta_{c1} = \theta_{p1} \text{ at } r = r_1 \qquad (2.26)$$

$$\theta_{c2} = \theta_{p2} \text{ at } r = r_2 \qquad (2.27)$$

The moment compatibility is given by

$$M_{r_{1c}} = M_{r_{1p}} \text{ at } r = r_1 \qquad (2.28)$$

$$M_{r_{2c}} = M_{r_{2p}} \text{ at } r = r_2 \qquad (2.29)$$

The displacement conditions have been evaluated using Equation (2.20) and are explicitly shown as Equations (2.30) - (2.31).

$$0 = -\frac{pr_1^2}{Et_c} + A_1\sin(\beta_1 b)\sinh(\beta_1 b) + B_1\cos(\beta_1 b)\cosh(\beta_1 b) \qquad (2.30)$$

$$0 = -\frac{pr_2^2}{Et_c} + A_2\sin(\beta_2 b)\sinh(\beta_2 b) + B_2\cos(\beta_2 b)\cosh(\beta_2 b) \qquad (2.31)$$

Explicit results for slope compatibility are as follows. Using the first derivative of Equations (2.13) and (2.20) evaluated at $r = r_1$ and $y = b$, along with Equation (2.26) yields

$$A_1\beta_1[\sin(\beta_1 b)\cosh(\beta_1 b) + \cos(\beta_1 b)\sinh(\beta_1 b)] + B_1\beta_1[\cos(\beta_1 b)\sinh(\beta_1 b)$$

$$- \sin(\beta_1 b)\cosh(\beta_1 b)] - C_2\left(\frac{2}{r_1}\right) - C_1\left(\frac{1}{r_1}\right) = -\frac{r_1^3 p}{16D_p} + C_3\left(\frac{1}{r_1}\right) \qquad (2.32)$$

Using the first derivative of Equations (2.13) and (2.20) evaluated at $r = r_2$ and $y = b$ in Equation (2.27) yields

$$-A_2\beta_2[\sin(\beta_2 b)\cosh(\beta_2 b) + \cos(\beta_2 b)\sinh(\beta_2 b)] - B_2\beta_2[\cos(\beta_2 b)\sinh(\beta_2 b)$$

$$- \sin(\beta_2 b)\cosh(\beta_2 b)] - C_2\left(\frac{2r_2}{r_1^2}\right) - C_1\left(\frac{1}{r_2}\right)$$

$$= -\frac{r_2^3 p}{16D_p} + C_3\left(\frac{r_2}{r_1^2}\right)\left[1 + 2\ln\left(\frac{r_2}{r_1}\right)\right] \qquad (2.33)$$

Explicit results for moment compatibility are as follows. Equations (2.14) and (2.22) evaluated at $r = r_1$ using Equation (2.28) yields

$$A_1[2D_c\beta_1^2\cos(\beta_1 b)\cosh(\beta_1 b)] - B_1[2D_c\beta_1^2\sin(\beta_1 b)\sinh(\beta_1 b)]$$

$$- C_2(1 + v)\frac{2D_p}{r_1^2} + C_1(1 - v)\frac{D_p}{r_1^2} = -\frac{r_1^2 p}{16}(3 + v) + C_3 D_p\left(\frac{3 + v}{r_1^2}\right) \qquad (2.34)$$

Equations (2.15) and (2.23) evaluated at $r = r_2$ using Equation (2.29) yields

$$A_2[-2D_c\beta_2^2\cos(\beta_2 b)\cosh(\beta_2 b)] + B_2[2D_c\beta_2^2\sin(\beta_2 b)\sinh(\beta_2 b)]$$

$$+ C_2 (1 + \nu) \frac{2D_p}{r_1^2} - C_1 (1 - \nu) \frac{D_p}{r_2^2} = \frac{r_2^2 p}{16} (3 + \nu)$$

$$- C_3 D_p[\frac{1}{r_1^2} (3 + \nu) + \frac{2}{r_1^2} \ln (\frac{r_2}{r_1})(1 + \nu)] \qquad (2.35)$$

The six unknown constants of integration are A_1, B_1, A_2, B_2, C_1 and C_2 which are calculated by solving Equations (2.30) - (2.35) simultaneously.

In summary, given the system parameters: F_0, p, r_1, r_2, t_p, t_c, E and ν, we calculate

$$Q_{r_2} = \frac{1}{2\pi r_2} (F_0 + \pi r_2^2 p) \qquad (2.36)$$

$$C_3 = \frac{r_1^2 r_2^2 p}{8D_p} - \frac{r_1^2 r_2}{4} \frac{Q_{r_2}}{D_p} \qquad (2.37)$$

$$D_p = \frac{E t_p^3}{12(1-\nu^2)} \qquad (2.38)$$

$$D_c = \frac{E t_c^3}{12(1-\nu^2)} \qquad (2.39)$$

$$\beta_1 = (\frac{E t_c}{4r_1^2 D_c})^{1/4} \qquad (2.40)$$

$$\beta_2 = (\frac{E t_c}{4r_2^2 D_c})^{1/4} \qquad (2.41)$$

Solving the six simultaneous Equations (2.30) - (2.35) will yield the unknown constants of integration. The deflection of the plate Δ at $r = r_2$ is

then computed from Equation (2.13), or

$$\Delta = w|_{r=r_2} = - (r_2^4 - r_1^4) \frac{p}{64D_p} + C_3(\frac{r_2}{r_1})^2 \ln (\frac{r_2}{r_1})$$

$$+ C_2 [(\frac{r_2}{r_1})^2 - 1] + C_1 \ln (\frac{r_2}{r_1}) \tag{2.42}$$

For a unit axial load P, compute the deflection Δ using Equation (2.42). Then, compute the effective modulus E' of the equivalent cylinder using Equation (2.2a).

E. Numerical Results

Define a nondimensional bellows parameter.

$$\lambda = \frac{Rt}{b^2} \tag{2.43}$$

Let

$$\frac{1}{S} = \frac{Et}{E'R} \tag{2.44}$$

be a measure of system response i.e. flexibility. The inverse of flexibility i.e. stiffness is

$$S = \frac{E'R}{Et} \tag{2.45}$$

The FORTRAN program SHELL.FOR, whose listing is given in Appendix A, computes the effective modulus E' for a given set of system parameters. A numerical example is shown below. Table (2.1) lists the numerical values chosen as input parameters.

The results of the computation are as follows:

Input Parameter	Numerical Value
p	15 psi
F_0	0 lb
E	2480 psi
ν	0.5
b	0.1 in
r_1	0.1 in
r_2	0.5 in
t_p	0.09 in
t_c	0.09 in

Table 2.1   Input parameters to the program SHELL.FOR for the chosen numerical example.

$$\Delta = 0.1003 \quad \text{in}$$

$$E' = 49.85 \quad \text{psi}$$

$$\frac{E}{E'} = 49.75$$

$$\lambda = 3.6$$

$$S = 0.0893$$

Design curves for stiffness S vs. nondimensional parameter λ are plotted in Figure (2.6) for different height to mean radius and height to one-fourth length of corrugation ratio. These curves can be used to compute the effective modulus E' for a given geometry of the bellows.
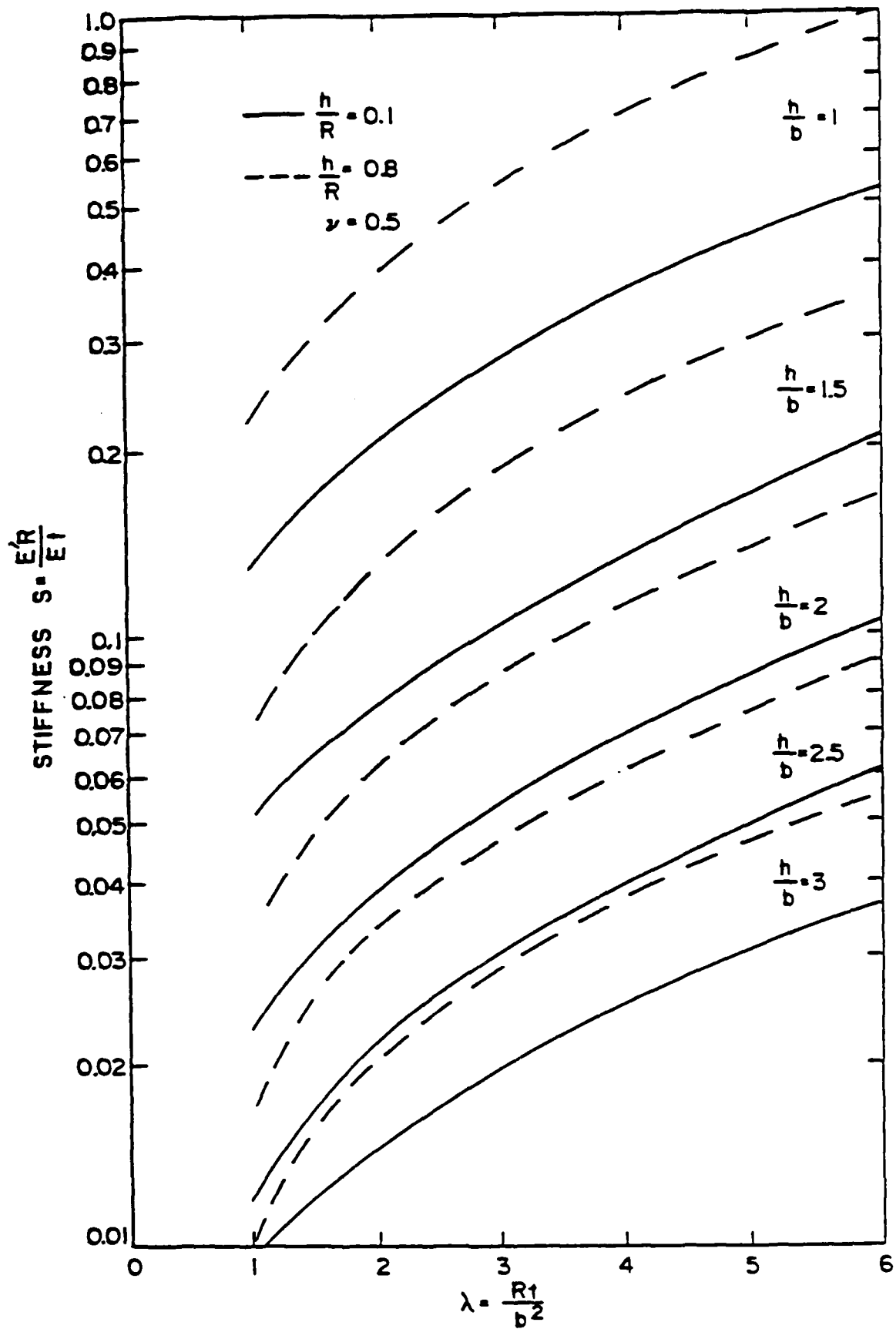
Figure 2.6 Design charts for stiffness S vs. nondimensional parameter λ.

3. ANALYSIS OF CANTILEVER BEAM ELEMENTS

A. Mathematical Model

A typical element of the manipulator arm has a bellows configuration with the ends sealed and with reinforcement on the underside as shown in Figure (3.1). To achieve the bending effect of the manipulator arm in either direction, we use double sided elements placed back to back as shown in Figure (3.2).

Each element of the arm consists of several corrugations, and the exact number is determined by the length of the element and the maximum desired transverse displacement or rotation at the tip of the cantilever.

The maximum tip rotation will typically be 90° or 180° depending on the function of the element. Elements that are designed to coil around the load need to rotate more than the elements that help in the lifting of the load.

A relationship between the geometry, length, the degree of rotation and the number of corrugations in the double sided element is derived as follows. Assume that the corrugations on the convex surface just touch at the maximum degree of bend. With reference to Figure (3.3), these two relations are
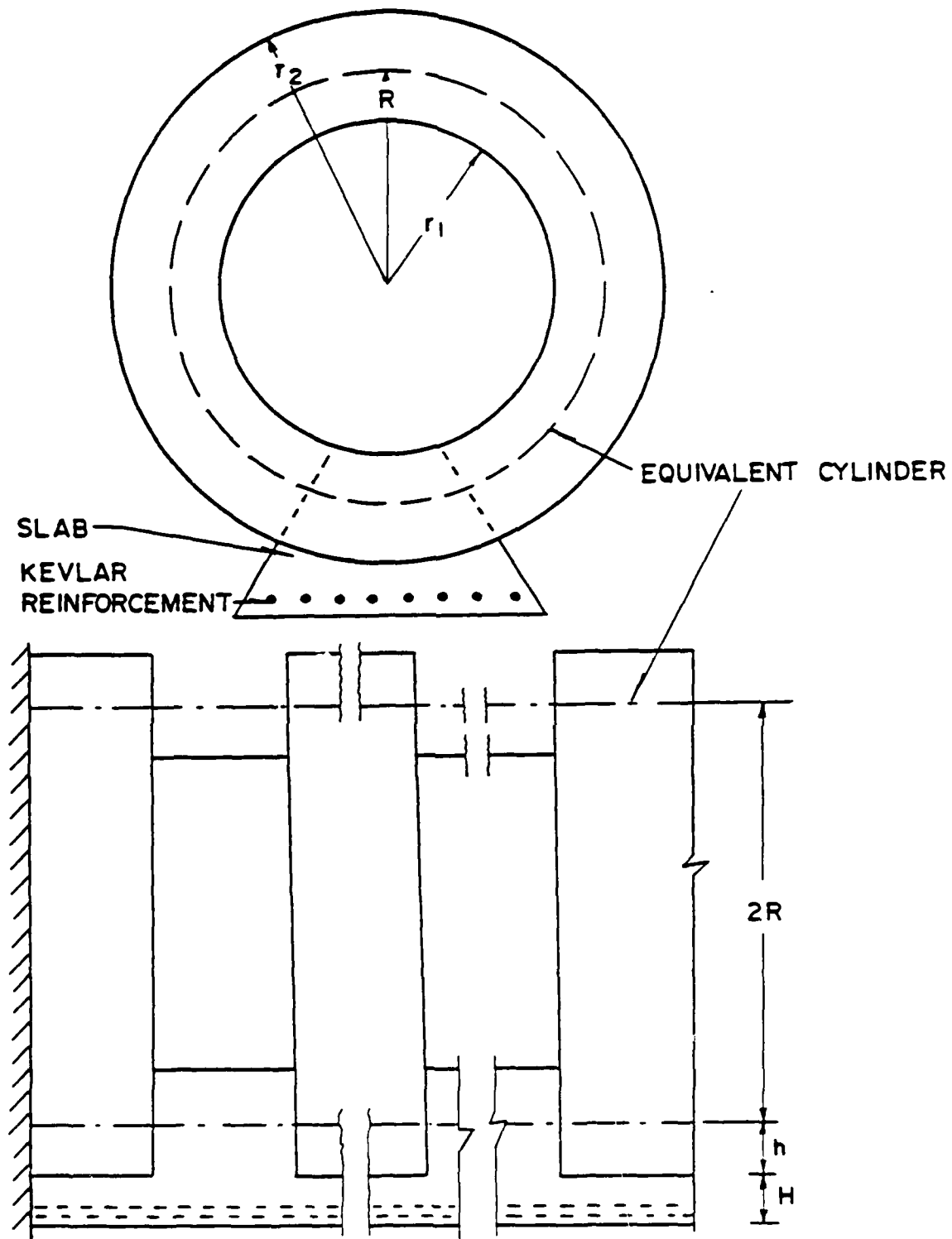
Figure 3.1 Cross section and elevation view of single-sided bellows with

kevlar reinforcement on the underside.
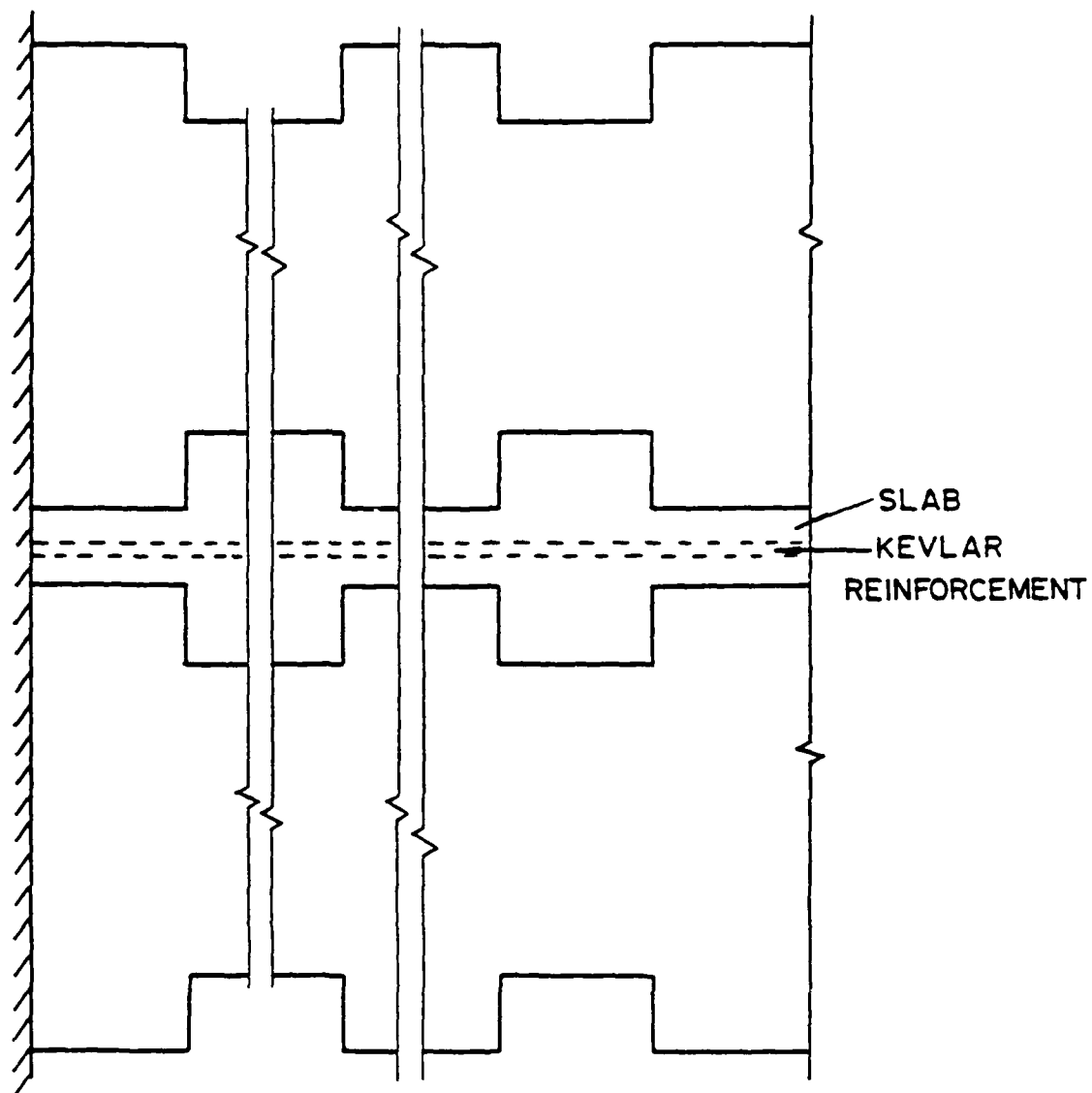
Figure 3.2 Elevation view of double-sided bellows with kevlar reinforcement, placed back-to back.
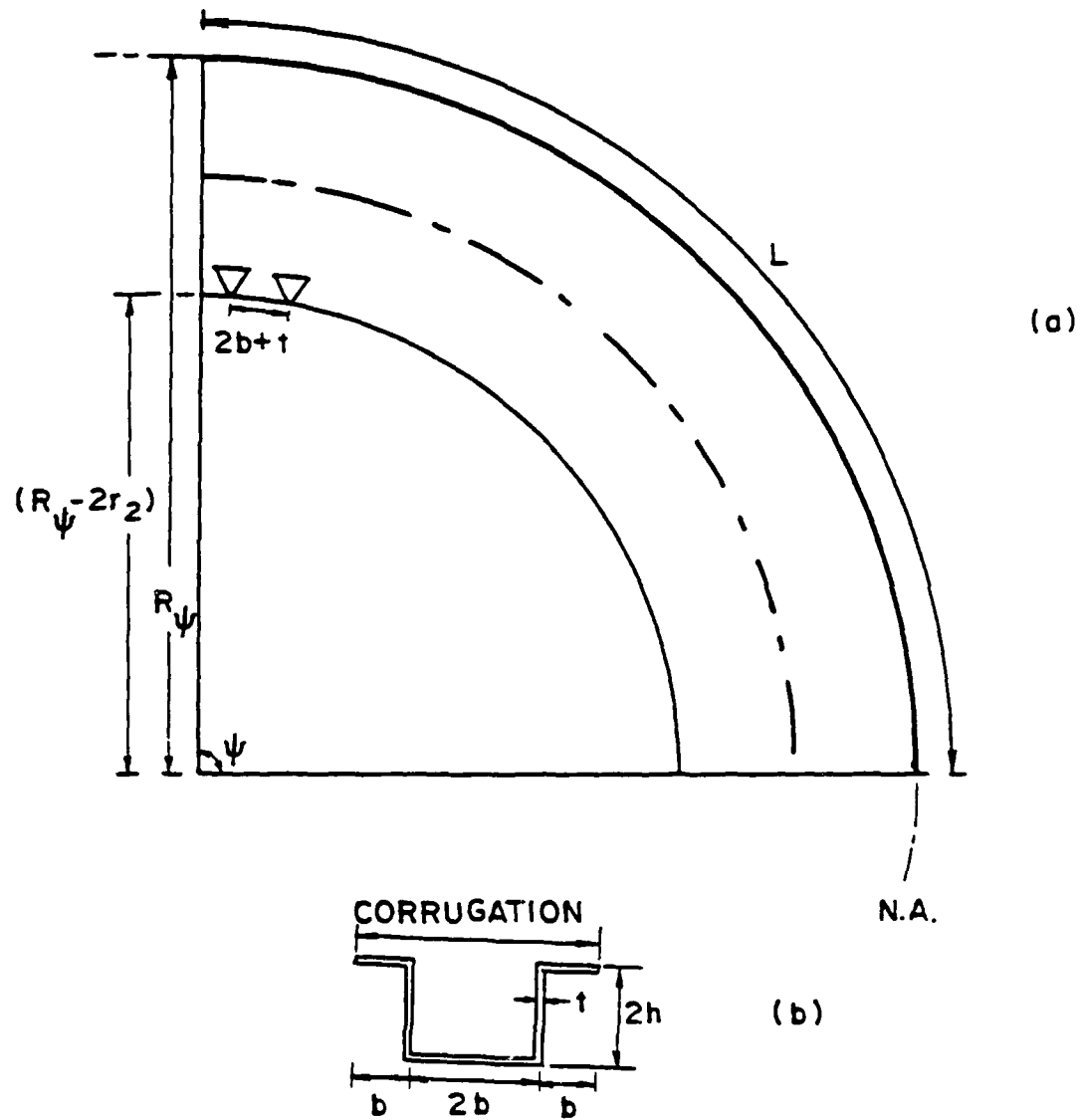
Figure 3.3 Criteria for gap size : corrugation gap away from neutral axis just closed (a); end view of a corrugation (b).

$$L = R_\psi \psi \tag{3.1}$$

$$(R_\psi - 2r_2)\psi = (2b + t)n \tag{3.2}$$

where

n is the number of corrugations

b is the one-fourth length of the corrugations

ψ is the maximum degree of bend of the element

t is the uniform thickness of the bellows

L is the length of the element

r_2 is the outer radius of the bellows

From Equations (3.1) - (3.2), it follows that

$$n = \frac{(\frac{L}{\psi} - 2r_2)\psi}{2b + t} \tag{3.3}$$

The second constraint is that the number of corrugations and the corrugation length should satisfy

$$(4b)n = L \tag{3.4}$$

The two unknowns n, b are solved simultaneously using Equations (3.3)-(3.4) yielding

$$n = \frac{\frac{L}{2} - 2r_2}{t}\psi \tag{3.5}$$

$$b = \frac{L}{4n} \tag{3.6}$$

The elements of the manipulator arm will be analyzed as a cantilever beam with an equivalent modulus E' (refer to Chapter II) and second area moment $\bar{I}$ of the composite single or double sided finger element.

The composite double sided element is symmetric about its neutral axis. Considering half of this section, we have the equivalent cylinder, slab and reinforcement as shown in Figure (3.1). For analysis purpose, we

consider only the equivalent cylinder, a flat slab of modulus E and two different types of reinforcement: n threads of modulus E_r and radius R_r, or rectangular reinforcement of modulus E_r, as shown in Figure (3.4).

For double sided finger elements with circular threads, the second area moment is

$$\bar{I} = 2\{\pi R^3 t_e + 2\pi R t_e (R + h + H)^2 + \frac{1}{3} d_1 H^3 + (\frac{E_r}{E} - 1)n(0.3927 R_r^4)\} \quad (3.7a)$$

For double sided finger elements with rectangular reinforcements

$$\bar{I} = 2\{\pi R^3 t_e + 2\pi R t_e (R + h + H)^2 + \frac{1}{3} d_1 H^3 + (\frac{E_r}{E} - 1) \frac{1}{3} s_1 h_1^3\} \quad (3.7b)$$

where the equivalent thickness of the corrugated tube is

$$t_e = t \frac{E'}{E} \quad (3.8)$$

B. Deflection Analysis

The manipulator arm is made up of a number of elements joined end to end. The function of the arm determines the size and number of elements in the arm. The cantilever beam analysis of a typical element with an equivalent stiffness $E\bar{I}$ is presented.

Large deflection is taken into account. Shear deformations are neglected. The shape of the elastic curve is found from the exact differential equation.

This cantilever is subjected to a coplanar terminal loading consisting of an axial compressive force P_ℓ, a transverse force P_b and a bending moment M_b. A floating coordinate system is chosen at the tip of the cantilever as shown in Figure (3.5a). In previous analysis of the elastica (Timoshenko and Gere, 1961), the only loading was an axial compressive force P_ℓ.
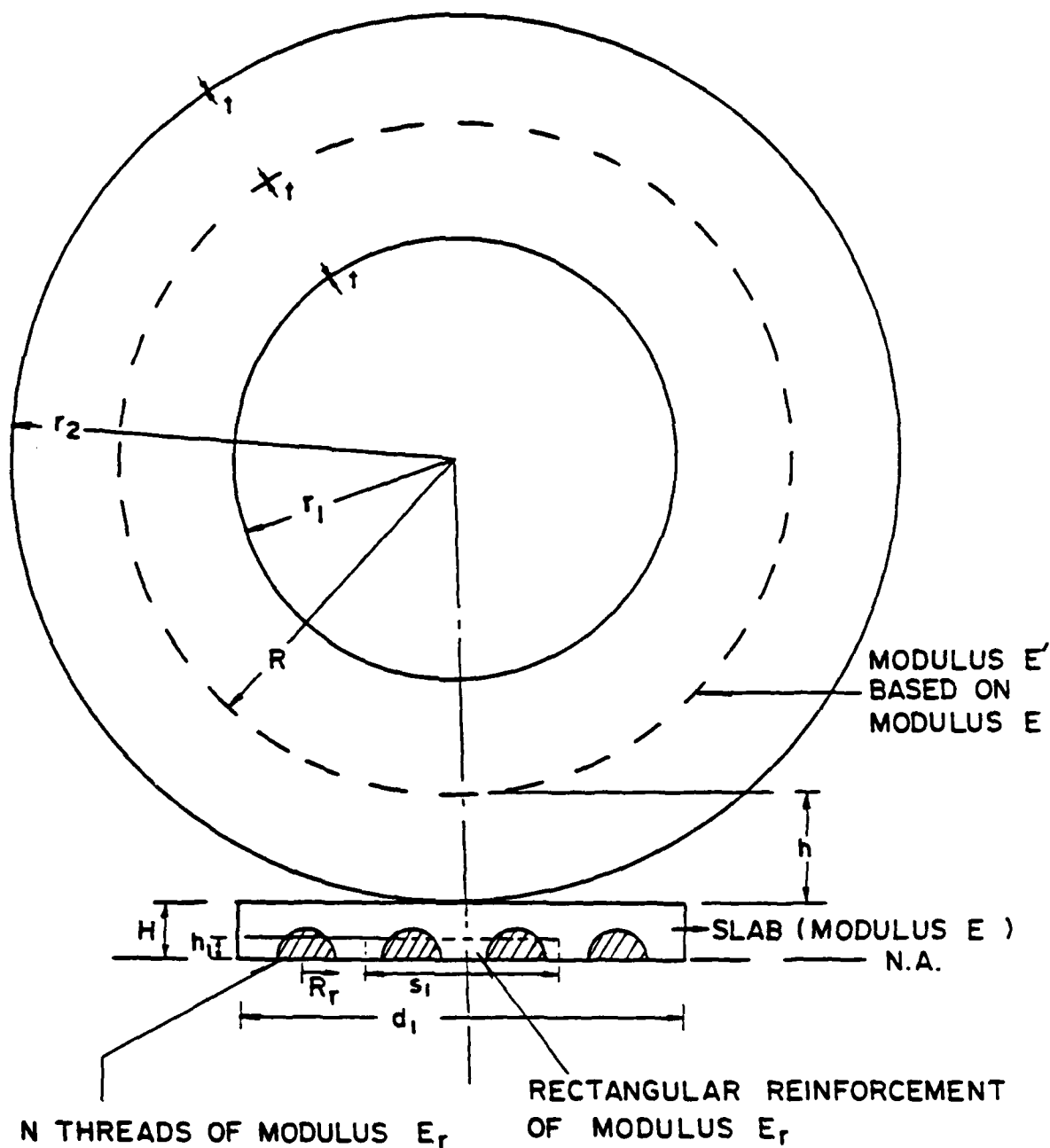
Figure 3.4 Cross section view of one-half of double-sided bellows used

for computing composite section moment of inertia.

(a)   (b)
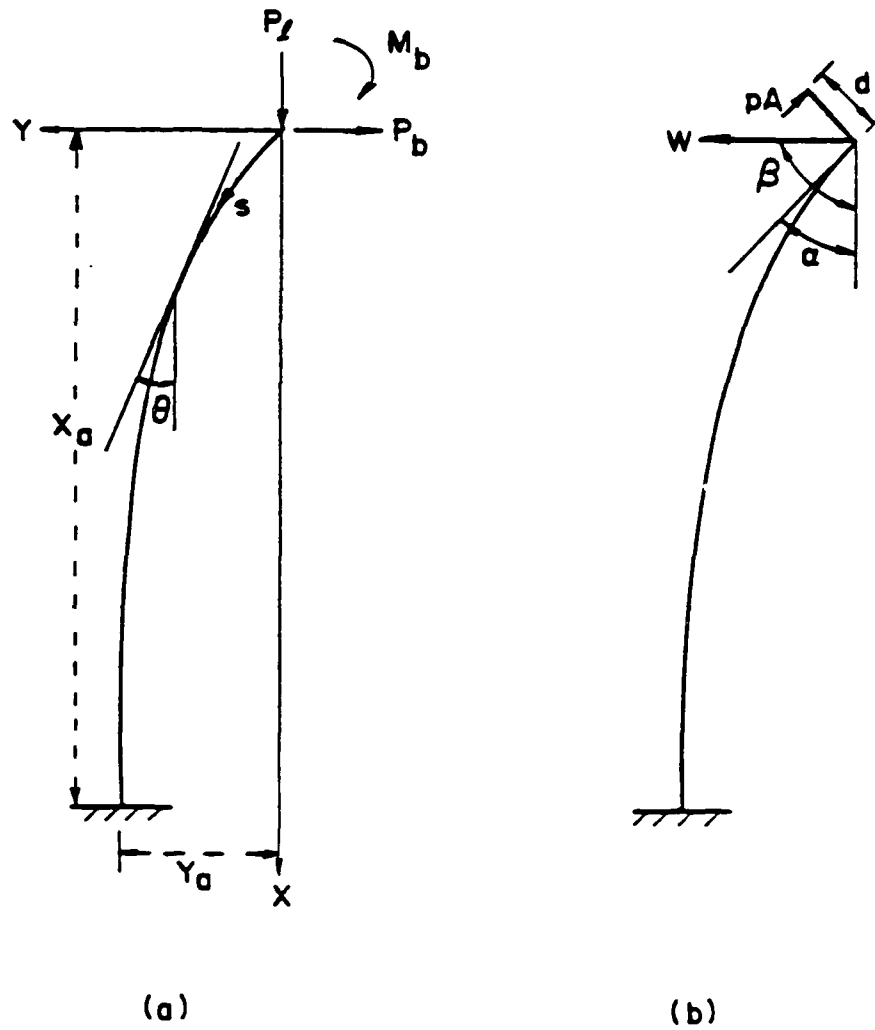
Figure 3.5 Cantilever deflection model with coordinate system at the
tip subjected to coplanar terminal loading (a); loading of
cantilever element (b).

The exact differential equation of the deflection curve is

$$M = - E\bar{I} \frac{d\theta}{ds} \tag{3.9}$$

where

$$\left|\frac{d\theta}{ds}\right| = \left|\frac{y''}{(1 + y'^2)^{3/2}}\right|$$

$$E\bar{I} \frac{d\theta}{ds} = - P_\ell y - P_b x - M_b \tag{3.10}$$

Differentiating Equation (3.10) with respect to s and using the relations

$$\frac{dy}{ds} = \sin \theta \qquad \frac{dx}{ds} = \cos \theta$$

we obtain

$$E\bar{I} \frac{d^2\theta}{ds^2} = - P_\ell \sin \theta - P_b \cos \theta \tag{3.11}$$

Integrating Equation (3.11) with respect to $\frac{d\theta}{ds}$ ds, we obtain

$$\frac{1}{2} E\bar{I} \left(\frac{d\theta}{ds}\right)^2 = P_\ell \cos \theta - P_b \sin \theta + K_1 \tag{3.12}$$

We solve for the constant K_1 from the edge condition: At $s = 0$, $\theta = \alpha$ and $\frac{d\theta}{ds} = - \frac{M_b}{E\bar{I}}$. Hence, Equation (3.12) reduces to

$$\frac{1}{2} E\bar{I} \left(\frac{d\theta}{ds}\right)^2 = P_\ell(\cos \theta - \cos \alpha) + P_b(\sin \alpha - \sin \theta) + \frac{1}{2} \frac{M_b^2}{E\bar{I}} \tag{3.13}$$

Since $\frac{d\theta}{dx}$ is known to be negative, Equation (3.13) can be rearranged as

$$ds = - [2 \frac{\bar{P_\ell}}{EI} (\cos \theta - \cos \alpha) + \frac{2 \bar{P_b}}{EI} (\sin \alpha - \sin \theta) + (\frac{\bar{M_b}}{EI})^2]^{-1/2} d\theta \quad (3.13a)$$

Integrating, nondimensionalizing and simplifying Equation (3.13a), we obtain

$$1 = \int_o^\alpha \frac{d\theta}{(A \cos \theta - B \sin \theta + c)^{1/2}} \quad (3.14)$$

where

$$A = 2 \bar{P_\ell}$$

$$B = 2 \bar{P_b}$$

$$C = -2\bar{P_\ell} \cos \alpha + 2 \bar{P_b} \sin \alpha + \bar{M_b}^2$$

$$\bar{P_\ell} = \frac{P_\ell \ell^2}{E\bar{I}}$$

$$\bar{P_b} = \frac{P_b \ell^2}{E\bar{I}}$$

$$\bar{M_b} = \frac{M_b \ell}{E\bar{I}}$$

Let $A \cos \theta - B \sin \theta = D \cos (\theta + \theta_0)$. Rearranging Equation (3.14), we obtain

$$1 = \int_o^\alpha \frac{d\theta}{[D \cos (\theta + \theta_0) + C]^{1/2}} \quad (3.15)$$

where

$$D = \sqrt{A^2 + B^2}$$

$$\theta_0 = \tan^{-1} \frac{B}{A}$$

Writing $\theta + \theta_0 = 2x$ and simplifying Equation (3.15) we obtain

$$1 = \frac{2}{(C + D)^{1/2}} \int_{\frac{\theta_0}{2}}^{\frac{\alpha + \theta_0}{2}} \frac{dx}{[1 - K^2 \sin^2 x]^{1/2}} \qquad (3.16)$$

where

$$K^2 = \frac{2D}{C+D}$$

Equation (3.16) represents an indefinite elliptic integral of the first kind. Note that K and θ_0 depends on the angle α and the loads. Solutions of this elliptical integral are available in tabulated form, given α, for pure lateral, longitudinal or moment loading.

Figure (3.5b) shows an element subjected to a pressure loading p over a uniform area $A(= \pi R^2)$ acting at a distance d and a dead weight W acting at an angle β.

Resolving these loads into its components, we obtain

$$P_\ell = -pA \cos \alpha + W \cos \bar{\beta} \qquad (3.17a)$$

$$P_b = pA \sin \alpha - W \sin \beta \qquad (3.17b)$$

$$M_b = pAd \qquad (3.17c)$$

An iterative procedure using the secant method and the IMSL subroutine DCADRE was written to compute the unknown angle α which is involved in the limits of Equation (3.16). A FORTRAN program CANT, whose listing is given in Appendix B, was written to invoke this procedure and to compute the shape of the elastic curve. The initial guess value of α is taken to be 0.

A numerical example for a typical element was computed. The length and stiffness of the element were chosen as $\ell = 1$ in and $\bar{EI} = 1$ lb in^2, respectively. The pressure loading acts at an eccentricity of 0.1 times the length. For increasing pressure loading, the corresponding values of the

eccentric end load P and the end moment M_b chosen are listed in Table (3.1).
The calculated deflection curves at these loads are shown in Figure (3.6).
The deflection pattern resembles that of the elastica. Table (3.1) shows the
tip angle α corresponding to each level of loading.

Eccentric end load P lb	End moment M_b lb-in	Calculated tip angle α deg.
0	0	0
2	0.2	16
4	0.4	41
6	0.6	78
8	0.8	124
10	1.0	173

Table 3.1 End loads and the corresponding tip angle for
$W = 0$, $\ell = 1$ in, $\overline{EI} = 1$ lb-in^2 and $d/\ell = 0.1$.
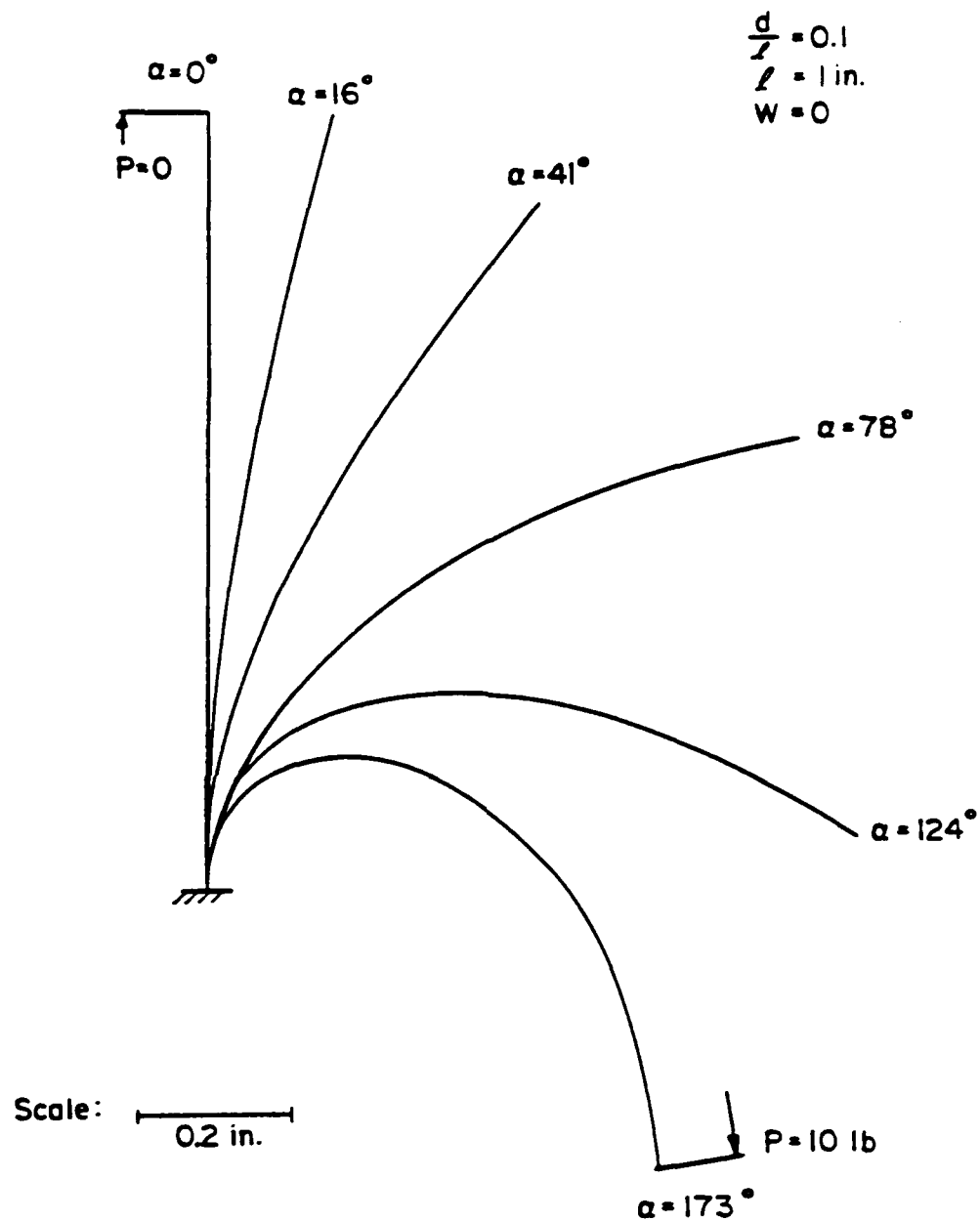
Figure 3.6 Elastic curve of the deflection pattern of the cantilever subjected to an increasing pressure together with the maximum angle at the tip.

4. ELEMENT STRINGS

A. Transformation Equations

The manipulator arm is made up of a number of elements connected by rigid links. One end of the arm is the supporting base of the cantilever beam while the last few elements near the tip act as a gripper or end effector. These tip elements grip the payload by coiling around it. The points of contact between the element and the load are sufficient to prevent the load from slipping. The rigid links do not bend. They merely translate and rotate.

Let the number of elements in the "lifting" arm be n and the elements numbered consecutively from the supporting base 1,2...n. Each element of the arm is modeled as a cantilever beam starting from the base. The end of the rigid link after element i is the fixed end of the cantilever beam for element i + 1. Given a coplanar terminal loading, we can calculate the end deflections of that element by the methods presented in the last chapter. Hence, we have determined the end coordinates of the element with respect to the local coordinate system.

Determining the position and orientation of any element in the arm relative to its base coordinate requires the transformation of coordinates

through all other elements and links between the base reference and the element whose coordinates are being determined. Similarly, by carrying out the transformation for each of the elements, we get the overall orientation of the "lifting" arm in the global coordinate system. Figure (4.1) shows a relation between the local and global coordinate system.

A transformation matrix relating the (i) frame to the (i+1) frame is of the form:

$$
\begin{bmatrix} X_{i,p} \\ \\ Y_{i,p} \end{bmatrix} = \begin{bmatrix} X_{i+1} \\ \\ Y_{i+1} \end{bmatrix} + \begin{bmatrix} \cos(\alpha_{i+1}) & \sin(\alpha_{i+1}) \\ \\ -\sin(\alpha_{i+1}) & \cos(\alpha_{i+1}) \end{bmatrix} \begin{bmatrix} X_{i+1,p} \\ \\ Y_{i+1,p} \end{bmatrix}
$$

where

α_{i+1} is the angle measured clockwise from frame (i) to frame (i+1).

X_{i+1}, Y_{i+1} are the coordinates of the origin of frame (i+1) in the coordinate system of frame (i).

$X_{i+1,p}, Y_{i+1,p}$ are the coordinates of any point P in frame (i+1).

$X_{i,p}, Y_{i,p}$ are the coordinates of the same point P in frame (i).

A FORTRAN program TRANS, whose listing is given in Appendix C, models each lifting element as a cantilever beam in the local coordinate system. The slope computed at the tip of element i is the angle α_{i+1} which is used to transform the element (i+1) from its local coordinate system to that of element i. The position of the tip of the element in the local coordinate system is then computed. Provision is made for the transformation between an element and the link before it. As the link is rigid, the angle α_{i+1} is zero degrees. The transformation matrix relating the tip of element i and the base reference is the product of all matrices relating the elements and the links
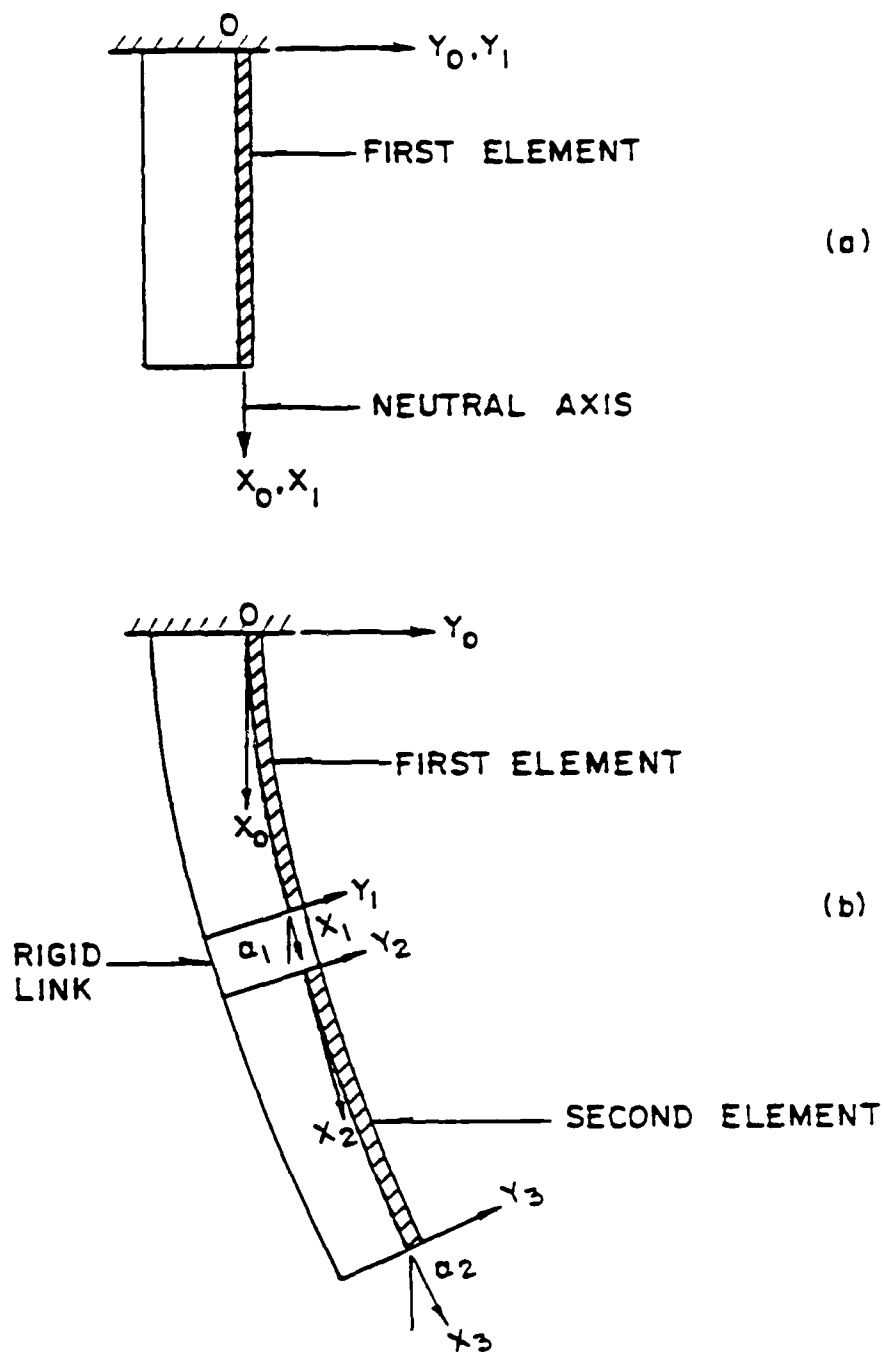
Figure 4.1 First element showing coincidence of local and global axes

(a); rigid link showing translation and second element show-

ing displaced local axis (b).

between them. Hence, the program TRANS determines the position of the tip of each lifting element of the arm in the global coordinate system.

B. Typical Design

Figure (4.2) shows the motion of a manipulator arm. Double or single sided elements could be used as the structural section of the elements. The stiffness of double sided elements were derived in part A of Chapter III. The advantage of double sided elements is that they may bend the arm in either the clockwise or counter clockwise direction. For instance, if the elements on the left side are pressurized, the arm will bend in the counter clockwise direction.

Given a destination coordinate in the feasible work space, we want to know a pressure history in all the elements that will move the load from the starting to the given destination coordinate. Note that there are many possible solutions or different pressure histories that could achieve the same result. The solution procedure described below picks a solution that may not necessarily be the one where the payload tranverses the least path distance to achieve its target point. Mahajan (1985) investigated the problem of optimal paths.

The end effector is designed separately. The number of these elements is determined by the length of the element and the size of the object to be lifted. The end effector bends in the opposite direction to that of the lifting arm. The angle θ_1 to which these end effector elements should coil around the load to prevent it from slipping is determined by a simple geometrical drawing. The slope α at the end of each of these elements is

$$\alpha = \frac{\theta_1}{N_e} \tag{4.1}$$
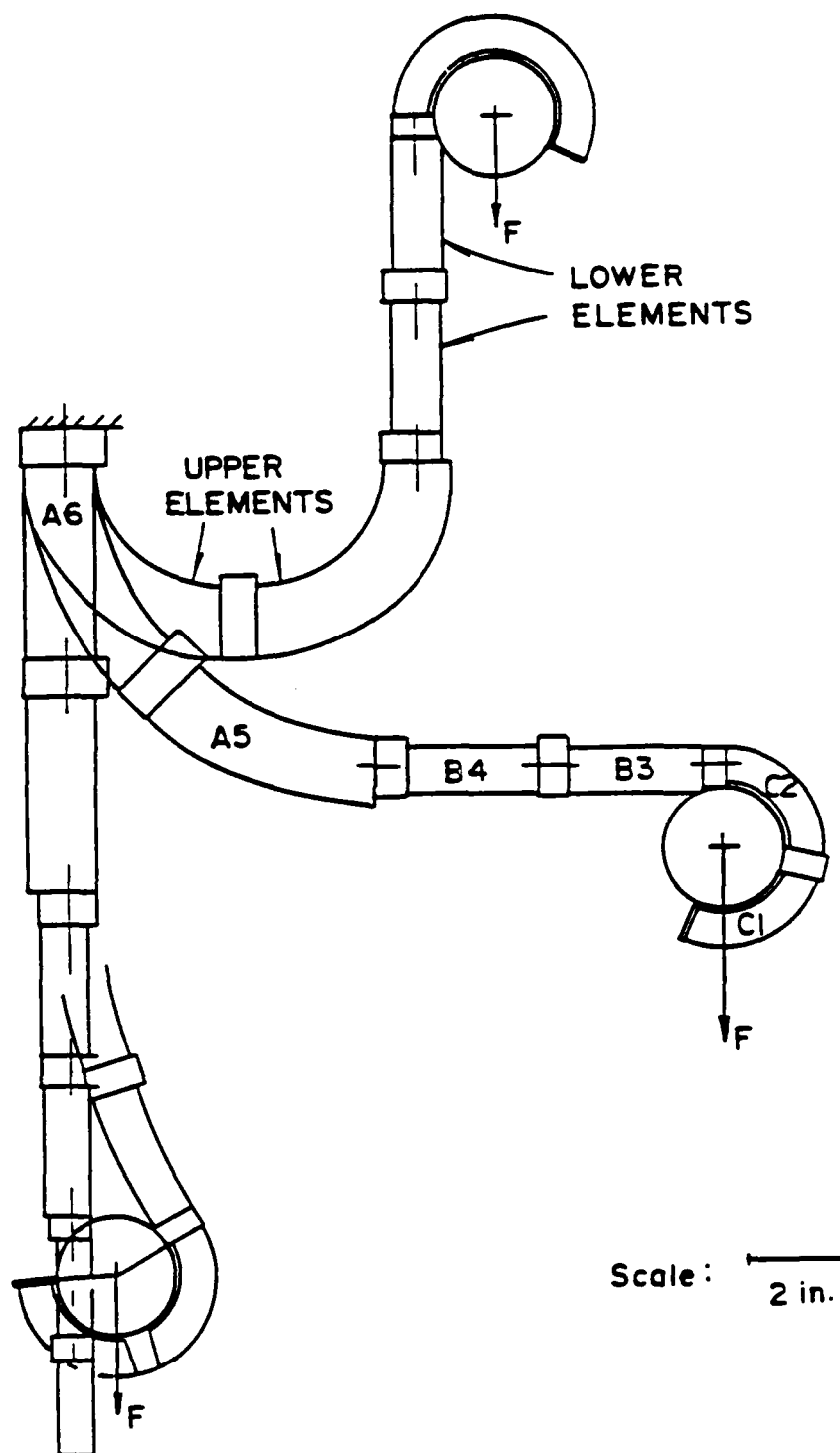
Figure 4.2 One possible trajectory of a six SIMRIT finger arm consisting of three different types of elements.

where N_e is the number of end effector elements. Then, using the program CANT, we make runs of varying pressure levels. Since we do not know the point of contact between the load and the end effector elements, we assume the worst case or the case of highest moment. That is

$$\beta = 180° - \alpha \qquad (4.2)$$

$$M_0 = W(R_\ell + 2R + d + H) \qquad (4.3a)$$

$$M_0 = W R_\ell \qquad (4.3b)$$

The moment expressions in Equations (4.3a) - (4.3b) are for the double and single sided elements respectively. Hence, the pressure history in the end effector elements is determined by that pressure level whose slope at the tip of the element is closest to α.

The lifting elements are designed as an element string. Initially, the moment due to the payload is assumed to be zero. Referring to Figure (3.5b), the angle β at which the load acts is updated from the slopes of all the previous elements. For the ith element, the angle β is given by

$$\beta_i = 180° - \sum_{k=1}^{i-1} \alpha_k \qquad i=2,3...n \qquad (4.4a)$$

$$\beta_1 = 180° \qquad (4.4b)$$

Then, for a given set of internal pressures in each of the elements, we compute the position of the tip of the element in the global coordinate system using the transformation matrices developed in part A. Knowing the geometry of the link joining the lifting elements to the end effector and the radius of the load, we can compute the coordinates of the load. Referring to Figure (4.3), we compute the coordinates of the load as follows.

$$R_{TPL} = 2 R_B + H + R_L \qquad (4.5)$$

$$\phi = \tan^{-1} \frac{X_L}{R_L + Y_L} \qquad (4.6)$$
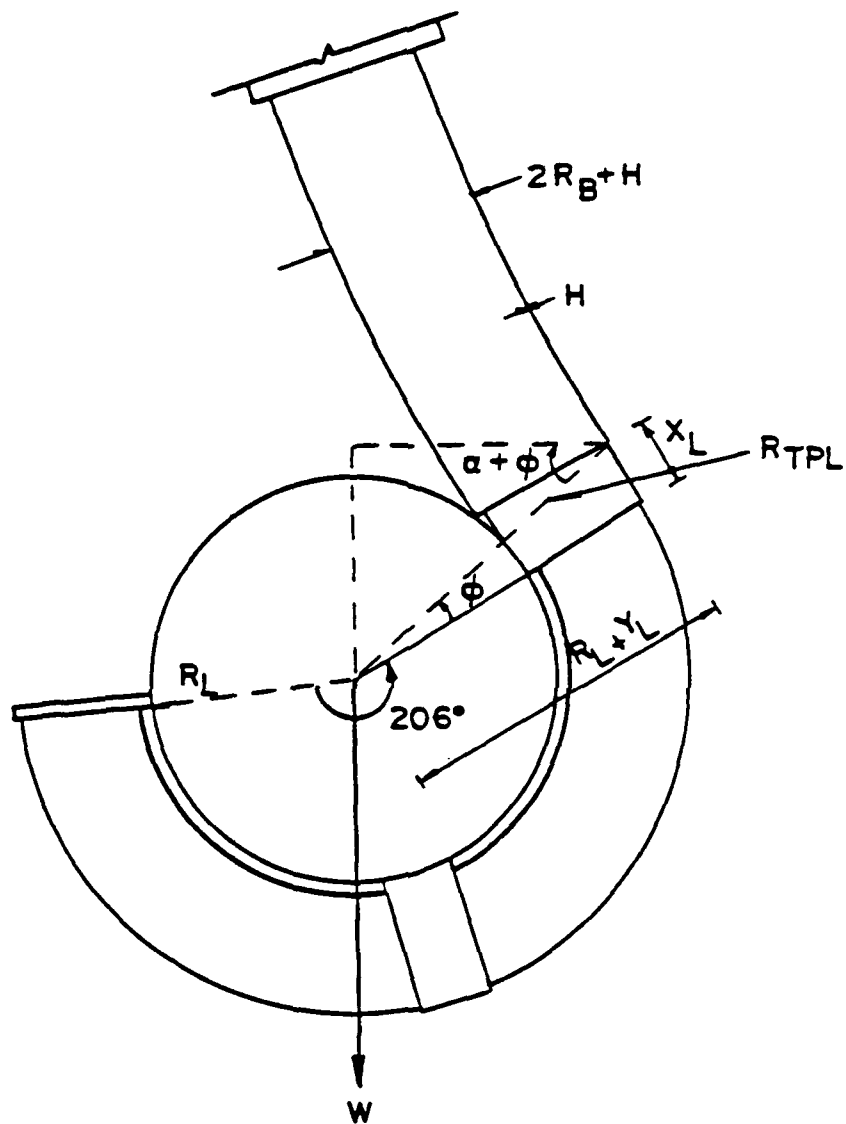
Figure 4.3 Deriving relations between the tip of the lifting elements and the coordinates of the center of the load.

$$Gx = \text{x-coordinate of } n^{th} \text{ element} + R_{TPL} \sin\left(\sum_{k=1}^{n} \alpha_k + \phi\right) \qquad (4.7)$$

$$Gy = \text{y-coordinate of } n^{th} \text{ element} - R_{TPL} \cos\left(\sum_{k=1}^{n} \alpha_k + \phi\right) \qquad (4.8)$$

Knowing the coordinates of the load, we can compute the moment due to the load acting on each element. The entire procedure is repeated. The following inequalities must be simultaneously satisfied for the specified tolerance limit δ.

$$|Gx_{current} - Gx_{earlier}| < \delta \qquad (4.9)$$

$$|Gy_{current} - Gy_{earlier}| < \delta \qquad (4.10)$$

The iteration stops when both the inequalities are satisfied. Hence, for a given set of pressures, we can compute the global element deflections of the manipulator arm.

A systematic procedure is adopted to vary the pressure in the elements to move the load from the initial or present coordinates of the load (X_p, Y_p) to the destination coordinates (X_f, Y_f). The present position of the load can be in any one of the four regions, as shown in Figure (4.4). With reference to Figure (4.2).

    i) The load is in the upper-right region, or

        $X_p < X_f$

        $Y_p > Y_f$

        Then decrease the pressure in all the elements.

    ii) The load is in the upper-left region, or

        $X_p < X_f$

        $Y_p < Y_f$

        Then decrease the pressure in the lower elements.
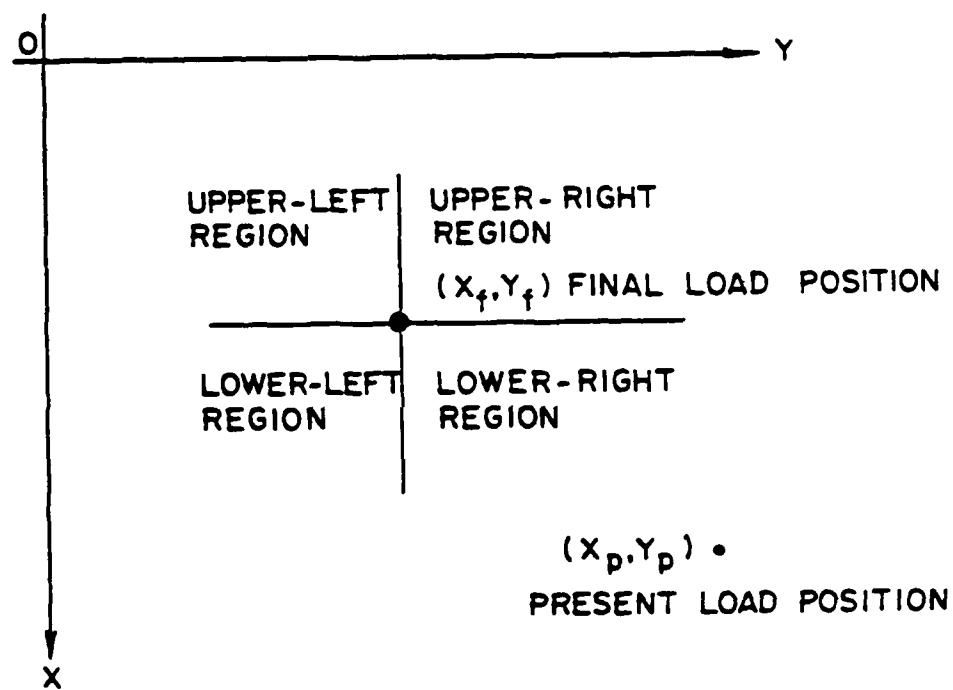
Figure 4.4 The four possible regions in which the load could be presently positioned.

iii)   The load is in the lower-right region, or

$$X_p > X_f$$

$$Y_p > Y_f$$

Then increase the pressure in the lower elements.

iv)   The load is in the lower-left region, or

$$X_p > X_f$$

$$Y_p < Y_f$$

Then increase the pressure in all the elements.

The iteration procedure is repeated until the following conditions are satisfied:

$$|X_p - X_f| < \epsilon_1 \qquad\qquad (4.11)$$

$$|Y_p - Y_f| < \epsilon_2 \qquad\qquad (4.12)$$

where ϵ_1 and ϵ_2 are specified tolerance limits.

C. Numerical Results

The manipulator arm shown in Figure (4.2) is composed of six single-sided SIMRIT finger elements connected by rigid links. The first four elements are the lifting elements while the last two form the end effector. There are three different types of elements A, B and C. Figure (4.5) shows a cross section through the SIMRIT finger. Table (4.1) summarizes the geometry for these elements. The object to be lifted is a cylinder of radius 1.25 in. and weighing 0.5 lb. The stiffness $\overline{EI}$ for these elements were derived by Wilson (1986) and calculated by Walker (1986).

From a scale drawing, refer to Figure (4.3), we note that the tip angle relative to its own base for the last 2 elements (type C) is 206°. In addition to the geometry of this element, the other input parameters to the program CANT are
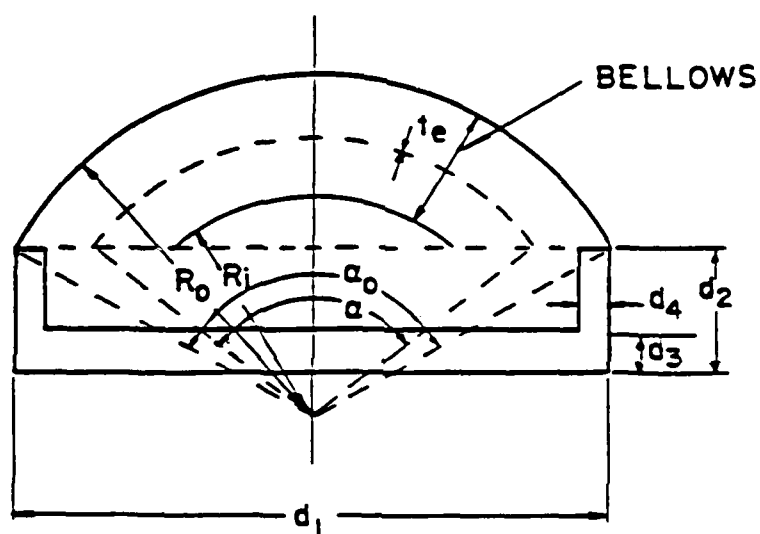
Figure 4.5 Cross section through a SIMRIT finger showing the geometry

Dimension (unit)	Size A	Size B	Size C
b (in)	0.1150	0.0828	0.0603
d_1 (in)	1.563	1.063	0.8000
d_2 (in)	0.7087	0.4930	0.3260
d_3 (in)	0.2314	0.1882	0.1380
d_4 (in)	0.0948	0.0694	0.0700
h (in)	0.1745	0.1286	0.0960
L (in)	3.875	2.688	1.730
R (in)	0.6875	0.4625	0.2550
t (in)	0.0943	0.0826	0.0700
α (rad)	2.950	2.827	3.013
y_p (in)	0.7156	0.4875	0.3133
A_p (in^2)	1.296	0.5366	0.2150
$\bar{I}$ (in^4)	0.3700	0.0730	0.0150
E' (lb/in^2)	137.2	189.7	240.9
E (lb/in^2)	2120.	2120.	2120.
$\bar{EI}$ (lb-in^2)	50.77	13.92	3.640

Table 4.1 Geometry for three different types of SIMRIT finger elements.

$$\beta = 77°$$
$$M_0 = -0.656 \text{ lb-in}$$
$$W = 0.5 \text{ lb.}$$

The pressure loading that corresponds to a maximum slope of 103° is 37.2 psi.

The lifting elements are analyzed using the program TRANS. The first two elements are of type A while the other two are of type B. Initially, the moment due to the load is assumed to be zero in all of the elements. Noting that the rigid link does not bend (i.e. $\alpha = 0°$), the transformation matrix is given as input data. Each of the other elements is modeled as a cantilever beam in its local axis and the corresponding transformation matrix is computed. The subroutine TRANS is then invoked to obtain the coordinates of the tip of each lifting element in the global coordinate system. Then, using Equations (4.5) - (4.8), the coordinates of the center of gravity of the load is computed. The moment due to the load is then updated. The iteration continues till the conditions given in Equations (4.9) - (4.10) are satisfied. In addition to the geometry of the two elements, the other input parameters to the program TRANS are

$$R_L = 1.25 \text{ in.}$$
$$X_L = 0.5 \text{ in.}$$
$$Y_L = 0.75 \text{ in.}$$
$$H = 0.1 \text{ in.}$$

The results of the computation is summarized in Table (4.2). The trajectories corresponding to the pressure loading shown in Table (4.2) are plotted in Figure (4.6).

The program TRANS can handle many different options. An element in the arm may or may not be pressurized. The elements can be of varying geometry. However, for large nondimensional pressure parameters ($\bar{P}_\ell$, $\bar{P}_b > 10$)

Curve	Pressure p(psi)		Global cood. of load (in)		Global tip cood. of element (in)							
					A6		A5		B4		B3	
	Type A	Type B	x	y	x	y	x	y	x	y	x	y
A	0.0	0.0	13.67	-2.28	2.79	0.01	6.45	-0.01	9.76	-0.16	13.06	-0.09
B	0.77	1.86	14.83	1.26	2.87	0.05	6.56	0.28	9.83	0.70	12.77	2.22
C	1.54	3.73	13.65	4.79	2.87	0.10	6.54	0.53	9.65	1.51	11.50	4.21
D	3.09	7.45	8.03	8.15	2.87	0.22	6.45	1.06	8.75	3.12	7.59	5.92
E	6.17	14.91	1.50	2.38	2.82	0.50	6.03	2.25	5.70	4.63	3.66	3.07

Note: Type C has constant pressure of 37.2 psi in all configurations.

It is the end effector coiling around a cylinder of radius 1.25 in.

It coils in a reverse curvature to that of the lifting elements.

Table 4.2 Tip coordinates of the lifting elements and the load in the global coordinates when subjected to different pressures.
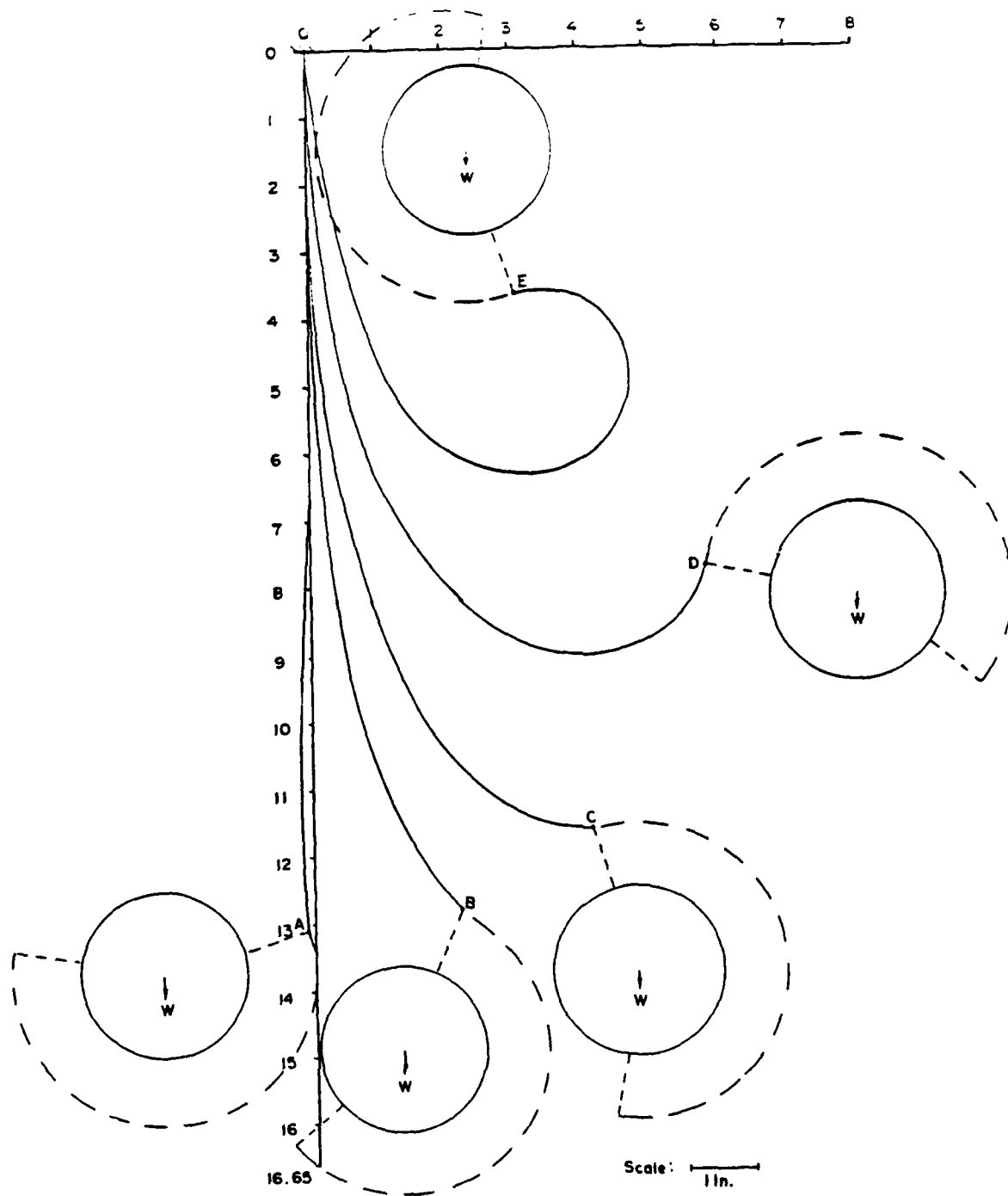
Figure 4.6 Calculated trajectory of a six SIMRIT finger arm consisting of three different types of elements with pressure history as in Table 4.2.

the results of this program should be used cautiously as numerical instability may occur. This needs further investigation.

Using the systematic procedure described in part B, one possible pressure loading to lift the load to a vertical position (-0.3, 7.2) is

Element	Pressure (psi)
A6	9.26
A5	9.26
B4	7.45
B3	7.45
C2	37.20
C1	37.20

5. CONCLUSIONS AND DISCUSSION

The design curves for stiffness vs. the nondimensional parameter λ was found to be within ± 6% of that predicted by the Haringx model. In his paper, Wilson (1984-b), has shown that the Haringx model correlates well with that of the experimental data.

The elastic curve of the deflection pattern of the cantilever subjected to an increasing pressure loading was found to resemble that of the elastica. The elastica problem (Timoshenko and Gere, 1961), in which only the longitudinal loads were considered, were verified using this model.

The calculated trajectories of a six SIMRIT finger arm subjected to increasing pressure histories are shown. These trajectories represent feasible equilibrium positions of the arm. The actual position of the arm in the global coordinate system will be verified by experiment in due course.

There are several possible extensions of this research. The numerical example shown in Chapter IV consists of single sided elements with the neutral axis for all the lifting elements on the same side. In this configuration, the arm can move only in the counter clockwise direction through 180° in the same plane. To achieve reversal of curvature, we could either pressurize double sided elements judiciously or have the neutral axis for part of the arm on one side and for the remaining part of the arm on the opposite side. With the reversal of curvature, the arm could move ± 180° in the same plane. The mathematical model for plane motion can be extended to include out-of-plane motion. This can be achieved by arranging the bellows in a satellite
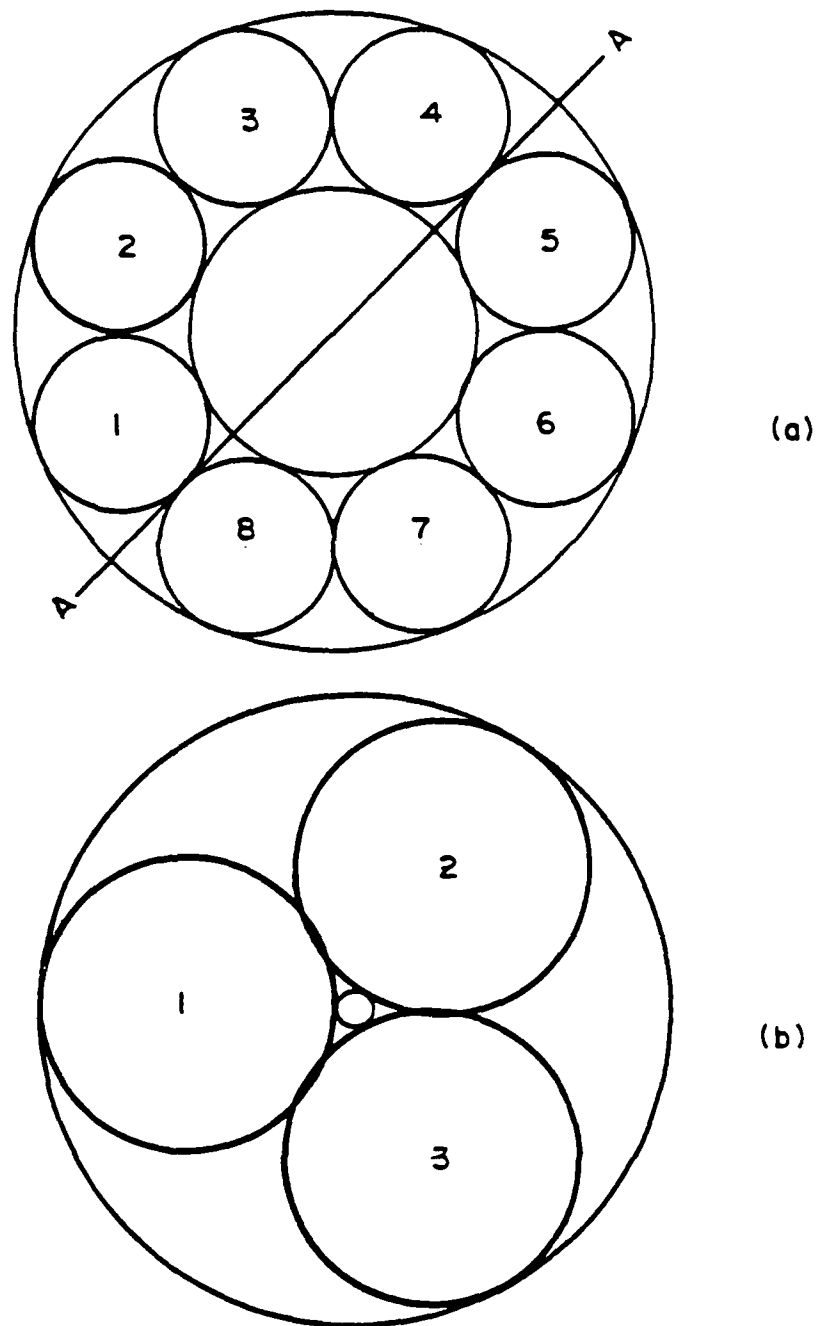
Figure 5.1 Satellite arrangement of bellows in an element : an even arrangement -eight (a); an odd arrangement -three (b).

configuration as shown in Figure (5.1). In the case of an even number of the bellows (Figure (5.1a)), we can pressurize the bellows (1,2,3,4) to achieve bending about the axis A-A. Hence, the flexible arm can have a work space consisting of volume of revolutions in each of the four quadrants.

Provision is made in the program TRANS to include the self weight of the element. The self weight of the element is assumed to be a concentrated mass acting in the direction of gravity at the tip of the element.

A 'Learning Program' was developed by (Mahajan, 1985) to vary the pressure in a systematic way to achieve rapid convergence to the destination coordinate. In his model, only the end moment was considered. Mahajan's program could be extended to include the mathematical model presented in Chapter IV, a model that includes end moment, longitudinal and transverse loading.

Computational efficiency could be improved. The numerical instability that occurs in the program TRANS *for nondimensional pressure loading of* $\bar{P}_\ell >$ 10 or $\bar{P}_b > 10$ could be overcome. In addition, the number of iterations required to compute the tip angle α in Equation (3.16) may be reduced. We could form a data base for the three different nondimensional loading parameters $\bar{P}_\ell$, $\bar{P}_b$ and $\bar{M}_b$. The angle α should lie between $0°$ and $180°$. For a particular combination of $\bar{P}_\ell$, $\bar{P}_b$ and $\bar{M}_b$, we can store that value of α which satisfies Equation (3.16). Hence, the program TRANS can pick the right angle α from this data base without having to perform the numerous iterations.

Another bending geometry that could be investigated is that of a tapered section, with the broader end at the supporting base. This could be an optimal bending geometry since the moment arm due to the load will be higher at the supporting base, decreasing towards the gripper. Such tapered configurations would have a much higher payload to self weight ratio than uniform configurations.

REFERENCES

Bisshopp, K. E. and Drucker, D. C., "Large Deflection of Cantilever Beams," Quart. of Appl. Math., 3-272 (1945).

Calladine, C. R., "Flexibility of Axially Symmetric Bellows under Axial Loading," Int. J. Mech. Sci., 16, 843 (1974).

Critchlow, A. J., Introduction to Robotics, MacMillan Publishing Company, New York.

Donnell, L. H., "The Flexibility of Corrugated Pipes Under Longitudinal Forces and Bending," ASME Trans. J. Appl. Mech. APM-54-7, 69 (1932).

Haringx, J. A., "Instability of Bellows Subjected to Internal Pressure," Philips Res. Rep. 7, 189 (1952).

Lewis, G. and Monasa, F., "Large Deflections of Cantilever Beams of Non-Linear Materials of the Ludwick Type Subjected to an End Moment, Int. J. Non-Lin. Mech., 17-1-1 (1982).

Mahajan, U., "Mechanics of a Continuous Manipulator Made of a Nonlinear Composite Material," M.S. Thesis, Duke Univ., (1985).

Scott, E. J. and Carver, D. R., "Nonlinear Differential Equation for Beam Deflection," ASME App. Mech. 54-A-35 (1953).

Theocaris, P. S. and Panayotounakos, D. E., "Exact Solution of the Non-Linear Differential Equation Concerning the Elastic Line of a Straight Rod due to Terminal Loading," Int. J. Non-Lin. Mech., 17-5/6-395 (1982).

Timoshenko and Gere, "Theory of Elastic Stability," Eng. Soc. Monographs, McGraw-Hill Book Company, 76-82 (1961).

Walker, T., "Analysis of a Six-Finger Arm," Senior Independent Study, Dept. of Civil & Environ. Eng., Duke Univ., (1986).

Wilson, J. F., "Robotic Mechanics and Animal Morphology," NATO ASI Series, Vol. F11, Robotics and Artificial Intelligence, Springer-Verlag Berlin Heidelberg, (1984a).

Wilson, J. F., "Mechanics of Bellows: A Critical Survey," Int. J. Mech. Sc., Vol. 26, No. 11/12, 593-605, (1984b).

Wilson, J. F. "Material Properties and Mechanics of Pneumoelastic Bending Elements," Lord Company Report, (1986).

APPENDIX A

COMPUTER PROGRAM FOR THE COMPUTATION OF REDUCED MODULUS

```
        real a(10,10),x(10),y(10),mu,Mr1c,Mr2c,Mr1p,Mr2p
        real c(10,10),f,eps,cmax,temp(10),w,lambda
        integer s(10)

c       Input and output file declarations.

        OPEN(7,FILE='SHE.DAT')
        OPEN(8,FILE='SHE.OUT')

c       Read in axial load and internal pressure on bellows.

        read(7,1)F0,p
        write(8,3)F0,p
3       format(//' Axial load=',F10.4/' Pressure=',F10.4//)

c       Read in Young's Modulus and Poisson's ratio.

        read(7,1)E,mu
        write(8,21)E,mu
21      format(' Youngs Modulus='F10.4/' Poiss.ratio=',F10.4)

c       Read in number of intervals along plate, inner and outer
c       cylinders at which deflections are desired.

        read(7,22)int
        write(8,23)int
23      format(/' Interval at which defln. is desired=',I4//)

c       Read in mean radius.

        read(7,1)Rm
        write(8,43)Rm
43      format(/' Mean radius=',F10.4//)

c       Loop to control variations in depth of corrugation.

        do 100 kk=1,2

c       Read in half depth of corrugation.

        read(7,1)h
        r1=Rm-h
        r2=Rm+h
        write(8,4)r1,r2
4       format(/' Inner cyl. radius=',F10.4/' Outer cyl. radius=',F10.4)

c       Loop to control variations of corrugation length.

        do 101 jj=1,5

c       Read in one-forth length of corrugation.

        read(7,1)b
        write(8,10)b
10      format(/' Half lenth of cyl.=',F10.4)

c       Thickness of plate and cylinders is assumed to be the same.

c       Loop to control variations in cylinder thickness.
```

```
        do 102 ii=1,7
c       Read in cylinder thickness.
```

```
        read(7,1)tc
        tp=tc
        write(8,20)tp,tc
20      format(/' Thick. of plate=',F10.4/' Thick. of shell=',F10.4)
22      format(20I4)
1       format(6F10.4)

c       Number of unknown constants of integration is 6.

        n=6
        ratio=r2/r1
        do 12 i=1,n
        do 12 j=1,n
12      A(i,j)=0.0

c       Compute the known constant and other parameters to be used
c       in the formulation of the linear system.

        Qr2=(FO-3.14159*r2*r2*p)/(2*3.14159*r2)
        Dp=E*tp*tp*tp/(12*(1-mu*mu))
        Dc=E*tc*tc*tc/(12*(1-mu*mu))
        c3=r1*r1*r2/Dp*(r2*p/8-Qr2/4)
        B1=sqrt(sqrt(E*tc/(4*r1*r1*Dc)))
        B2=sqrt(sqrt(E*tc/(4*r2*r2*Dc)))

c       Formulation of the 6 x 6 simultaneous linear system.

        y(1)=p*r1*r1/(E*tc)
        y(2)=p*r2*r2/(E*tc)
        temp1=-r1*r1*r1*p/16
        y(3)=temp1/Dp+c3/r1
        y(4)=(3+mu)*(temp1/r1+Dp*c3/(r1*r1))
        temp2=-r2*r2*r2*p/16
        y(5)=temp2/Dp+c3*r2/(r1*r1)*(1+2*log(r2/r1))
        temp3=r2*r2*p*(3+mu)/16
        temp4=c3*Dp/(r1*r1)*((3+mu)+2*(1+mu)*log(r2/r1))
        y(6)=temp3-temp4
        bb1=B1*b
        bb2=B2*b
        a(1,1)=sin(bb1)*sinh(bb1)
        a(1,2)=cos(bb1)*cosh(bb1)
        a(2,3)=sin(bb2)*sinh(bb2)
        a(2,4)=cos(bb2)*cosh(bb2)
        a(3,1)=B1*(sin(bb1)*cosh(bb1)+cos(bb1)*sinh(bb1))
        a(3,2)=B1*(cos(bb1)*sinh(bb1)-sin(bb1)*cosh(bb1))
        a(3,5)=-1/r1
        a(3,6)=-2/r1
        a(4,1)=2*Dc*B1*B1*cos(bb1)*cosh(bb1)
        a(4,2)=-2*Dc*B1*B1*sin(bb1)*sinh(bb1)
        a(4,5)=Dp/(r1*r1)*(1-mu)
        a(4,6)=-2*Dp/(r1*r1)*(1+mu)
        a(5,3)=-B2*(sin(bb2)*cosh(bb2)+cos(bb2)*sinh(bb2))
        a(5,4)=-B2*(cos(bb2)*sinh(bb2)-sin(bb2)*cosh(bb2))
        a(5,5)=-1/r2
        a(5,6)=-2*r2/(r1*r1)
        a(6,3)=-2*Dc*B2*B2*cos(bb2)*cosh(bb2)
        a(6,4)=2*Dc*B2*B2*sin(bb2)*sinh(bb2)
        a(6,5)=-Dp/(r2*r2)*(1-mu)
        a(6,6)=2*Dp/(r1*r1)*(1+mu)

        do 40 i=1,n
        s(i)=i
```

```
            x(i)=y(i)
            co 40 j=1,n
40          c(i,j)=a(i,j)
            eps=1e-15

c           Call subroutines lr and rb to solve the 6 x 6 simultaneous equations.

            call lr(c,n,s,eps,sucess)
            call rb(c,n,s,x)

c           Re-order solution vector x.

            do 47 i=1,n
47          temp(i)=x(s(i))
            do 48 i=1,n
48          x(i)=temp(i)
            write(8,6)(x(i),i=1,n)
6           format(//' The constants A1,B1,A2,B2,C1,C2 are resp.:'//6d13.6)

c           Compute slope and moment at junctions between plate and
c           inner and outer cylinders.

            Thetac1=x(1)*a(3,1)+x(2)*a(3,2)
            Thetac2=x(3)*a(5,3)+x(4)*a(5,4)
            Thetap1=2/r1*x(6)+x(5)/r1+y(3)
            Thetap2=2*r2*x(6)/(r1*r1)+x(5)/r2+y(5)
            Mr2c=x(3)*a(6,3)+x(4)*a(6,4)
            Mr1c=x(1)*a(4,1)+x(2)*a(4,2)
            Mr1p=y(4)-a(4,6)*x(6)-a(4,5)*x(5)
            Mr2p=y(6)-a(6,6)*x(6)-a(6,5)*x(5)
            write(8,25)Mr1c
25          format(//,' Moment Mr1c at r=r1 of inner cylinder',F10.4)
            write(8,26)Mr2c
26          format(/,' Moment Mr2c at r=r2 of outer cylinder',F10.4)
            write(8,27)Thetac1
27          format(/,' slope Thetac1 at r=r1 of inner cylinder',F10.4)
            write(8,28)Thetac2
28          format(/,' slope Thetac2 at r=r2 of outer cylinder',F10.4)
            write(8,29)Thetap1
29          format(/,' slope Thetap1 at r=r1 of plate',F10.4)
            write(8,30)Thetap2
30          format(/,' slope Thetap2 at r=r2 of plate',F10.4)
            write(8,31)Mr1p
31          format(/,' Moment Mr1p at r=r1 of plate',F10.4)
           write(8,32)Mr2p
32          format(/,' Moment Mr2p at r=r2 of plate',F10.4)

            write(8,35)
35          format(//'      radii      deflection'//)
            hh=(r2-r1)/int
            r=r1

c           Compute axial deflections of the plate at the specified intervals.

            do 33 i=1,int+1
            w1=-(r**4-r1**4)*p/(64*Dp)
            rr=r/r1
            w2=c3*rr*rr*log(rr)
            w3=(rr*rr-1)*x(6)
            w4=log(rr)*x(5)
            w=w1-w2+w3+w4
            write(8,34)r,w
33          r=r-hh
            delta=w
            write(8,37)
37          format(//' Outer cyl dist    deflection'//)
```

```
            nn=p/int
            dist=0.
            const=-p*r2*r2/(E*tc)

      c     Compute deflections of outer cylinder at the specified intervals.

            do 36 i=1,int+1
            bb2=B2*dist
            z=const+x(3)*sin(bb2)*sinh(bb2)+x(4)*cos(bb2)*cosh(bb2)
            write(8,34)dist,z
  36        dist=dist+hh
            dist=0.
            write(8,38)
  38        format(//' Inner cyl dist     deflection'//)
            const=-p*r1*r1/(E*tc)

      c     Compute deflections of inner cylinder at the specified intervals.

            do 39 i=1,int+1
            bb1=B1*dist
            z=const+x(1)*sin(bb1)*sinh(bb1)+x(2)*cos(bb1)*cosh(bb1)
            write(8,34)dist,z
  39        dist=dist+hh

      c     Compute effective modulus and modulus ratio.

            E1=(F0+3.14157*Rm*Rm*p)*b/(3.14157*Rm*tc*delta)
            EE1=E/E1
            write(8,41)E1,EE1
  41        format(//' Effective Modulus E1=',d13.6//' Modulus ratio EE1=',
     1      d13.6//)
  34        format(2d13.6/)

      c     Compute nondimensional parameter lambda, flexibility and stiffness.

            lambda=tc/(b*b)*Rm
            flex=EE1*tc/Rm
            stiff=1/flex
            write(8,49)stiff,lambda
  49        format(//,' STIFFNESS=',F15.6/' LAMBDA=',F15.6//)
 102        continue
 101        continue
 100        continue

            stop
```

```
c     THIS SUBROUTINE FACTORISES THE COEFFICIENT MATRIX A
c     INTO ITS L-R FACTORS AND WRITES THEM OVER MATRIX A.
c     PREF INDICATES OPTIONS: PREF=S(1)=0 FOR NO PARTIAL PIVOT SEARCH.
c     PREF=1 FOR PARTIAL PIVOT SEARCH.

      subroutine lr(a,n,s,eps,sucess)
      integer s(10),temp,pref
      character sucess*1
      dimension a(10,10)

      pref=1
      if(s(1).eq.0)then
        pref=s(1)
        s(1)=1
      endif

c     THIS BLOCK INTERCHANGES ROWS IN THE CASE OF PARTIAL PIVOT SEARCH.

      if(pref.ne.0)then
        amax=0.
        do 10 i=1,n
        if(abs(a(i,1)).ge.amax)then
          amax=abs(a(i,1))
          k=i
        endif
10      continue
        if(k.ne.1)then
          temp=s(1)
          s(1)=s(k)
          s(k)=temp
        endif
      endif

c     PIVOTING ABOUT PIVOT ELEMENT (1,1)

      do 30 i=2,n
      n2=s(i)
      if(abs(a(s(1),1)).lt.eps)then
        sucess='n'
        go to 130
      else
        a(n2,1)=a(n2,1)/a(s(1),1)
      endif
30    continue

c     PIVOTING ABOUT ANY GENERAL PIVOT ELEMENT

      do 40 k1=2,n
        do 50 k2=k1,n
          sum=0.0
          do 60 j=1,k1-1
60          sum=sum+a(s(k2),j)*a(s(j),k1)
50      a(s(k2),k1)=a(s(k2),k1)-sum
      if(k1.lt.n)then
        if(pref.ne.0)then
        amax=0.
        do 70 k3=k1,n
          if(abs(a(s(k3),k1)).ge.amax)then
            amax=abs(a(s(k3),k1))
            k4=k3
```

```
              endif
70        continue
              if(k4.ne.k1)then
                  temp=s(k1)
                  s(k1)=s(k4)
                  s(k4)=temp
              endif
          endif
          if(abs(a(s(k1),k1)).lt.eps)then
              sucess='n'
          go to 130
          else
          do 80 i1=k1+1,n
80        a(s(i1),k1)=a(s(i1),k1)/a(s(k1),k1)
              do 90 j1=k1+1,n
              sum=0.
                  do 100 i2=1,k1-1
100               sum=sum+a(s(k1),i2)+a(s(i2),j1)
90                a(s(k1),j1)=a(s(k1),j1)-sum
          endif
      endif
40        continue

130       return
          end
```

127

```
c     THIS SUBROUTINE DOES FORWARD AND BACKWARD PASSES ON
c     ANY  B  VECTOR. THE RESULTS OF THE PASSES ARE OVERWRITTEN ON B.

      subroutine fb(a,n,s,b)
        integer s(10)
        dimension  a(10,10),b(10)

c     THIS PORTION DOES FORWARD PASS

      do 10 i=2,n
      sum=0.
      do 20 j=1,i-1
20      sum=sum+a(s(i),j)*b(s(j))
10    b(s(i))=b(s(i))-sum

c     THIS PORTION DOES BACKWARD PASS

      b(s(n))=b(s(n))/a(s(n),n)
      do 30 i=n-1,1,-1
       sum=0.
      do 40 j=i+1,n
40    sum=sum+a(s(i),j)*b(s(j))
30    b(s(i))=(b(s(i))-sum)/a(s(i),i)

      return
      end
```

APPENDIX B

COMPUTER PROGRAM FOR THE BENDING OF A

SINGLE CANTILEVER BEAM

```
C
C
C       ****************************************
C       *       MAIN PROGRAM BEGINS            *
C       ****************************************
C
        INTEGER IER
        REAL DCADRE,AERR,RERR,ERROR,F,F1,NEW,CURR,OLD,LLIM
        REAL BETA,L,STIFF,P,W,D,PL,PB,MB,PLBAR,PBBAR,MBBAR
        REAL A,B,C,DL,THETA,KSQ,CONST,EPS,XA,YA,NEWDEG,PLD
        REAL LOLIM,UPLIM,M0
C
C       EXTERNAL FUNCTIONS FOR THE INTEGRATION SUBROUTINE DCADRE.
C
        EXTERNAL FLEN,XCOD,YCOD
C
C       COMMON BLOCKS BETWEEN FUCTIONS, SUBROUTINES AND THE MAIN
C       PROGRAM FOR THE DATA TO BE COMMUNICATED.
C
        COMMON/AREA1/BETA,L,STIFF,P,W,D,MBBAR
        COMMON /AREA3/DL,C,THETA,KSQ,CONST
C
C       DEFINE ERROR LIMITS AND TOLERANCES.
C
        EPS=1.0E-5
        AERR=0.0
        RERR=1.0E-2
C
C       READ IN GEOMETRY AND LOAD ON THE ELEMENT.
C
        READ(1,*)BETA,L,STIFF,PLD,W,DBYL,M0
C
C       OBTAIN PRESSURE LOAD ECCENTRICITY FROM ECCENTRICITY/LENGTH RATIO.
C
        D=DBYL*L
C
C       LOOP TO DETERMINE TRAJECTORY DUE TO VARYING LEVELS OF PRESSURE.
C
        DO 81 K=1,7
        P=PLD*FLOAT(K)
        MB=P*D+M0
        MBBAR=MB*L/STIFF
C
C       INITIALLY ASSUMED EXTREME ANGLES FOR THE SECANT METHOD.
C
        CURR=0./180.*3.14159
        NEW=175./180.*3.14159
        CALL COMP(CURR)
        UPLIM=(THETA+CURR)/2.
C
C       IF(1-KSQ*SIN(X)*SIN(X)) >=0 SET THE UPPER BOUND SUCH THAT
C       THE EQUALITY HOLDS.
C
        UPTEMP=SQRT(1./KSQ)
        IF(UPTEMP.GT.1.) THEN
            UPPER=1.57
        ELSE
            UPPER=ASIN(UPTEMP)
        ENDIF
C
C       SET THE UPPER INTEGRATION LIMIT TO THE LIMITING UPPER BOUND IN
C       EITHER THE POSITIVE OR NEGATIVE RANGE.
C
        IF(UPLIM.GT.0.0)THEN
          IF(UPLIM.GT.UPPER)UPLIM=UPPER
```

```
            ELSE
                IF(UPLIM.LT.-UPPER)UPLIM=-UPPER
            ENDIF
            F=CONST*DCADRE(FLEN,THETA/2.,UPLIM,AERR,
          + RERR,ERROR,IER)-1.
C
C           ITERATIVE LOOP TO DETERMINE THE TIP SLOPE OF THE ELEMENT.
C
10          F1=F
            OLD=CURR
            CURR=NEW
            CALL COMP(CURR)
            UPLIM=(THETA+CURR)/2.
C
C           IF(1-KSQ*SIN(X)*SIN(X) >= 0 , SET THE UPPER BOUND SUCH THAT
C           THE EQUALITY HOLDS.
C
            UPTEMP=SQRT(1./KSQ)
            IF(UPTEMP.GT.1.) THEN
                UPPER=1.57
            ELSE
                UPPER=ASIN(UPTEMP)
            ENDIF
C
C           SET UPPER INTEGRATION LIMIT TO THE LIMITING BOUND IN EITHER
C           THE POSITIVE OR THE NEGATIVE RANGE.
C
            IF(UPLIM.GT.0.0)THEN
                IF(UPLIM.GT.UPPER)UPLIM=UPPER
            ELSE
                IF(UPLIM.LT.-UPPER)UPLIM=-UPPER
            ENDIF
            F=CONST*DCADRE(FLEN,THETA/2.,UPLIM,AERR,RERR,
          + ERROR,IER)-1.
C
C           IF THE DIFFERENCE BETWEEN THE TWO EXTREME FUNCTIONS IN THE
C           SECANT METHOD IS < EPS THEN WRITE WARNING MESSAGE AND QUIT
C           TIP ANGLE COMPUTATION LOOP. USE THE LAST COMPUTED ANGLE
C           ALPHA AS THE TIP ANGLE.
C
            IF(ABS(F-F1).LT.EPS)THEN
              . WRITE(3,23)
23            FORMAT(//5X,'F AND F1 DIFFER BY LESS THAN EPS')
                GO TO 20
            ENDIF
C
C           UPDATE THE ANGLE ALPHA USING THE SECANT METHOD.
C
            NEW=CURR-F*(CURR-OLD)/(F-F1)
C
C           ERROR CRITERION TO QUIT TIP ANGLE COMPUTATION LOOP.
C
            IF (ABS(NEW-CURR).LT.EPS)GO TO 20
            WRITE(3,1)NEW
1           FORMAT(//' NEW ALPHA=',F10.4)
            GO TO 10
20          NEWDEG=NEW*180./3.14159
            WRITE(3,2)NEWDEG
2           FORMAT(//' ALPHA=',F10.4,' DEGREES' )
            CALL COMP(NEW)
            UPLIM=(THETA+NEW)/2.
C
C           IF(1-KSQ*SIN(X)*SIN(X)) >= 0 , SET THE UPPER BOUND SUCH THAT
C           THE EQUALITY HOLDS.
C
            UPTEMP=SORT(1./KSO)
```

```fortran
            IF(UPTEMP.GT.1.)THEN
                UPPER=1.57
            ELSE
                UPPER=ASIN(UPTEMP)
            ENDIF
C
C       SET UPPER INTEGRATION LIMIT TO THE LIMITING BOUND IN EITHER THE
C       POSITIVE OR NEGATIVE RANGE.
C
            IF(UPLIM.GT.0.0)THEN
                IF(UPLIM.GT.UPPER)UPLIM=UPPER
            ELSE
                IF(UPLIM.LT.-UPPER)UPLIM=-UPPER
            ENDIF
            ANS=CONST*DCADRE(FLEN,THETA/2.,UPLIM,AERR,
          + RERR,ERROR,IER)
            WRITE(3,7)ANS
7           FORMAT(//' ANSWER OBTAINED BY INTEGRATION IS ',F10.4)
            LOLIM=THETA/2.
C
C       COMPUTE TIP DEFLECTIONS OF THE ELEMENT.
C
            XA=CONST*DCADRE(XCOD,LOLIM,UPLIM,AERR,RERR,ERROR,IER)
            YA=CONST*DCADRE(YCOD,LOLIM,UPLIM,AERR,RERR,ERROR,IER)
            WRITE(3,12)
            WRITE(3,11)XA*L,YA*L
12          FORMAT(//' THE NEW COORDINATES FOR THE TIP IS :'//)
11          FORMAT(' XA=',F10.4,' YA=',F10.4//)
            WRITE(3,13)
13          FORMAT(//2X,'NO.',9X,'THETA (RADIANS)',8X,'XCOOD',10X,
          + 'YCOOD'//)
C
C       COMPUTE DEFLECTIONS OF ELEMENT NEARER THE TIP.
C
            COUNT=1.
            DO 21 J=1,10
            LLIM=NEW/(2.*COUNT)+LOLIM
            XCOOD=CONST*DCADRE(XCOD,LLIM,UPLIM,AERR,RERR,ERROR,IER)
            YCOOD=CONST*DCADRE(YCOD,LLIM,UPLIM,AERR,RERR,ERROR,IER)
            WRITE(3,9)J,LLIM,XCOOD,YCOOD
9           FORMAT(/I3,5X,E20.6,5X,F10.4,5X,F10.4)
            COUNT=COUNT+0.1
21          CONTINUE
C
C       COMPUTE DEFLECTIONS OF ELEMENT NEARER THE BASE.
C
            DO 22 J=3,6
            LLIM=NEW/(2.*FLOAT(J))+LOLIM
            XCOOD=CONST*DCADRE(XCOD,LLIM,UPLIM,AERR,RERR,ERROR,IER)
            YCOOD=CONST*DCADRE(YCOD,LLIM,UPLIM,AERR,RERR,ERROR,IER)
            M=J+8
            WRITE(3,9)M,LLIM,XCOOD*L,YCOOD*L
22          CONTINUE
81          CONTINUE
            STOP
            END
C
C       ****************************************************
C       *     FUNCTION FLEN TO COMPUTE THE INTEGRAND      *
C       ****************************************************
C
            FUNCTION FLEN(X)
            REAL X,KSQ
            COMMON /AREA3/DL,C,THETA,KSQ,CONST
             DEFN=1.-KSQ*SIN(X)*SIN(X)
            IF(DEFN.LT.0.0)DEFN=1.E-4
```

```fortran
      FLEN=1/SQRT(DEFN)
      RETURN
      END
C
C     **************************************************
C     *      SUBROUTINE COMP TO COMPUTE THE            *
C     *      INTERMEDIATE VALUES FOR THE               *
C     *      INTEGRATION                               *
C     **************************************************
C
      SUBROUTINE COMP(CURR )
      REAL CURR,THETA,KSQ,CONST
      REAL BETA,L,STIFF,P,W,D,MBBAR
      COMMON /AREA1/BETA,L,STIFF,P,W,D,MBBAR
      COMMON /AREA3/DL,C,THETA,KSQ,CONST
      PL=-P*COS(CURR)+W*COS(BETA)
      PB=P*SIN(CURR)-W*SIN(BETA)
      PLBAR=PL*L*L/STIFF
      PBBAR=PB*L*L/STIFF
      A=2.*PLBAR
      B=2.*PBBAR
      C=-2.*PLBAR*COS(CURR)+2.*PBBAR*SIN(CURR)+MBBAR*MBBAR
      DL=SQRT(A*A+B*B)
      THETA=ATAN2(B,A)
      KSQ=2.*DL/(C+DL)
      CONST=2./SQRT(C+DL)
      RETURN
      END
C
C     **************************************************
C     *      FUNCTION XCOD TO COMPUTE THE              *
C     *      INTEGRAND FOR THE COMPUTATION             *
C     *      OF THE TIP AND INTERMEDIATE               *
C     *      X-COORDINATE                              *
C     **************************************************
C
      FUNCTION XCOD(X)
      REAL X
      COMMON /AREA3/DL,C,THETA,KSQ,CONST
      XCOD=COS(2.*X-THETA)*FLEN(X)
      RETURN
      END
C
C     **************************************************
C     *      FUNCTION YCOD TO COMPUTE THE              *
C     *      INTEGRAND FOR THE COMPUTATION             *
C     *      OF THE TIP AND INTERMEDIATE               *
C     *      Y-COORDINATE                              *
C     **************************************************
C
      FUNCTION YCOD(X)
      REAL X
      COMMON /AREA3/DL,C,THETA,KSQ,CONST
      YCOD=SIN(2.*X-THETA)*FLEN(X)
      RETURN
      END
```

APPENDIX C

COMPUTER PROGRAM FOR THE ELEMENT STRING

```
C
C        *****************************************
C        *       MAIN PROGRAM BEGINS          *
C        *****************************************
C
         INTEGER IER
         REAL DCADRE,AERR,RERR,ERROR,F,F1,NEW,CURR,OLD,LLIM
         REAL BETA,L,STIFF,P,W,D,PL,PB,MB,PLBAR,PBBAR,MBBAR
         REAL A,B,C,DL,THETA,KSQ,CONST,EPS,XA,YA,NEWDEG,PLD
         REAL LOLIM,UPLIM,M0,X(10),Y(10),ALPHA(10),XXX(10),YYY(10)
         REAL LEN(10),EI(10),INTLD(10),SLFWT(10),DLRAT(10)
         REAL EXTMOM(10)
C
C        EXTERNAL FUNCTIONS FOR THE INTEGRATION SUBROUTINE DCADRE.
C
         EXTERNAL FLEN,XCOD,YCOD
C
C        COMMON BLOCKS BETWEEN FUNCTIONS, SUBROUTINES AND THE MAIN PROGRAM
C        FOR THE DATA TO BE COMMUNICATED.
C
         COMMON/AREA1/BETA,L,STIFF,PA,W,D,MBBAR
         COMMON /AREA3/DL,C,THETA,KSQ,CONST
C
C        DEFINE ERROR LIMITS AND TOLERANCES.
C
         EPS=1.0E-5
         AERR=0.0
         RERR=1.0E-2
         DEL=0.2
C
C        INITIALLY ASSUMED GLOBAL COORDINATES OF LOAD.
C
         GLXP=0.0
         GLYP=0.0
C
C        READ IN DATA OF LOAD , LINK JOINING LIFTING ELEMENTS AND END
C        EFFECTOR AND THE LAST LIFTING ELEMENT.
C
         READ(1,*)WL,RL,XL,YL,H,RB
C
C        READ IN TRANSFORMATION MATRICES FOR EACH OF THE LINKS IN THE
C        LIFTING ELEMENTS.
C
         DO 82 K=2,6,2
         READ(1,*)X(K),Y(K),ALPHA(K)
82       CONTINUE
C                              .
C        READ IN GEOMETRY AND LOADS ON EACH OF THE LIFTING ELEMENTS.
C
         DO 81 K=1,4
         READ(1,*)LEN(K),EI(K),INTLD(K),SLFWT(K),DLRAT(K),EXTMOM(K)
C
C        ITERATIVE LOOP TO DETERMINE THE GLOBAL LOAD POSITION DUE TO A
C        SET OF PRESSURES.
C        SET ANGLE AT WHICH SHEAR LOAD AND SELF WEIGHT ACTS TO 180
C        DEGREES FOR THE FIRST ELEMENT.
C
81       CONTINUE
87       BETA=3.14159
C
C        LOOP TO DETERMINE THE LOCAL (X,Y) COORDINATES FOR THE TIP OF
C        EACH ELEMENT.
C
         ALPSUM=0.0
```

```
              DO 85 K=1,4
              L=LEN(K)
              STIFF=EI(K)
              PA=INTLD(K)
C
C     SHEAR LOAD AND SELF WEIGHT ACTING ON ELEMENT K.
C
              W=WL+SLFWT(K)
              DBYL=DLRAT(K)
              MO=EXTMOM(K)
              D=DBYL*L
              MB=PA*D+MO
              MBBAR=MB*L/STIFF
C
C     INITIALLY ASSUMED EXTREME ANGLES FOR THE SECANT METHOD.
C
              CURR=0./180.*3.14159
              NEW=175./180.*3.14159
              CALL COMP(CURR)
              UPLIM=(THETA+CURR)/2.
C
C     IF(1-KSQ*SIN(X)*SIN(X)) >= 0 SET THE UPPER BOUND SUCH THAT
C     THE EQUALITY HOLDS.
C
              UPTEMP=SQRT(1./KSQ)
              IF(UPTEMP.GT.1.) THEN
                  UPPER=1.57
              ELSE
                  UPPER=ASIN(UPTEMP)
              ENDIF
C
C     SET UPPER INTEGRATION LIMIT TO THE LIMITING UPPER BOUND IN
C     EITHER THE POSITIVE OR NEGATIVE RANGE.
C
              IF(UPLIM.GT.0.0)THEN
                  IF(UPLIM.GT.UPPER)UPLIM=UPPER
              ELSE
                  IF(UPLIM.LT.-UPPER)UPLIM=-UPPER
              ENDIF
              LOLIM=THETA/2.
              F=CONST*DCADRE(FLEN,LOLIM,UPLIM,AERR,
     +        RERR,ERROR,IER)-1.
C
C     ITERATIVE LOOP TO DETERMINE THE TIP ANGLE ALPHA IN EACH ELEMENT.
C
10            F1=F
              OLD=CURR
              CURR=NEW
              CALL COMP(CURR)
              UPLIM=(THETA+CURR)/2.
C
C     IF(1-KSQ*SIN(X)*SIN(X)) >= 0 , SET THE UPPER BOUND SUCH THAT
C     THE EQUALITY HOLDS.
C
              UPTEMP=SQRT(1./KSQ)
              IF(UPTEMP.GT.1.) THEN
                  UPPER=1.57
              ELSE
                  UPPER=ASIN(UPTEMP)
              ENDIF
C
C     SET UPPER INTEGRATION LIMIT TO THE LIMITING BOUND IN EITHER
C     THE POSITIVE OR NEGATIVE RANGE.
C
              IF(UPLIM.GT.0.0)THEN
                  IF(UPLIM.GT.UPPER)UPLIM=UPPER
```

```
              ELSE
                  IF(UPLIM.LT.-UPPER)UPLIM=-UPPER
              ENDIF
              LOLIM=THETA/2.
              F=CONST*DCADRE(FLEN,LOLIM ,UPLIM,AERR,RERR,
          +   ERROR,IER)-1.
C
C         IF THE DIFFERENCE BETWEEN THE TWO EXTREME FUNCTIONS IN THE
C         SECANT METHOD IS < EPS THEN WRITE WARNING MESSAGE AND QUIT
C         TIP ANGLE COMPUTATION LOOP. USE THE LAST COMPUTED ANGLE
C         ALPHA AS THE TIP ANGLE.
C
              IF(ABS(F-F1).LT.EPS)THEN
                  WRITE(3,23)
23                FORMAT(//5X,'F AND F1 DIFFER BY LESS THAN EPS')
                  GO TO 20
              ENDIF
C
C         UPDATE THE ANGLE ALPHA USING THE SECANT METHOD.
C
              NEW=CURR-F*(CURR-OLD)/(F-F1)
C
C         ERROR CRITERION TO QUIT TIP ANGLE COMPUTATION LOOP.
C
              IF (ABS(NEW-CURR).LT.EPS)GO TO 20
              WRITE(3,1)NEW
1             FORMAT(//' NEW ALPHA=',F10.4)
              GO TO 10
20            NEWDEG=NEW*180./3.14159
              WRITE(3,2)NEWDEG
2             FORMAT(//' ALPHA=',F10.4,' DEGREES' )
              CALL COMP(NEW)
              UPLIM=(THETA+NEW)/2.
C
C         IF(1-KSQ*SIN(X)*SIN(X)) >= 0 , SET THE UPPER BOUND SUCH THAT
C         THE EQUALITY HOLDS.   .
C
              UPTEMP=SQRT(1./KSQ)
              IF(UPTEMP.GT.1.)THEN
                  UPPER=1.57
              ELSE
                  UPPER=ASIN(UPTEMP)
              ENDIF
C
C         SET UPPER INTEGRATION LIMIT TO THE LIMITING BOUND IN EITHER THE
C         POSITIVE OR NEGATIVE RANGE.
C
              IF(UPLIM.GT.0.0)THEN
                  IF(UPLIM.GT.UPPER)UPLIM=UPPER
              ELSE
                  IF(UPLIM.LT.-UPPER)UPLIM=-UPPER
              ENDIF
              LOLIM=THETA/2.
              ANS=CONST*DCADRE(FLEN,LOLIM,UPLIM,AERR,
          +   RERR,ERROR,IER)
              WRITE(3,7)ANS
7             FORMAT(//' ANSWER OBTAINED BY INTEGRATION IS ',F10.4)
              LOLIM=THETA/2.
              XA=CONST*DCADRE(XCOD,LOLIM,UPLIM,AERR,RERR,ERROR,IER)
              YA=CONST*DCADRE(YCOD,LOLIM,UPLIM,AERR,RERR,ERROR,IER)
C
C         STORE TIP DEFLECTIONS AND CLOCKWISE ANGLE ROTATION IN
C         ARRAYS X,Y AND ALPHA.
C
              X(2*K-1)=XA*L
              Y(2*K-1)=YA*L
```

```
            ALPHA(2*K-1)=-NEW
C
C           TOTAL CHANGE IN ANGLE FROM THE SUPPORTING BASE.
C
            ALPSUM=ALPSUM+NEW
C
C           WRITE THE TIP DEFLECTIONS OF THE ELEMENT IN THE LOCAL COORDINATE
C           SYSTEM.
C
            WRITE(3,21)X(2*K-1),Y(2*K-1)
21          FORMAT(//5X,'XTIP=',F7.3,5X,'YTIP=',F7.3)
C
C           UPDATE THE ANGLE AT WHICH THE DEAD LOAD ACTS.
C
            IF(K.NE.4)BETA=BETA-NEW
85          CONTINUE
C
C           CALL TO TRANSFORM TIP DEFLECTIONS IN LOCAL COORDINATE SYSTEM
C           TO GLOBAL COORDINATE SYSTEM.
C
            CALL TRANS(X,Y,ALPHA,XXX,YYY,4)
C
C           WRITE GLOBAL TIP DEFLECTIONS OF ELEMENTS.
C
            DO 83 K=1,4
            WRITE(3,115)K,XXX(K),K,YYY(K)
83          CONTINUE
115         FORMAT(//5X,'GLTPXEL(',I2,')=',F7.3,5X,'GLTPYEL(',I2,')=',
           + F7.3)
C
C           COMPUTE COORDINATES OF LOAD.
C
            RTPL=2.*RB+H+RL
            PSI=ATAN2(XL,RL+YL)
            GLXC=XXX(4)+RTPL*SIN(ALPSUM+PSI)
            GLYC=YYY(4)-RTPL*COS(ALPSUM+PSI)
C
C           CRITERION TO QUIT GLOBAL LOAD POSITION ITERATION DUE TO
C           A SET OF PRESSURES.
C
            IF((ABS(GLXC-GLXP).LE.DEL).AND.(ABS(GLYC-GLYP).LE.DEL))GO TO 86
C
C           UPDATE EXTERNAL MOMENT IN EACH ELEMENT DUE TO LOAD.
C
            DO 84 I=1,4
            EXTMOM(I)=(SLFWT(I)+WL)*(YYY(I)-GLYF)
84          CONTINUE
C
C           UPDATE GLOBAL LOAD POSITION.
C
            GLXP=GLXC
            GLYP=GLYC
            GO TO 87
C
C           WRITE FINAL GLOBAL LOAD POSITION DUE TO A SET OF PRESSURES.
C
86          WRITE(3,22)GLXC,GLYC
22          FORMAT(//5X,'GL. XCOOD. LD.=',F10.4,5X,'GL. YCOOD. LD.=',F10.4)
            STOP
            END
C
C           ***********************************************************
C           *       FUNCTION FLEN TO COMPUTE THE INTEGRAND        *
C           ***********************************************************
C
            FUNCTION FLEN(X)
```

```fortran
      REAL X,KSQ
      COMMON /AREA3/DL,C,THETA,KSQ,CONST
       DEFN=1.-KSQ*SIN(X)*SIN(X)
      IF(DEFN.LE.0.0)DEFN=1.0E-4
      FLEN=1./SQRT(DEFN)
      RETURN
      END
C
C
C     **********************************************
C     *      SUBROUTINE COMP TO COMPUTE THE        *
C     *      INTERMEDIATE VALUES FOR THE           *
C     *      INTEGRATION                           *
C     **********************************************
C
      SUBROUTINE COMP(CURR)
      REAL CURR,THETA,KSQ,CONST
      REAL BETA,L,STIFF,P,W,D,MBBAR
      COMMON /AREA1/BETA,L,STIFF,P,W,D,MBBAR
      COMMON /AREA3/DL,C,THETA,KSQ,CONST
      PL=-P*COS(CURR)+W*COS(BETA)
      PB=P*SIN(CURR)-W*SIN(BETA)
      PLBAR=PL*L*L/STIFF
      PBBAR=PB*L*L/STIFF
      A=2.*PLBAR
      B=2.*PBBAR
      C=-2.*PLBAR*COS(CURR)+2.*PBBAR*SIN(CURR)+MBBAR*MBBAR
      DL=SQRT(A*A+B*B)
      THETA=ATAN2(B,A)
      KSQ=2.*DL/(C+DL)
      CONST=2./SQRT(C+DL)
      RETURN
      END
C
C
C     **********************************************
C     *      FUNCTION XCOD TO COMPUTE THE          *
C     *      INTEGRAND FOR THE COMPUTATION         *
C     *      OF THE TIP X-COORDINATE               *
C     **********************************************
C
      FUNCTION XCOD(X)
      REAL X
      COMMON /AREA3/DL,C,THETA,KSQ,CONST
      XCOD=COS(2.*X-THETA)*FLEN(X)
      RETURN
      END
C
C
C     **********************************************
C     *      FUNCTION YCOD TO COMPUTE THE          *
C     *      INTEGRAND FOR THE COMPUTATION         *
C     *      OF THE TIP Y-COORDINATE               *
C     **********************************************
C
      FUNCTION YCOD(X)
      REAL X
      COMMON /AREA3/DL,C,THETA,KSQ,CONST
      YCOD=SIN(2.*X-THETA)*FLEN(X)
      RETURN
      END
C
C
C     **********************************************
C     *      SUBROUTINE TRANS TO TRANSFORM         *
C     *      THE LOCAL COORDINATES TO THE          *
C     *      GLOBAL COORDINATES                    *
C     **********************************************
C
```

```
            SUBROUTINE TRANS(X,Y,ALPHA,XXX,YYY,IELEM)
            REAL X(10),Y(10),ALPHA(10),TRAN(3,3),TEMP(3,3),TRAN2(3,3)
            REAL XXX(10),YYY(10)
      C
      C     INITIALIZE TRANSFORMATION MATRIX TO AN IDENTITY MATRIX.
      C
            DO 11 I=1,3
               DO 12 J=1,3
                  IF (I.EQ.J) THEN
                     TRAN(I,J)=1.
                  ELSE
                     TRAN(I,J)=0.
                  ENDIF
      12       CONTINUE
      11    CONTINUE
      C
      C     GLOBAL AND LOCAL COORDINATES FOR FIRST ELEMENT COINCIDES.
      C
            XXX(1)=X(1)
            YYY(1)=Y(1)
            DO 15 J=2,IELEM
            DO 10 I=2*J-3,2*(J-1)
               CALL UTOI(X(I),Y(I),ALPHA(I),TEMP)
               CALL TMULT(TRAN,TEMP,TRAN2)
      C
      C     UPDATE TRANSFORMATION MATRIX TILL ELEMENT(J-1) AND
      C     THE RIGID LINK AFTER IT.
      C
            DO 51 II=1,3
               DO 50 JJ=1,3
                  TRAN(II,JJ)=TRAN2(II,JJ)
      50       CONTINUE
      51    CONTINUE
      10    CONTINUE
      C
      C     COMPUTE GLOBAL TIP COORDINATES FOR ELEMENT J.
      C
            XXX(J)=TRAN(1,1)*X(2*J-1)+TRAN(1,2)*Y(2*J-1)+TRAN(1,3)
            YYY(J)=TRAN(2,1)*X(2*J-1)+TRAN(2,2)*Y(2*J-1)+TRAN(2,3)
      15    CONTINUE
            RETURN
            END
      C
      C     ********************************************
      C     *     SUBROUTINE UTOI TO FORM THE          *
      C     *     TRANSFORMATION MATRIX BETWEEN        *
      C     *     FRAME (I) AND FRAME (I-1)            *
      C     ********************************************
      C
            SUBROUTINE UTOI(X,Y,ALPHA,IFORM)
            REAL X,Y,ALPHA,IFORM(3,3)
            IFORM(1,1)=COS(ALPHA)
            IFORM(2,1)=-SIN(ALPHA)
            IFORM(3,1)=0.0
            IFORM(1,2)=SIN(ALPHA)
            IFORM(2,2)=COS(ALPHA)
            IFORM(3,2)=0.0
            IFORM(1,3)=X
            IFORM(2,3)=Y
            IFORM(3,3)=1.0
            RETURN
            END
      C
      C     ********************************************
      C     *     SUBROUTINE TMULT TO MULTIPLY         *
      C     *     TWO MATRICES                         *
```

```
C     ******************************************
C
      SUBROUTINE TMULT(BRELA,CRELB,CRELA)
      REAL BRELA(3,3),CRELB(3,3),CRELA(3,3)
      DO 10 I=1,3
         DO 20 J=1,3
            CRELA(I,J)=BRELA(I,1)*CRELB(1,J)+BRELA(I,2)*
     -      CRELB(2,J)+BRELA(I,3)*CRELB(3,J)
20       CONTINUE
10    CONTINUE
      RETURN
      END
```